Coherence bandwidth characterisation for indoor mobile radio microcells at microwave and millimetre wave frequencies

Jean Philippe Kermoal

A thesis submitted in partial fulfilment of the requirements of the University of Glamorgan for the degree of Master of Philosophy

University of Glamorgan

April 1998

This to certify that, except where specific reference is made, the work described in this thesis is the result of the candidate. Neither this thesis, nor any part of it, has been presented, or is currently submitted, in candidature for any degree at any University.

Signed _____

Jean Philippe Kermoal

Acknowledgements

I wish to thank my director of studies, Dr. Akram Hammoudeh for his thorough guidance, enthusiastic discussion and support throughout the research. With gratitude, I would also acknowledge Dr. Christopher Haslett for his help while he was with the University of Glamorgan.

I would not forget Dr. Manuel García Sánchez from the University of Vigo (Spain) for our long and interesting conversation.

I am also very grateful to my colleagues and ex-colleagues of the Radiowave Propagation Research Unit, Mr. Jean Pierre Pugliese, Mr. Jürgen Richter, Dr. Ming Sheng Ding and Richard Stephens for their useful discussion. Furthermore, I would like to thank the member of the Postgraduate Research Centre particularly Mr. Ulrich Wienrich, Ralf Patz, Ingo Lüdtke, Dr. Katherine Ann Compton, Dr. Patrick Megasson and Dr. Sami Sasak. I shall not forget Mr. Tim Jones and Mr. Michael Weiss for their invaluable assistance in my nightmarish software trouble.

Special thanks to the porters Mrs. Priscilla Downes and Mr. Leonard Davies for their help and understanding during the measurement campaigns.

Last but not least, I would like to thank my parents and sister for their support, inspiration and understanding during the difficult moments.

Abstract

This thesis reports measured and predicted results of the coherence bandwidth of indoor mobile radio microcells at 11 GHz and 62.4 GHz. Furthermore, the influence of the antennas radiation patterns and the effect of furniture on the value of the coherence bandwidth has been investigated.

A two branch frequency diversity system has been developed and used to simultaneously record the amplitude variation of the sideband signals. Frequency separations in the range between 5 and 240 MHz have been used at both 11 GHz and 62.4 GHz. In order to assist in explaining experimental results, a ray-tracing algorithm based on the image method, has been developed. It considers reflections up to the third order and assumes smooth walls, all with the same dielectric parameters.

The correlation coefficients between signal envelopes separated in frequency are measured and expressed as functions of distance between terminals. The level below which the correlation stays for a given percentage of time has been measured and plotted against frequency spacing to generate the frequency correlation function of the microcell. The coherence bandwidth, corresponding to correlation levels of 0.5, 0.7 and 0.9, are determined from these functions. The coherence bandwidth has also been measured at each position in the microcell and its value for a given percentage of mobile terminal locations is given. The difference between results obtained from both methods are outlined and explained.

Results are presented for three corridors and a room. A comparison between experimental results obtained at 11 GHz and 62.4 GHz is also given.

List of symbols and abbreviations

ACTS	Advanced Communication Technologies and Services
AMPS	Advanced Mobile Phone Service
C/I	Carrier to Interference ratio
CDF	Cumulative Distribution Function
CDMA	Code Division Multiple Access
CEPT	Conférence Européenne des Postes et Télécommunications
COST	Cooperation in the Field of Scientific and Technical Research
CT	Cordless Telephone
CW	Continuous Wave
DECT	Digital European Cordless Telecommunication
E	electrical field intensity (V)
ERMES	European Digital Radio Messaging System
ETSI	Trans-European Trunk Radio System
f	frequency (Hz)
FDMA	Frequency Division Multiple Access
FM	Frequency Modulation
FPLMTS	Future Public Land Mobile Telecommunication System
FSK	Frequency Shift Keying
GSM	Groupe spécial mobile / Global System for Mobile communication
G_{Rx}	receiving antenna gain (dB)
G_{Tx}	transmitting antenna gain (dB)

HIPERLAN	High Performance Radio Local Area Network
IBC	Integrated Broadband Communication
ISDN	Integrated Services Digital Network
IMT	International Mobile Telecommunication
ITU-R	International Telecommunication Union - Radio communication Sector
ITU-T	International Telecommunication Union - Telecommunication Sector
L	path loss (dB)
LOS	Line-Of-Sight
l_{los}	line-of-sight path length (m)
l_n	n^{th} ray path length (m)
MBS	Mobile Broadband System
NLOS	Non Line-Of-Sight
NMT	Nordic Mobile Telephone
NTT	Nippon Telephone and Telegraph
MVDS	Multipoint Video Distribution Systems
OBS	Obstructed Line-of-Sight
PBX	Private Branch Exchange
PDF	Probability Density Function
PDP	Power Delay Profile
PMR	Private Mobile Radio
Pr	received power (dBm)
Pt	transmitted power (dBm)
QWSS	Quasi Wide Sense Stationary
RACE	Research and Development in Advanced Communication Technologies in Europe
SNR	Signal to Noise Ratio
TACS	Total Acces Communication System
TDD	Time Division Duplex
TDMA	Time Division Multiple Access

TETRA	Trans-European Trunk Radio System
UMTS	Universal Mobile Telecommunication System
US	Uncorrelated Scattering
v	speed (ms^{-1})
WARC	World Administrative Radio Conference
WBS	Wireless Broadband Systems
WLAN	Wireless Local Area Network
WSSUS	Wide Sense Stationary Uncorrelated Scattering
α_n	n^{th} ray arrival angle (degree)
λ	wavelength (m)
$\rho_{\parallel}$	parallel reflection coefficient
$\rho_{\perp}$	perpendicular reflection coefficient
τ	time delay (s)
$\Delta\theta$	phase difference (degree)
Δ_l	path length difference (m)

Contents

Acknowledgements 1

Abstract 2

List of symbols and abbreviations 3

Contents 6

List of Figures 10

List of Tables 19

1 Introduction 22

1.1 The radio frequency spectrum congestion : Issues and solutions 22

1.2 Wireless personal communication 23

1.2.1 An overview of the mobile radio system : First and second generation 23

1.2.1.1 Cellular system 24

1.2.1.2 Cordless telephone system 26

1.2.2 The future of the mobile radio systems : Third generation 27

1.2.3 Wireless data network 28

1.3 The propagation channel 29

1.4 Objectives of the research 30

2 Indoor radio channel 32

2.1 Introduction 32

2.2 Propagation characteristics 33
2.2.1 Path loss 35
2.2.2 Statistics of the mobile radio channel 37
2.2.2.1 Rayleigh distribution 38
2.2.2.2 Rician distribution 38
2.2.3 Power delay profile 39
2.2.4 RMS delay spread 41
2.2.5 Coherence bandwidth 41

3 Ray tracing theory and modelling **45**

3.1 Introduction 45
3.2 Overview of indoor propagation models 46
3.2.1 Ray-tracing models 46
3.2.1.1 The ray launching method 47
3.2.1.2 The image method 47
3.3 Principles of electromagnetic wave propagation and ray theory 49
3.4 Development of a three-dimensional ray-tracing tool 50
3.4.1 From single to N order two-dimensional reflection model 51
3.4.1.1 Parallel walls scenario 51
3.4.1.2 Perpendicular walls scenario 51
3.4.2 A three dimensional indoor model 52
3.4.3 Indoor radio wave propagation model 52
3.4.4 Ray tracing algorithm 54
3.4.5 Ray path length 55
3.4.6 Reflection coefficient 55
3.4.7 Antenna parameters 58
3.5 Limitation of the model 58

4 Experimental hardware and geometry **67**

4.1 Introduction 67
4.2 The mechanical mobile system 68

4.3 The 62.4 GHz system . . . 70
4.3.1 Transmitter . . . 70
4.3.2 Receiver . . . 70
4.3.3 Antennas . . . 71
4.4 The 11 GHz System . . . 71
4.4.1 Transmitter . . . 71
4.4.2 Receiver . . . 72
4.4.3 Antennas . . . 72
4.5 The data acquisition system . . . 73
4.6 Description of the indoor environment . . . 73
4.6.1 J Block corridor 2^{nd}floor : corridor J2 . . . 74
4.6.2 J Block corridor 3^{nd}floor : corridor J3 . . . 74
4.6.3 H Block corridor : corridor H . . . 75
4.6.4 B 68 . . . 75

5 Characterisation of the indoor mobile radio channel and its coherence bandwidth at 11 GHz 87

5.1 Introduction . . . 87
5.2 Experimental and theoretical characterisation using horn to omnidirectional antenna . . . 88
5.2.1 Corridor J2 . . . 88
5.2.1.1 Received signal envelopes . . . 88
5.2.1.2 Correlation coefficient as a function of distance . . . 91
5.2.1.3 Method 1 : Characterisation of the coherence bandwidth using the microcell frequency correlation function . . . 92
5.2.1.4 Method 2 : Coherence bandwidth characterisation using the frequency correlation function at each position . . . 93
5.2.1.5 Theoretical investigation of the relationship between the coherence bandwidth and RMS delay spread . . . 95
5.2.2 Corridor J3 . . . 110
5.2.3 Corridor H . . . 118

5.2.4 Interim summary 125
5.2.5 Room B68 125
5.3 Effects of the antennas radiation patterns on coherence bandwidth 133
5.3.1 Corridor J2 133
5.3.2 Corridor J3 140
5.3.3 Corridor H 143
5.3.4 Interim summary 146
5.4 Effects of furniture in room B68 146

6 Coherence bandwidth characterisation at 62.4 GHz and comparison with results at 11 GHz **152**
6.1 Introduction 152
6.2 Corridor J2 152
6.3 Room B68 163
6.4 Effects of furniture on the coherence bandwidth 170

7 Conclusion and further work **175**
7.1 Conclusion 175
7.2 Further work 178

References **179**

List of Figures

2-1 Cumulative distribution function of the Rayleigh and Rician fading for several values of k 44

3-1 3-D representation of the definition of the plane of incidence 61
3-2 Illustration of of the image method using the forward (a) and backward (b) ray-tracing technique 61
3-3 First order reflection with two single refiections 62
3-4 A second order reflection ray-tracing model 62
3-5 A third order reflection ray-tracing model 63
3-6 Ray-tracing model with two perpendicular walls 63
3-7 Three dimensional representation of the image boxes for a first order layer . 64
3-8 Creation of fades in multipath environment 64
3-9 Coordinate of the incident field 65
3-10 Vectorial representation of the electric field E 65
3-11 Determination of the reflected E field for multireflection scenario 66
3-12 Reference vectors for the determination of the gain of the antennas 66

4-1 First setup : Detail of the horizontal guiding wheels 76
4-2 Second setup : Detail of the rail track design 76
4-3 Description of the finalised mechanical set up 76
4-4 Stationary trolley fully equiped 77
4-5 Mobile trolley equiped with the 62.4 GHz system 77
4-6 Block diagram of the transmitter at 62.4 GHz 78

4-7 Block diagram of the receiver at 62.4 GHz and the two-branch diversity system 78
4-8 Omnidirectional antenna and the transmitter at 62.4 GHz 79
4-9 Radiation pattern in elevation of the omnidirectional antenna at 62.4 GHz . 79
4-10 Omnidirectional antenna mounted on the mobile trolley for measurements at 11 GHz 80
4-11 Radiation pattern in elevation of the omnidirectional antenna at 11 GHz . . 80
4-12 Block diagram of the transmitter at 11.0 GHz 81
4-13 Block diagram of the receiver at 11 GHz 81
4-14 Calibration setup of the omnidirectional antenna at 11 GHz 81
4-15 Lay out of the measurement set up for corridor J2 (not to scale) 82
4-16 Corridor J2, view of wall B 82
4-17 lay out of the measurement set up for corridor J3 (not to scale) 83
4-18 Corridor J3, view of wall B 83
4-19 Lay out of the measurement set up for the corridor H (not to scale) 84
4-20 Corridor H, view of wall D 84
4-21 Lay out of the measurement set up of the room B68 without furniture (not to scale) 85
4-22 Room B68 with the 62.4 GHz system, view of the wall B 85
4-23 lay out of the measurement set up for the room B68 with furniture (not to scale) 86
4-24 Room B68 with furniture, view of the wall D 86

5-1 Received envelopes for a frequency spacing of 5 MHz in corridor J2 using a horn to omnidirectional antenna at 11 GHz 97
5-2 Predicted envelopes using a third order ray-tracing model computed for a frequency spacing of 5 MHz in corridor J2 using a horn to omidirectional antenna at 11 GHz 97
5-3 Power spectra of the signal envelope received as function of distance between terminals in corridor J2 using a horn to omnidirectional antenna at 11 GHz 98

5-4 Power spectrum of the received signal envelope with the terminals 20 m apart in corridor J2 using a horn to omnidirectional antenna at 11 GHz . . 98
5-5 Power spectrum of the predicted signal envelope with the terminals 20 m apart in corridor J2 using a horn to omnidirectional antenna at 11 GHz . . 99
5-6 K-parameter in the Rice distribution as function of distance between terminals in corridor J2 using a horn to omnidirectional antenna at 11 GHz . 100
5-7 Time delay for a two-ray model 100
5-8 Correlation between the envelopes separated by 5 MHz versus distance between terminals 101
5-9 Correlation between the envelopes separated by 40 MHz versus distance between terminals 101
5-10 Correlation between the envelopes separated by 132 MHz versus distance between terminals 101
5-11 Correlation between the predicted envelopes separated by 5 MHz versus distance between terminals 102
5-12 Correlation between the predicted envelopes separated by 40 MHz versus distance between terminals 102
5-13 Correlation between the predicted envelopes separated by 130 MHz versus distance between terminals 102
5-14 Cumulative distribution functions of the correlation coefficient for different frequency spacings in corridor J2 using a horn to omnidirectional antenna at 11 GHz 103
5-15 Cumulative distribution functions of the predicted correlation coefficient for different frequency spacings in corridor J2 using a horn to omnidirectional antenna at 11 GHz 103
5-16 Frequency correlation functions measured in corridor J2 using a horn to omnidirectional antenna at 11 GHz 104
5-17 Frequency correlation functions predicted in corridor J2 using a horn to omnidirectional antenna at 11 GHz 105

5-18 Frequency correlation function measured at a distance of 0.8 m from the receiver in corridor J2 using a horn to omnidirectional at 11 GHz 106
5-19 Frequency correlation function measured at a distance of 12 m from the receiver in corridor J2 using a horn to omnidirectional at 11 GHz 106
5-20 Frequency correlation function measured at a distance of 23.2 m from the receiver in corridor J2 using a horn to omnidirectional at 11 GHz 106
5-21 Coherence bandwidth for three correlation levels as a function of distance between terminals in corridor J2 using a horn to onmnidirectional antenna at 11 GHz 107
5-22 Predicted coherence bandwidth for three correlation levels as a function of distance between terminals in corridor J2 using a horn to omnidirectional antenna at 11 GHz 108
5-23 Predicted RMS delay spread versus distance between terminals 109
5-24 Coherence bandwidth for a 0.7 correlation level versus RMS delay spread . 109
5-25 Received envelopes for a frequency spacing of 5 MHz in corridor J3 using a horn to omnidirectional antenna at 11 GHz 113
5-26 Predicted envelopes using a third order ray-tracing model computed with a frequency spacing of 5 MHz in corridor J3 using a horn to omidirectional antenna at 11 GHz 113
5-27 Power spectra of the signal envelope as function of distance between terminals in corridor J3 using a horn to omnidirectional antenna at 11 GHz . . . 114
5-28 K factor in the Rice distribution as function of distance between terminals in corridor J3 using a horn to onmidirectional antenna at 11 GHz 114
5-29 Frequency correlation functions measured in corridor J3 using a horn to omnidirectional antenna at 11 GHz 115
5-30 Coherence bandwidth for a correlation level of 0.9 versus distance between terminals in corridor J3 at 11 GHz 116
5-31 Frequency correlation functions predicted in corridor J3 using a horn to omnidirectional antenna at 11 GHz 117

5-32 Received envelopes for a frequency spacing of 5 MHz in corridor H using a horn to omnidirectional antenna at 11 GHz 120
5-33 Predicted envelopes using a third order ray-tracing model computed with a frequency spacing of 5 MHz in corridor H using a horn to omidirectional at 11 GHz 120
5-34 Power spectra of the signal envelope as a function of distance between terminals in corridor H using a horn to omnidirectional antenna at 11 GHz . . 121
5-35 K factor in the Rice distribution as a function of distance between terminals in corridor H using a horn to omnidirectional antenna at 11 GHz 121
5-36 Frequency correlation function measured in corridor H using the horn to omnidirectional antenna at 11 GHz 122
5-37 Coherence bandwidth at a correlation level of 0.9 versus distance between terminals in corridor H at 11 GHz 123
5-38 Frequency correlation function predicted in corridor H using the horn to omnidirectional antenna at 11 GHz 124
5-39 Received envelopes for a frequency spacing of 5 MHz in room B68 empty using a horn to omnidirectional antenna at 11 GHz 128
5-40 Predicted envelopes using a third order ray-tracing model computed using a frequency separation of 5 MHz for the room B68 using a horn/omidirectional configuration at 11 GHz 128
5-41 Power spectra of the signal envelopes as function of distance for B68 empty using a horn to omnidirectional antenna configuration 129
5-42 K factor in the Rice distribution with distance for B68 empty at 11 GHz using a horn to omnidirectional antenna configuration 129
5-43 Frequency correlation function for different percentage of time for the room B68 empty using a horn to omnidirectional antenna configuration at 11 GHz130
5-44 Coherence bandwidth at a correlation level of 0.9 versus distance between the terminals using a horn to omnidirectional antenna configuration for the room B68 empty at 11 GHz 131

5-45 Predicted frequency correlation function for different percentage of time for the room B68 empty using a horn to omnidirectional antenna configuration 132
5-46 Received envelopes for a frequency spacing of 5 MHz in corridor J2 using a horn to horn configuration at 11 GHz 135
5-47 Predicted envelopes using a third order ray-tracing model computed with a frequency spacing of 5 MHz in corridor J2 using a horn to horn antenna at 11 GHz 135
5-48 Power spectra of the signal envelope received as function of distance between terminals in corridor J2 using a horn to horn antenna at 11 GHz 136
5-49 K factor in the Rice distribution as function of distance between terminals in corridor J2 using a horn to horn and a horn to omnidirectional antenna at 11 GHz 136
5-50 Frequency correlation functions measured in corridor J2 for 70 and 95 % of the time using a horn to horn and a horn to omnidirectional antenna at 11 GHz 137
5-51 Coherence bandwidth for correlation level of 0.9 versus distance between terminals in corridor J2 using a horn to horn and a horn to omnidirectional antenna at 11 GHz 138
5-52 Frequency correlation function predicted in corridor J2 for 70 and 95 % of the time using a horn to horn and a horn to omnidirectional antenna at 11 GHz 139
5-53 Power spectra of the signal envelope received as a function of distance between terminals in corridor J3 using a horn to horn antenna at 11 GHz . . 141
5-54 K factor in the Rice distribution as a function of distance between terminals in corridor J3 using a horn to horn and a horn to omnidirectional antenna at 11 GHz 141
5-55 Frequency correlation function measured in corridor J3 for 70 and 95 % of the time using a horn to horn and a horn to omnidirectional antenna at 11 GHz 142

5-56 Power spectra of the signal envelope as a function of distance between terminals in corridor H using a horn to horn antenna at 11 GHz 144
5-57 K factor in the Rice distribution with distance between terminals in corridor H using a horn to horn and a horn to omnidirectional antenna at 11 GHz . 144
5-58 Frequency correlation function measured in corridor H for 70 % and 95 % of the time using a horn to horn and a horn to omnidirectional antenna at 11 GHz 145
5-59 Received envelopes for a frequency spacing of 5 MHz in room B68 furnished using a horn to omnidirectional antenna at 11 GHz 148
5-60 Power spectra of the signal envelope as a function of distance between terminals in room B68 furnished using a horn to omnidirectional antenna at 11GHz 148
5-61 K factor in the Rice distribution with distance between terminals in B68 empty and furnished using a horn to omnidirectional antenna at 11 GHz . . 149
5-62 Frequency correlation function measured fro 70 % and 95 % of the time in room B68 furnished using a horn to omnidirectional antenna at 11 GHz . . 150
5-63 Coherence bandwidth at a correlation level of 0.9 in room B68 with and without furniture using a horn to omnidirectional antenna at 11 GHz 151

6-1 Received envelopes for a frequency spacing of 5 MHz in corridor J2 using a horn to omnidirectional antenna at 62.4 GHz 156
6-2 Predicted envelopes using third order ray-tracing with a frequency spacing of 5 MHz in corridor J2 using a horn to omnidirectional antenna at 62.4 GHz156
6-3 Power spectra of the signal envelope as function of distance between terminals in corridor J2 using a horn to omnidirectional antenna at 62.4 GHz . . 157
6-4 K factor in the Rice distribution with distance between terminals in corridor J2 using a horn to omnidirectional antenna at 62.4 GHz 157
6-5 Correlation between the envelopes separated by 5 MHz versus distance between terminals 158
6-6 Frequency correlation functions mesured in corridor J2 using a horn to omnidirectional antenna at 62.4 GHz 159

6-7 Frequency correlation function measured in corridor J2 for 90 % of the time using a horn to omnidirectional antenna at 11.0 GHz and 62.4 GHz 160
6-8 Coherence bandwidth for a correlation level of 0.9 as a function of distance between terminals in corridor J2 using a horn to omnidirectional antenna at 62.4 GHz 161
6-9 Frequency correlation functions predicted for 90 % of the time using double (o) and triple (*) order ray-tracing in corridor J2 at 62.4 GHz 162
6-10 Received envelopes for a frequency separation of 5 MHz in room B68 empty using a horn to omnidirectional antenna at 62.4 GHz 165
6-11 Predicted received envelopes using a third order ray-tracing model computed with a frequency spacing of 5 MHz in room B68 using a horn to omnidirectional antenna at 62.4 GHz 165
6-12 Power spectra of the signal envelope as a function of distance between terminals in room B68 empty using horn to omnidirectional antenna at 62.4 GHz 166
6-13 K factor in the Rice distribution with distance between terminals in room B68 empty using horn to omnidirectional antenna at 62.4 GHz and 11 GHz 166
6-14 Frequency correlation function measured in room B68 empty using a horn to omnidirectional antenna at 62.4 GHz 167
6-15 Frequency correlation function measured for 90 % of the time in room B68 empty at 62.4 GHz and 11.0 GHz 168
6-16 Coherence bandwidth for a correlation level of 0.9 as a function of distance between terminals using a horn to omnidirectional antenna at 11.0 GHz and 62.4 GHz 169
6-17 Received envelopes for a frequency spacing of 5 MHz in room B68 with furniture using a horn to omnidirectional antenna at 62.4 GHz 171
6-18 Power spectra of the signal envelope as function of distance between terminals in room B68 with furniture using a horn to omnidirectional antenna at 62.4 GHz 171

6-19 K factor in the Rice distribution with distance between terminals for B68 with and without furniture using a horn to omnidirectional antenna at 62.4 GHz 172
6-20 Frequency correlation functions measured for 70 % and 90 % of the time in room B68 with and without furniture using a horn to omnidirectional antenna at 62.4 GHz 173
6-21 Coherence bandwidth for a correlation level of 0.9 as function of distance between terminals with and without furniture using a horn to omnidirectional antenna at 62.4 GHz 174

List of Tables

5.1 coefficients of the best fit function $\rho = 1/(1 + c\Delta f^n)$ 92

5.2 Coherence bandwidth for 0.5 ($B_{0.5}$), 0.7 ($B_{0.7}$) and 0.9 ($B_{0.9}$) correlation levels computed from the above frequency correlation functions 104

5.3 Coherence bandwidth for 0.5 ($B_{0.5}$), 0.7 ($B_{0.7}$) and 0.9 ($B_{0.9}$) correlation levels computed from the above predicted frequency correlation functions . 105

5.4 Coherence bandwidth for 0.5 ($B_{0.5}$), 0.7 ($B_{0.7}$) and 0.9 ($B_{0.9}$) correlation levels computed from the above coherence bandwidth function 107

5.5 Coherence bandwidth for 0.5 ($B_{0.5}$), 0.7 ($B_{0.7}$) and 0.9 ($B_{0.9}$) correlation levels computed from the above predicted coherence bandwidth function . . 108

5.6 Coherence bandwidth for 0.5 ($B_{0.5}$), 0.7 ($B_{0.7}$) and 0.9 ($B_{0.9}$) correlation levels computed from the above frequency correlation functions 115

5.7 Coherence bandwidth for 0.5 ($B_{0.5}$), 0.7 ($B_{0.7}$) and 0.9 ($B_{0.9}$) correlation levels for the corridor J3 using a horn to omnidirectional antenna configuration at 11 GHz 116

5.8 Coherence bandwidth for 0.5 ($B_{0.5}$), 0.7 ($B_{0.7}$) and 0.9 ($B_{0.9}$) correlation levels computed from the above predicted frequency correlation functions . 117

5.9 Coherence bandwidth for 0.5 ($B_{0.5}$), 0.7 ($B_{0.7}$) and 0.9 ($B_{0.9}$) correlation levels computed from the above frequency correlation functions 122

5.10 Coherence bandwidth for 0.5 ($B_{0.5}$), 0.7 ($B_{0.7}$) and 0.9 ($B_{0.9}$) correlation levels computed fron the coherence bandwidth functions in corridor H using a horn to omnidirectional antenna at 11 GHz 123

5.11 Coherence bandwidth for 0.5 ($B_{0.5}$), 0.7 ($B_{0.7}$) and 0.9 ($B_{0.9}$) correlation levels from the above predicted frequency correlation functions 124
5.12 Coherence bandwidth for 0.5 ($B_{0.5}$), 0.7 ($B_{0.7}$) and 0.9 ($B_{0.9}$) correlation levels for the room B68 empty using a horn to omnidirectional antenna configuration at 11 GHz 130
5.13 Coherence bandwidth for 0.5 ($B_{0.5}$), 0.7 ($B_{0.7}$) and 0.9 ($B_{0.9}$) correlation levels for the room B68 empty using a horn to omnidirectional antenna configuration at 11 GHz 131
5.14 Coherence bandwidth for 0.5 ($B_{0.5}$), 0.7 ($B_{0.7}$) and 0.9 ($B_{0.9}$) correlation levels from the prediction for the room B68 using a horn to omnidirectional antenna configuration at 11 GHz 132
5.15 Coherence bandwidth for 0.5 ($B_{0.5}$), 0.7 ($B_{0.7}$) and 0.9 ($B_{0.9}$) correlation levels computed from the above frequency correlation fuctions 137
5.16 Coherence bandwidth for 0.5 ($B_{0.5}$), 0.7 ($B_{0.7}$) and 0.9 ($B_{0.9}$) correlation levels in corridor J2 computed from the coherence bandwidth functions for 70 and 95 using horn to horn and horn to omnidirectional antenna at 11 GHz138
5.17 Coherence bandwidth for 0.5 ($B_{0.5}$), 0.7 ($B_{0.7}$) and 0.9 ($B_{0.9}$) correlation levels computed from the above predicted frequency correlation functions . 139
5.18 Coherence bandwidth for 0.5 ($B_{0.5}$), 0.7 ($B_{0.7}$) and 0.9 ($B_{0.9}$) correlation levels computed from the above frequency correlation functions 142
5.19 Coherence bandwidth for 0.5 ($B_{0.5}$), 0.7 ($B_{0.7}$) and 0.9 ($B_{0.9}$) correlation levels computed from the above frequency correlation function 145
5.20 Coherence bandwidth for 0.5 ($B_{0.5}$), 0.7 ($B_{0.7}$) and 0.9 ($B_{0.9}$) correlation levels computed from the above frequency correlation functions 150
5.21 Coherence bandwidth for 0.5 ($B_{0.5}$), 0.7 ($B_{0.7}$) and 0.9 ($B_{0.9}$) correlation levels computed from the coherence bandwidth functions in room B68 with and without furniture for 70 and 95 % of the time using a horn to omnidirectional antenna at 11 GHz 151

6.1 coefficients of the best fit function $\rho = 1/(1 + c\Delta f^n)$ 154

6.2 Coherence bandwidth for 0.5 ($B_{0.5}$), 0.7 ($B_{0.7}$) and 0.9 ($B_{0.9}$) correlation levels computed from the above frequency correlation function 159
6.3 Coherence bandwidth for 0.5 ($B_{0.5}$), 0.7 ($B_{0.7}$) and 0.9 ($B_{0.9}$) correlation levels computed from the above frequency correlation functions 160
6.4 Coherence bandwidth for 0.5 ($B_{0.5}$), 0.7 ($B_{0.7}$) and 0.9 ($B_{0.9}$) correlation levels computed from the coherence bandwidth functions in corridor J2 using a horn to omnidirectional antenna configuration at 62.4 GHz 161
6.5 Predicted and measured Coherence bandwidth for 0.5 ($B_{0.5}$), 0.7 ($B_{0.7}$) and 0.9 ($B_{0.9}$) correlation levels computed from the frequency correlation function for 90 % of the time in corridor J2 using a horn to omnidirectional antenna configuration at 62.4 GHz 162
6.6 Coherence bandwidth for 0.5 ($B_{0.5}$), 0.7 ($B_{0.7}$) and 0.9 ($B_{0.9}$) correlation levels computed from the above frequency correlation functions 167
6.7 Coherence bandwidth for 0.5 ($B_{0.5}$), 0.7 ($B_{0.7}$) and 0.9 ($B_{0.9}$) correlation levels computed from the above frequency correlation functions 168
6.8 Coherence bandwidth for different percentage of time computed from the above coherence bandwidth functions 169
6.9 Coherence bandwidth for 0.5 ($B_{0.5}$), 0.7 ($B_{0.7}$) and 0.9 ($B_{0.9}$) correlation levels computed from the above frequency correlation functions in room B68 with and without furniture using a horn to omnidirectional antenna at 62.4 GHz 173

Chapter 1

Introduction

1.1 The radio frequency spectrum congestion : Issues and solutions

The recent years have seen a formidable growth in the mobile radio communication technology. From the first mobile radio link established by Marconi in 1897 to now, different generations of mobile communication systems have followed one upon the other [1] [2].

The development of the first generation cellular mobile radio system started slowly in the 1970s and lasted until 1980s. Cellular radio and cordless telephones arose from this development and used analogue technology. Cellular systems were originally targeted at vehicular subscribers in urban areas and limited to a certain group of users (police, hospital, business). Cordless telephones, on the other hand were designed to operate as a radio extension of a home telephone line. Even though the systems operated successfully, they suffered some drawbacks due to the technology employed, the restriction in the capacities offered, and the lack of harmonisation between countries in the case of the cellular network.

The second generation met the challenges of digital technology [2]. In Europe, efforts were concentrated on the standardisation and harmonisation of mobile systems. For instance, the Pan European Cellular System successfully proved the need of a Pan-European roaming facilities by its success. Digital cordless CT2 (Cordless telephone), an improved

version of the analogue cordless telephone, provides facilities such as telepoint call-out-only systems in public environments and conventional cordless telephones in home environments [3]. The introduction of ERMES (European Digital Radio Messaging System) in 1987 and TETRA (Trans-European Trunk Radio System) in 1994 were also responses to the internal European market [4].

Nevertheless, the services and capacities offered by the second generation personal communication system are still limited to voice transmission and low data rates. In general, the unpredictable expansion of the mobile system market caused the spectrum frequency, allocated around 800 MHz and 1800 MHz, to suffer from congestion. Efficient modulation techniques and new frequency bands are required to accommodate more users and increase capacity of personal communication networks.

Research works to explore the feasibility of using the microwave (1 to 30 GHz) and millimetre (30 to 300 GHz) frequencies for a number of applications has already been reported world wide. Therefore the higher part of the frequency spectrum may be used to alleviate the congestion in the radio frequency spectrum that faces the personal wireless mobile market.

1.2 Wireless personal communication

On account of the large number of wireless personal communication systems available world wide today, it is necessary to have a succinct understanding and knowledge of the past, present and future of the mobile radio communication technologies. A brief introduction to the history of the first and second generation personal communication systems is given. Following this, the perspectives of future systems are discussed. Finally the different wireless data network standards are discussed.

1.2.1 An overview of the mobile radio system : First and second generation

A mobile radio system is usually optimised to operate in a certain type of environment, depending on the mobility of the user, and with respect to the capacity demand of the

system. The main mobile radio systems in use are the cellular and the cordless telephony systems.

1.2.1.1 Cellular system

In the 1970s, Bell Laboratories launched the first cellular system known as AMPS (Advanced Mobile Phone Service) [1]. The principle of cellular systems when compared to previous conventional mobile radio systems like PMR (Private Mobile Radio) or trunked mobile radio system is the use of many base stations so defining a cell structure. The main advantage of using cells is that they allow frequency re-use and hence increase frequency spectrum share efficiency. The size of the cell is dependant on the concentration of users per square metre and the capacity required. High user concentration and/or large system capacity demands require small cells. The cell is usually referred to as a "picocell" for home or office, a "microcell" for large indoor or outdoor environment such as a suburban area and a "macrocell" for rural environment.

In the USA, the AMPS cellular service has been available to the public since 1983. This cellular system, which works in the 800 MHz band, uses analogue frequency modulation (FM) for voice transmission and digital frequency shift keying (FSK) for the signalling channel. To allow different users in the same cell to access the system the frequency channel is split up between different users. This technique is referred to as Frequency Division Multiple Access (FDMA) protocol. Originally operated in North America, the AMPS is also used in Canada, Central and South America and Australia.

In Europe, similar AMPS systems have been deployed as first generation systems. This includes the British Total Access Communication System (TACS) for the U.K, Italy, Spain, Austria and Ireland. The TACS uses the 800 - 900 MHz band. The Scandinavian Nordic Mobile Telephone models NMT 450 and the NMT 900 work on the frequency bands 450 and 900 MHz respectively. The German C 450 working in the 450 MHz band is also used in Portugal. The French system Radiocom 2000 works on several frequency bands from 190 MHz up to about 430 MHz. A detailed technical description of the different analog cellular systems is summarised in [1]. Although the TACS is available in Italy, another analogue system called Radio Telephone Mobile System is employed in that country.

In 1979, the Japanese Nippon Telephone and Telegraph (NTT) was operational in the Tokyo metropolitan area. In 1987, new operators were introduced on the Japanese cellular radio market and NTT evolved to JTACS/NTACS (Japanese TACS/ Nippon TACS).

The transition from the first analogue to the second digital generation was rendered possible by the evolution of low data rate digital speech coding techniques and the constant increase in the device density of integrated circuits. Furthermore digital modulation provides an advantage to the second generation mobile systems since it operates with a smaller signal to noise ratio than that provided by analogue modulation. Consequently for an identical service quality smaller re-use distances are needed, which provides higher spectrum efficiency [5] [6].

For cost efficiency the sharing of the radio hardware at the base station among multiple users is possible with digital technology. Two multiple access techniques are in use contrary to the FDMA of the first generation . They are TDMA (Time Division Multiple Access) and CDMA (Code Division Multiple Access) protocols. In short, when using TDMA, a specific frequency is used in a cell by only a single mobile for a specific time slot combination, whereas CDMA using direct sequence spreading allows multiple mobiles to use the same frequency in a given cell since the signals are distinguished by spreading them with different codes.

Integration with the existing wireline network was taken into consideration when the second generation of mobile personal system was defined. Moreover efforts on flexibility for mixed voice and data transmission communication were applied to digital systems. Additionally digital systems feature new services and support higher capacities than with the analogue one. The possibility of reducing the RF transmit power permits an increased lifetime of the batteries. Last but not least, digital encryption of the signal transmitted allows total privacy with the second generation of personal communication systems.

The Pan-European GSM system ("Groupe Spécial Mobile" later renamed "Global System for Mobile Communication") was an initiative from the CEPT (Conférence Européenne des Postes et Télécommuncations) in 1982. GSM was operating in 1993 and experienced a tremendous growth. It is designed to operate in the 900 MHz band and

is based on TDMA. Under the influence of the UK Department of Trade and Industry (UK-DTI) the DCS 1800 (Digital Cellular System 1800) was developed. It is a version of GSM operating in the 1800 MHz band.

1.2.1.2 Cordless telephone system

Analogue cordless telephones are merely a wireless extension of residential telephones which provide a certain mobility to the user. Contrary to analogue cellular systems, the terminals transmitted low RF power thereby reducing the coverage area to about 100 metres [7].

In Europe, the analogue cordless telephones arose illegally with the imports from the Far East (Japan) and the United States. Soon this caused interference with "legal" systems sharing the same frequency band [8]. In response to this issue, the CEPT/CT1 (Cordless telephone 1) emerged as a European standard operating in the 914-915/959-960 MHz band. CT1 is usually incompatible with equipment from different manufacturers [1] since it is an interoperability standard rather than a coexisting standard.

The second generation cordless telecommunication system CT2 was launched in the UK. Its allocation was centred on the 800 MHz band and uses FDMA technology. It is designed to be used for wireless Private Branch Exchange (PBX) and key systems, cordless residential telephones and for public cordless access services [7]. In 1992, it was adopted by the European Telecommunication Standard Institute (ETSI) as an interim European standard for cordless telecommunications. Promoted as a telepoint standard which is merely a wireless pay phone services, CT2 could not support incoming calls. With such a poor service, CT2 never broke through into the British market [1]. The Digital European Cordless Telecommunication (DECT) standard was brought out by the ETSI and this standard is assigned to the 1900 MHz frequency band and handles TDMA/TDD (Time Division Duplex). It is designed to serve a wide range of applications such as residential systems, small and large business systems, public cordless access systems and wireless data access systems [7]. It is a flexible standard interface which provides cost effective communication services to high user densities in picocells. Contrary to the conventional cordless telephone DECT is close to cellular system principles.

1.2.2 The future of the mobile radio systems : Third generation

Facing the success of the second generation and due to the additional demand of users for advanced mobile services with broadband capacities and the seamless integration between fixed and mobile communication networks, the third generation of mobile radio communication system are already under investigation [9]. In 1992, the World Administrative Radio Conference WARC92 in Spain resulted in a global re-allocation of the frequency spectrum for mobile radio systems and the frequency band 1.7 to 2.7 GHz band was assigned to the third generation of the radio telecommunication system. The International Telecommunication Union - Radio communication Sector (ITU-R) and telecommunication sector (ITU-T) are developing the Future Public Land Mobile Telecommunication System (FPLMTS) also renamed for convenience International Mobile Telecommunication by the year 2000 (IMT2000). In Europe, a similar system called Universal Mobile Telecommunication System (UMTS) is initiated by the ETSI. The Mobile Broadband System (MBS) is also a European project operating in the 40 GHz and 60 GHz band for wireless digital transmission. These digital systems will be challenged to include cellular, cordless, satellite and fixed wireless system features. The future systems are characterised by their high flexibility and spectral efficiency. In addition to speech transmission they are required to provide data communication at rates up to 2 Mb/s. This should provide advanced video facilities and data services to meet the multimedia challenge. These systems will support integration of satellite links to provide world wide roaming and global coverage. They are expected to operate in a multitude of environments and to follow a hierarchical cell structure [8].

In Europe, there are three active research programs which promote the work towards a third generation standard. These include the Cooperation in the Field of Scientific and Technical Research (COST), the Research and Development in Advanced Communication Technologies in Europe (RACE), and it successor the Advanced Communication Technologies and Services (ACTS). Project lines were coordinated thereby minimising overlapping or redundancy between different programs.

COST is an open and flexible framework for research and development in Europe.

The COST actions 227 and 231 focused on the development of multiple access schemes for third generation cellular mobile radio systems [8]. The COST action 227 was entitled "Integrated Space/Terrestrial Mobile Networks" and the COST action 231 was referred to as "Evolution of Land Mobile Radio Communications". The joint European program RACE comprises two phases, RACE I and RACE II. RACE meant to be precompetitive, prenormative and it aims to define Integrated Broadband Communication (IBC) taking into account the evolution of the Integrated Services Digital Network (ISDN) [8]. The ACTS started in September 1995 and it aims to pursue further the research conducted under RACE projects. A project of RACE II called MBS is considering futuristic systems. Using millimetre wave band at 40 GHz or 60 GHz, MBS will allow a transmission rates up to 155 Mb/s [10] [11]. The CEPT recommendation T/R 52-01 also allocated the band 40.5 to 42.5 GHz to the Multipoint Video Distribution Systems (MVDS).

The microwave and the millimetre bands are advantageous when considering the amount of bandwidth that such frequencies can provide. Additionally at millimetre wave frequencies diffraction effects can be neglected [12] and loss attenuation through walls [13] is high and consequently the power radiated is confined to the room where the transmitter is located. This will reduce interference among transmitters, allow frequency re-use in adjacent rooms and increase the frequency spectrum efficiency. Consequently this band is very attractive for indoor Line-Of-Sight (LOS) applications [14] [15] [16] [17] [18]. However, when a severe obstruction appears between the two terminals, the millimetre band is no longer useful. The use of the microwave band becomes attractive since reliable systems can be implemented in an Obstructed Line-Of-Sight (OBS) scenarios [11] [19] as for the European High Performance Radio Local Area Network (HIPERLAN) which operating frequencies were allocated in the microwave band as discussed in the next section.

1.2.3 Wireless data network

Progress in digital communication, portable computers, multimedia and semiconductor technologies have resulted in the rapid expansion of Wireless Local Area Network (WLAN). WLANs were responding to the demand of users with high mobility and with a reasonable bandwidth requirement. Furthermore, environments where cable installation is expensive,

impracticable or impossible are suitable for using WLANs [20]. The growth of WLANs requires standardisation to allow interoperability between systems when expansion is needed. Two significant emerging physical and data link layer standards are called IEEE 802.11 and the European HIPERLAN.

The HIPERLAN has been developed so that it is indistinguishable in performance from Wired LAN. The philosophy behind this wireless LAN adopted by the ETSI was different than from the American standard IEEE 802.11 since it established first the standard and then developed the product [21]. Two frequency bands centred at 5 and 17 GHz have been assigned for the HIPERLAN [20] [21]. This European WLAN allows a useful rate up to 23.5 Mb/s for point to point data link. With a lower power requirements, the HIPERLAN provides a short range coverage of 10 to 100 m.

Wireless Broadband Systems (WBS) are also being discussed in order to alleviate the pressure on non wired operating with data rates higher than 2 Mb/s. As explained previously the European MBS could provide 155 Mb/s. However the features of the HIPERLAN and the MBS differ not only in their data rates but also in the mobility and in the range of operation offered.

1.3 The propagation channel

Implementation of a successful wireless personal communication system is strongly dependant on the knowledge of the environment, the mobility of the user and on the type of application considered. Propagation phenomenon suffers from interference due to specular reflection on large flat surfaces, diffuse scattering from surfaces exhibiting small irregularities or from small objects with respect to the wavelength (in the sense of Rayleigh criterion [22]), transmission or refraction through dense structure, or shadowing by obstacles found in the path of the waves.

This type of obstacles, and/or surfaces vary significantly depending on the radio environment. In an outdoor environment, obstacles and/or surfaces may be buildings, street corners, trees, mountains and traffic in motion while in an indoor situation surfaces include partition walls, doors, ceiling, floor and people in motion. The signal reaches the receiver

after having usually travelled by several different paths. Therefore the received signal consists of different components, each of which with a different time delay and phase. These components combine vectorially. Depending on their phase distribution they add constructively or destructively. This phenomenon is known as multipath fading. As a result of this mechanism, deep fades in the received signal envelope are experienced and pulse spreading, in the case of digital communication, can lead to intersymbol interference. Therefore estimation of the cell coverage and time dispersion are vital parameters in the design and planning of new radio links and services.

Although multipath fading occurs in both the indoor and outdoor channels, its characteristics are different. The multipath condition in an indoor environment is more severe than in an outdoor scenario. In general the outdoor radio channel may suffer from atmospherical effects like snow, hail, rain, clouds and temperature variation. Certain regions of the frequency spectrum behave specifically to water or oxygen. The 60 and 120 GHz spectral zone suffers drastically from oxygen attenuation while the water vapour absorption is excessive for the 23 and 180 GHz one [23].

The outdoor channel scenario may be interpreted by the summation of a direct ray and a ground reflected ray at the receiving terminals [24] in the case of the rural environment. For the suburban microcell "canyon" street, the direct ray is added to the ground reflected ray and the rays reflected from building surfaces located on both sides. The indoor scenario is much more complex since reflections occur from all surfaces of the enclosed environment. It will be analysed in details in Chapter 2.

1.4 Objectives of the research

The characterisation of the indoor radio channel has been the subject of studies by a number of researchers [14] [25] [26] [27] [28] [29] [30] in order to provide information for the development and planning of future mobile radio systems.

Multipath propagation causes time dispersion and frequency selective fading. One of the most important parameters that provide a measure of the varying frequency response of the channel is the coherence bandwidth. The coherence bandwidth determines the

maximum frequency separation needed to decorrelate two signals.

This project presents experiments and analysis made to measure and characterise the coherence bandwidth of several indoor channels at 11 and 62.4 GHz. Measurements were made in rooms and corridors by transmitting two sideband signals separated in frequency and recording their signal strength simultaneously. Frequency separations in the range between 5 and 240 MHz were used. A model using a ray tracing algorithm has been developed and used to estimate the coherence bandwidth. The model takes into account the transmit and receive antennas radiation patterns and considers specular reflections up to the third order. The behaviour of the correlation coefficient between the signal envelopes and the coherence bandwidth with respect to the mobile position is demonstrated and explained. The cumulative distribution functions of the correlation coefficient and the frequency correlation functions of the channel are also reported. The measured and predicted frequency correlation functions, together with values of the coherence bandwidth at several correlation levels, are presented for different percentages of time. Predictions obtained from the model are compared to the measured results and used to interpret them. The limitations of the model are also examined and outlined. The influence of the antennas radiation patterns used in estimating the coherence bandwidth of an indoor channel is studied. A comparison between results obtained at 11 and 62.4 GHz is also presented.

Chapter 2

Indoor radio channel

2.1 Introduction

The expansion of mobile personal communication and Wireless LAN over wired networks when used in residential houses, offices and factories initiates the demand for studying the indoor radio channel characteristics. The development of the second generation engenders lots of research and report in the frequency band 800 to 1800 MHz [31] [32] [33]. In response to the next generation of communication system, research work has also been undertaken for microwave and millimetre wave indoor radiowave propagation [34] [35] [25] [12] [36]. Narrowband and wideband measurements have been reported in the literature to characterise the propagation channel [11] [37] [27] [38] [31]. Narrowband is used to define received signals [39] [40] which do not exhibit frequency selectivity. This means that all the frequency components of the transmitted signal experience the same behaviour in the propagation channel. In this case, the frequency fading is commonly qualified as "flat". Narrowband measurements provide information about the path loss [41] and the time fading properties of the radio channel [25]. On the other hand wideband indoor channel measurements give power delay profile and RMS delay spread results.

In indoor environments, like rooms and corridors, the influence of people on the propagation characteristics has been reported [42] [43] [44] [45] [46] [18] [47]. It has been shown [44] that the effects of people on path loss when compared with results for an empty room, is small and no influence on the RMS delay spread was noted. These results relate to

experiments undertaken at 2.4, 4.75,and 11.5 GHz. In the 800-900 MHz band [45], [43] the effects of short time variations in the delay spread and the received multipath power caused by human traffic around a transmitter and receiver were outlined. [45] quantified those variations by an average propagation loss, due to the people present in a hallway, of 4 dB. [43] suggested that a negative correlation between the RMS delay spread and the fluctuation of the received envelope exists ; i.e. the fluctuation of the RMS delay spread and the multipath power received shows that when the received power signal is small, the RMS delay spread is large and vice-versa. Theoretically [46] demonstrated that the presence of people, when using portable handset at about 800 MHz, modifies the antennas radiation pattern and increases time dispersion of the signal. It was concluded that not only the narrowband radio channel characteristics but also the wideband ones are also affected. Canadian researchers [48] presented the effects of fluorescent light on signal fading characteristics for indoor radio channels. To ensure no frequency dependence in the measurement, frequencies ranging from 0.5 to 10 GHz were used. [48] suggested that plasma inside fluorescent light, reflects the signal at twice the frequency of the main power network.

Propagation characteristics of a channel are strongly dependent on the position of the terminals, the geometry and structure of the environment. This includes the interior construction, furniture and the electrical properties of the material. [31] summarised the work already undertaken indoors and provided a building classification. [32] also gave a description of different environments defining cells with soft or hard partitions. Hard partitions are defined as an obstruction within a building which can not be easily moved and soft partitions are described as movable obstructions. Soft partitions such as furniture panels are of interest since they are lower than the ceiling and consequently when they obstruct the line of sight, the use of artificial ceiling reflectors may be used [26].

2.2 Propagation characteristics

The indoor propagation characteristics exhibit a multipath mechanism [49] [50] [12] [51] [34]. The amplitude fluctuations of the measured received signal are commonly called

fades. Two types of fading are superimposed : "slow" and "fast" fading. The term "fast" refers to short term variations whereas "slow" describes the much longer term variations [39]. Indoors,when a mobile receiver moves away from a transmitter located at one end of a long narrow corridor, the slow fading is caused by the side wall reflections whereas the fast one is due to reflection from the end wall opposite to the transmitter. It will be shown later that the distribution of the received signal envelope may vary with distance and microcell geometry and structure. When the receiver is in motion, the received signal experiences an apparent shift in its frequency defined as the Doppler effect [47] [39]. This frequency shift f_n is related to the cosine of the angle α_n between the direction of arrival of the rays and the direction of motion of the vehicle and is determined by

$$f_n = \frac{v}{\lambda} \cos \alpha_n \tag{2.1}$$

where v is the speed of the mobile terminal, λ is the wavelength. Therefore, a negative and positive Doppler shift is experienced when the components are arriving from behind or ahead of the mobile respectively.

The concept of multipath and frequency shift are related to each other. With mobile radio propagation, the received signal experiences two effects simultaneously. In addition to frequency selective fading which results from the multipath mechanism, a time fading occurs due to the mobility of the terminals or people in motion. This time fading results in a spread of the frequency previously defined as Doppler spread. This concept of duality between frequency and time domain is presented and detailed in [52] [53] [54] [39] and is illustrated bellow :

$$\overbrace{\text{time spread}}^{\textit{time domain}} \quad \underset{\Uparrow}{\overset{\textit{duality}}{=}} \quad \overbrace{\text{frequency fading}}^{\textit{frequency domain}}$$

due to multipath phenomena

$$\overbrace{\text{time fading}}^{\textit{time domain}} \quad \underset{\Uparrow}{\overset{\textit{duality}}{=}} \quad \overbrace{\text{frequency spread}}^{\textit{frequency domain}}$$

due to the mobility of T_x and R_x or

the change of the environment

Mathematical and experimental modelling of the conventional mobile radio systems is well documented in the literature [55] [56] [39]. Conventional radio propagation theory [57] [58] [59] [54] [60] [61] [49] [27] [62] indicates that the received signal is composed of several plane waves of random phases with spatial angles of arrival. The phase angles are assumed to be statistically independent and uniformly distributed between 0 and 2π. Generally the slow variation of the received envelope results from the gross changes along the propagation path and in the local environment and follows a log-normal distribution whereas fast variations are Rayleigh distributed due to the large number of components of the received signal.

However, in the case of indoor line of sight propagation such as a corridor scenario, conventional mobile radio propagation theory is not applicable anymore. Amplitude variations are found to follow Rayleigh and Rician distributions. With one of the terminal located at one end of a long narrow corridor, [25] and [51] showed that fast fading is due to the reflections coming from the endwall opposite the stationary terminal which experience fast rate of change in their differential path length relative to the line of sight. On the other hand, slow variations were found to result from interference between the LOS and reflections from the side walls. The power spectrum of the received envelope, as will be demonstrated later, exhibits two distinct frequency regions which suggests that the distribution of the phase angles is not uniformly distributed between 0 to 2π.

2.2.1 Path loss

Local average or local mean received power is an important factor when link budget calculations are required. It is used to estimate the cell coverage and the Signal to Noise Ratio (SNR) or the Carrier to Interference ratio (C/I) [32] [63]. The local mean is calculated by averaging the received signal power. The path loss can be estimated using the Friis formula as expressed in equation 2.2 adapted in dB. The path loss $L(r)$ is expressed as:

$$P_r = P_t + G_{Rx} + G_{Tx} - L(r) \tag{2.2}$$

Where P_r is the received power in dBm, P_t is the transmitter power in dBm and G_{Rx}

and G_{Tx} are the antenna gains in dBi for the receiver and the transmitter respectively. The path loss is also defined such as [26] :

$$L(r) = L(r_o) + 10.\log_{10}(r)^n - 10.\log_{10}(r_o)^n \tag{2.3}$$

Where n is the path loss exponent, r_o is the reference distance usually chosen to be 1 m and L(r_o) is the normalised received path loss at a separation distance of r_o. In free space n=2.

The propagation mechanism at 800 to 1800 MHz band has been thoroughly investigated [31] to asses the capacities of the second generation indoor cellular or cordless telephone system. Recently a lot of research has been carried out at various higher frequencies like the microwave bands (2.4, 4.75, 11.5, 19, 21.6 GHz) and the millimetre wave bands (29, 37, 60, 94 GHz) [44] [64] [35] [65] [34] [66] [67] [28] [25] [36] [26] [68].

For the frequency range of 800 MHz to 1800 MHz, it is common practice to estimate the value of n in the range between 1.8 to 2.5 [31] [41] for LOS scenarios. Whereas an obstructed line of sight scenario results in the value of n being larger and ranging between 3 and 4 [49]. At 94 GHz [26] measurements undertaken in a hall, room and corridor have shown a path loss exponents of 1.2 to 1.8 under line of sight conditions and 3.6 to 4.1 when the line-of-sight is obstructed. Narrowband measurements [69] undertaken at 60 GHz in several indoor environments using omnidirectional antennas and circular polarization were also reported. Various path loss exponents were measured in different environments. For instance a corridor 18 m long, 1.8 m wide and 2.7 m high with metal lockers on one sidewall provides an exponent of 1.32 while a wider corridor (3m wide) with glass panelling on both side indicates a 1.20 exponent. Such low propagation laws suggest that in a corridor with smooth parallel walls, floor and ceiling, strong specular reflections exist and channel the transmitted power to the other terminal. Comparatively, a laboratory with large dimensions (24 m × 5.5 m × 3.75 m) exhibits similar channelling effects but with an exponent of 1.71. This was explained by the presence of furniture within the room which prevented strong specular reflections. On the other hand, an office with plaster covered concrete walls and a carpeted floor which was 15.5 × 3.5 × 5 m gave

a much higher path loss exponent of 2.17. This was also explained by the presence of furniture and the carpet which attenuates the amount of specular reflection. The lack of strong specular reflection results in the received envelope to suffer less sever fading than for the corridors and the laboratory. [18] also concluded that a high mean signal level was maintained as a result of the reflections from the walls for closed environment. A path loss exponent of 1.03 was reported for a corridor with metal partitions. An exponent of 1.3 was measured for a room with two metal walls, one plasterboard wall and one wall partially double glazed. It was also shown that radiated power leakage may occur through doors and windows. However this was found to be not enough to provide adequate room to room coupling excepts where a line of sight path exists. This is in agreement with works reported in [37] where it was confirmed that, as far as coverage was concerned at 60 GHz, the low attenuation of plasterboard allows substantial penetration through walls. Nevertheless other types of material cause higher losses. Therefore, the evaluation and estimation of the electrical properties of building material is important. Initial work at 60 GHz to determine the dielectric parameters of various materials have been reported in [70] [71] [72].

At 60 GHz, it has been demonstrated that diffraction is insignificant compared to reflected and penetrated rays. [12] reported theoretical and experimental results in a bent corridor and concluded that in the shadow region single and double reflections are predominant while at large distances from the corner, the contribution of reflections to the received power becomes weaker and the penetrating rays are the strongest. [18] compared results of diffraction measurement at 900 MHz and 60 GHz. It was concluded that at 60 GHz the propagation mechanism is ray like and depends on reflection rather than diffraction effects to give reasonable coverage of the indoor area.

2.2.2 Statistics of the mobile radio channel

The radio propagation mechanism is of complex form and statistical tools may be used to describe it. The probability density function (PDF) and the cumulative distribution function (CDF) are the two main statistical functions used in communication theory. In a line-of-sight indoor microcell the distribution of the received signal envelope varies with

distance. When the two terminals are close to each other the envelope of the received signal is Rician while it becomes Rayleigh when they are separated by larger distance [69]. It will be shown later in this thesis the evolution of the statistic of the received envelope as a function of distance between terminals by fitting the measured signal envelope to a parameter of the Rice distribution.

2.2.2.1 Rayleigh distribution

The Rayleigh distribution is applicable in the case where several vectors (more than three) with random phases uniformly distributed between 0 and 2π and with comparable amplitude are combined together [73] [25]. The PDF of the Rayleigh distribution is defined in [55] as :

$$p(r) = \begin{cases} \frac{r}{b} exp(-\frac{r^2}{2b}) & , r \geqslant 0 \\ 0 & , r < 0 \end{cases} \tag{2.4}$$

where b is the mean received power of the electric field. The CDF can be written as

$$P[r \leq R] = 1 - \exp(-\frac{R^2}{2b}) \tag{2.5}$$

2.2.2.2 Rician distribution

When stochastic variable components with a Rayleigh distribution are added to a steady (non fading) component, the signal envelope is said to be Rician distributed. The PDF of the Rician distribution is expressed as [54]:

$$p(r) = \frac{r}{b} exp[-\frac{(A^2 + r^2)}{2b}] I_o(\frac{rA}{b}) \tag{2.6}$$

where I_o is the modified Bessel function of the first kind and zeroth order and A is the LOS peak value and b is the mean received power. The Rician distribution is often described in terms of a parameters K which is given by :

$$K = \frac{A^2}{2b} \tag{2.7}$$

when $A \rightarrow 0$ then $K \rightarrow 0$ and the dominant path (i.e. the line-of-sight) becomes insignificant and the Rician distribution becomes Rayleigh as shown in Figure 2-1. This figure also shows the Rice distribution for various values of k.

2.2.3 Power delay profile

Wideband characteristics depend on the relationship between the bandwidth of the transmitted signal and the frequency response of the radio channel which was modelled as a linear time variant channel [52] [74] [39] [5].

A multipath radio propagation channel may be interpreted as a time variant impulse response $h(t,\tau)$. It is analogous to a filter which is time varying due to the motion of terminals or the traffic surrounding the stations. Then when applying a complex input signal $x(t)$ to the channel, the output signal equivalent to the received signal $y(t)$ is given by the convolution product expressed in equation.2.8

$$y(t) = x(t) * h(t) = \int_{-\infty}^{\infty} x(\tau)h(t-\tau)d\tau \tag{2.8}$$

$h(t,\tau)$ is one of the four system functions defined in [52]. As explained previously a symmetrical correspondence between the filter system functions in the time and frequency domain is established by Fourier transformations. $h(t,\tau)$ is a stochastic process and the correlation functions related to this system function is written as

$$R_h(t,t';\tau,\tau') = E\{h(t,\tau).h^*(t',\tau')\} \tag{2.9}$$

Equation 2.9 can be simplified under the Wide Sense Stationary Uncorrelated Scattering (WSSUS) assumption [75]. A WSS process means that the mean is constant and the correlation only depends on the difference between the time variable

$$R(t,t') = R(t-t') = R(\Delta t) \tag{2.10}$$

i.e. the fading in a propagation channel is assumed stationary over a short period of time (or small distances). The term Wide-sense is used rather than strict sense since a

Strict Sense Stationary process means that not only the mean is constant, but also all the statistical properties of the process are invariant when a time shift is applied [76]. A process that is WSS over a small distances is called Quasi-WSS (QWSS). The Uncorrelated Scattering (US) assumption is related to the time delay τ and τ' since the different path delay are uncorrelated, therefore the autocorrelation function R_h becomes singular in the time delay variable. The WSS and The US assumption leads to :

$$R_h(t, t + \Delta t; \tau, \tau') = \delta(\tau' - \tau) P_h(\Delta t, \tau) \tag{2.11}$$

which means that the correlation function R_h is merely described by the Cross-Power Spectral density $P_h(\Delta t, \tau)$. $\delta(.)$ is the impulse Dirac delta function.

$$P_h(\Delta t, \tau) = E\{h(t, \tau) h^*(t + \Delta t, \tau)\} \tag{2.12}$$

For $\Delta t = 0$ which means that the time separation of the observation is zero, the Cross-Power Spectral density becomes the Power Delay Profile $P_h(\tau)$.

$$P_h(\tau) = E\{h(t, \tau) h^*(t + \Delta t, \tau)\} = E\left\{|h(t, \tau)|^2\right\} \tag{2.13}$$

The equation 2.13 indicates that the power delay profile is directly connected to the response average in time for a WSSUS process.

In such multipath environment, the signals arrive with various powers and time delays. The indoor channel response is given in [49] or [5] and expressed as

$$h(t) = \sum_k \alpha_k e^{j\theta_k} \delta(t - \tau_k) \tag{2.14}$$

where α_k is the gain, τ_k is the propagation delays, θ_k is the associated phase shifts and k is the path index. Consequently the Power Delay Profile (PDP) is used to established the time distribution of the received signal power from a transmitted impulse Dirac [44]. The PDP is defined as

$$P_h(t) = \sum_{k=0}^{N} \alpha_k^2 \delta(t - \tau_k) \tag{2.15}$$

2.2.4 RMS delay spread

A measure of the spread of the channel power delay profile is useful since the inter-symbol interference in a digital signal is related to this parameter. The first moment of the PDP is the mean excess delay expressed as :

$$\bar{\tau} = \frac{\sum_k \alpha_k^2 \tau_k}{\sum_k \alpha_k^2} - \tau_0 \tag{2.16}$$

where α_k is the attenuation,τ_k is the time of arrival of each k^{th} ray. τ_0 is the line of sight power component.

Whereas the second moment of the PDP defines the Root Mean Square (RMS) delay spread. It is given as :

$$\sigma\tau = \sqrt{\frac{\sum_k (\tau_k - \bar{\tau})^2 \alpha_k}{\sum_k \alpha_k}} \tag{2.17}$$

It is to be noted that the RMS delay spread only gives an information for wideband channels. The information is limited as indicator of average system performance because for the same RMS delay spread value, the overall power delay profile may be different [77] [23].

For indoor environments values of the RMS delay spread have been reported in the literature. Values ranging from 20 ns to 75 ns at 60 GHz for different indoor environments [63] mainly in rooms with dimension ranging from 80 m^2 to 1800 m^2 and heights varying from 3 to 7 m have been reported. It has also been shown that delay spread exhibited a dependence on the dimensions of the environment and the reflectivity of the walls.

2.2.5 Coherence bandwidth

The coherence bandwidth is a measure of the minimum frequency difference such that the signals are correlated to each other [55] [78].

For conventional mobile radio systems, Jakes [55] defined the coherence bandwidth as being inversely proportional to the RMS delay spread. It is derived from the envelope

correlation coefficient expressed in equation 2.18

$$\rho(\Delta f,\tau) = \frac{\langle r_1 r_2\rangle - \langle r_1\rangle \langle r_2\rangle}{\sqrt{\left[\langle r_1^2\rangle - \langle r_1\rangle^2\right]\left[\langle r_2^2\rangle - \langle r_2\rangle^2\right]}} \tag{2.18}$$

where r_1 and r_2 are the amplitude envelopes of the signals for two frequencies. Δf is the frequency separation and τ is the time delay between the two envelopes. $\rho(\Delta f,\tau)$ is simplified to give

$$\rho(\Delta f,\tau) = \frac{J_0^2(\omega_m \tau)}{1+(2\pi\Delta f)^2\sigma^2} \tag{2.19}$$

where J_0 is the Bessel's equation of the first order and σ is the time delay spread. $\omega_m = 2\pi f_m$ where f_m is the maximum Doppler shift. In the assumption that the signals are recorded simultaneously, $\tau = 0$, then $J_0(0) = 1$, therefore the equation 2.19 becomes

$$\rho(\Delta f) = \frac{1}{1+(2\pi\Delta f)^2\sigma^2} \tag{2.20}$$

Therefore, for a desired level of correlation $\rho(\Delta f)$, the coherence bandwidth B_c is deduced from

$$B_c = [\Delta f]_{\rho(\Delta f)} = \frac{1}{2\pi\sigma}\sqrt{\frac{1-\rho(\Delta f)}{\rho(\Delta f)}} \tag{2.21}$$

However, recently Fleury in [79] proved a theoretical relationship based on the uncertainty of Eiselberg to describe the dependence that may exist between the coherence bandwidth and the RMS delay spread. In the case of an indoor environment, it was shown that the product of the coherence bandwidth and the delay spread exhibits a lower boundary. This indicates that the equality established by Jake for conventional mobile radio system is not applicable to the case of indoor line-of-sight channels.

Following the duality that exist between time and frequency parameters described by Bello it is possible the coherence bandwidth may be calculated from the power delay profile $P_h(t)$. As explained in [75], the inverse Fourier Transform of the power delay profile (referred as delay power density spectrum in [75]) gives the frequency correlation function $R\tau(\Delta f)$. The frequency correlation function may then be used to determine the frequency

separation required to achieve a certain level of correlation.

The use of the Fourier concept between different system functions has been reported in [80] [75] [78] [44] for an indoor channel while [77] [81] [82] use this technique for outdoor channel.

[9] reported direct measurements of the coherence bandwidth in a heavily built-up urban area. Two sidebands separated in frequency were transmitted and recorded simultaneously. The measurements were undertaken for three locations in the urban microcell over a short distance of about 4.9 m. This is equivalent to a sample time of 3.3 seconds at a speed of about 10 to 12 mph. Each run was repeated using different frequency separations. The correlation coefficient (equation 2.18) between the two envelopes was then computed over the whole recorded time. Thereafter, the frequency correlation function was produced using the results obtained from the three different locations. However work reported in this thesis will demonstrates that this method is inaccurate in estimating the coherence bandwidth for a propagation channel using three locations only and over such a small distance. This is because, as will be shown, the correlation coefficient is found to be highly variable over the distance. [83] reported a technique which directly predicts the coherence bandwidth by using ray-tracing. The method consists of evaluating the coherence bandwidth for each location in the microcell. Results obtained using this method need to be carefully considered since, as will be demonstrated in this thesis, the frequency correlation function is not necessarily a monotonously decreasing one at each position in the microcell. Therefore, this technique may result in inaccurate estimate of the coherence bandwidth.

To the best knowledge of the author, no direct measurement of the coherence bandwidth in indoor microcells has been reported in the literature. Therefore this thesis presents direct measured and predicted results of the coherence bandwidth for several indoor environments at microwave and millimetre wave frequencies under line-of-sight condition. The characterisation of the coherence bandwidth is completed using two different techniques. The differences in the result using these two methods are presented and explained.

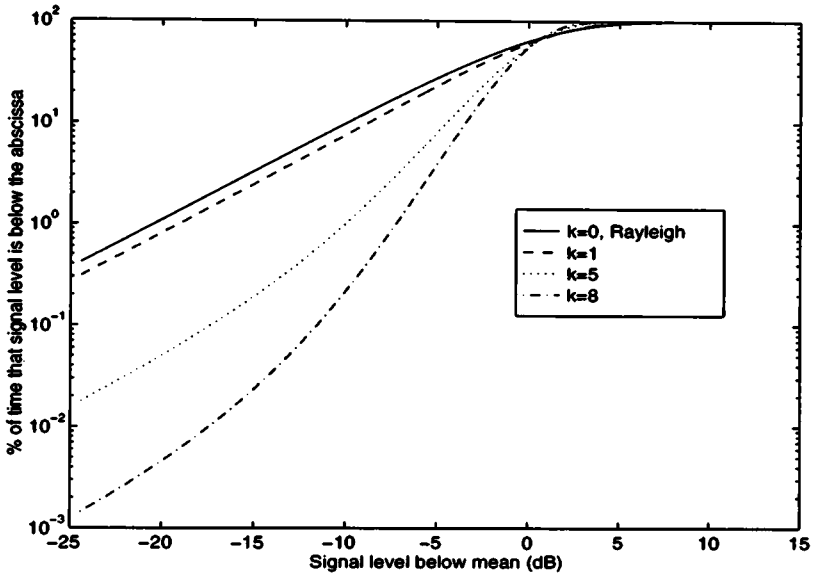

Figure 2-1: Cumulative distribution function of the Rayleigh and Rician fading for several values of k

Chapter 3

Ray tracing theory and modelling

3.1 Introduction

The indoor radio propagation channel characteristic is complex due to its multipath interference behaviour. To achieve reliable indoor links and optimizing systems for cost efficiency, it is not possible to conduct propagation measurement in every building to establish the propagation characteristic because it is time consuming and extremely expensive. Therefore a propagation model to predict the channel characteristics of the indoor environment is needed. Such a model provides a mathematical representation of the characteristics of the channel. After introducing the input parameters describing the environment being considered by the model and after a certain processing time (time being related to the complexity of the model, the algorithm, and the performance of the processor) relatively accurate results can be provided without exhaustive and expensive measurements campaigns.

An overview of the propagation models used to describe indoor radio propagation is given here. The development of a ray-tracing algorithm requires the basic knowledge of electromagnetic wave propagation. The principles of electromagnetic wave propagation and ray theory are discussed later in this chapter. A section is devoted to the model developed for the research presented in this thesis. Finally, the limitations are summarised and assumptions applied to the model are justified.

3.2 Overview of indoor propagation models

Radiowave propagation prediction could be obtained by solving Maxwell's Equation. However the computational demand would be unrealistic and therefore too heavy. Alternatively statistical and deterministic models have been used to model the propagation mechanism. The type of model to be used, when predicting coverage or network deployment, depends on the results sought.

Statistical models make use of measurements results and apply probability distribution functions and statistical moments to estimate the statistical properties of the channel. They contribute to a summary of comprehensive characteristics of numerous environments. In general accurate statistical indoor models rely on extensive measured data to determine the appropriate parameters describing a particular type of indoor environment. Indoor radiowave statistical models are well documented in the literature [84] [85] [50] [86] [87] [88] [89].

The second method is to use site specific propagation models also referred to as ray-tracing. This type of model is based on the use of electromagnetic theory and geometrical optics to characterise indoor radio propagation. This modelling technique is described in more details later in this chapter.

3.2.1 Ray-tracing models

Radiowave propagation models using ray tracing techniques have been under development for the last decade. Such models use optical geometry to predict the indoor propagation mechanism. Deterministic or site specific models do not depend on comprehensive measurement campaign in contrast with statistical models. Deterministic models are used to predict the characteristics of outdoor [90] and indoor channels. Such models require detailed description of the environment in terms of its geometrical description, dielectric constant of surfaces and exact position of the terminals

Deterministic models are established on the assumption that at high frequency, radio waves behave ray like [88] [25] [18] [91].Two types of ray-tracing methods are reported in the literature: the image method [86] [92] and the ray launching method [93]. Both

techniques [94] may be combined where the multiple-image and ray launching concepts were used to provide a three-dimensional model. This combination results in large improvements in terms of accuracy, computation efficiency, and memory requirements when compared to the ray launching method.

3.2.1.1 The ray launching method

The ray launching method is often presented in the literature as "brute force" ray-tracing technique and is largely documented in [95] [96] [97] [38] [98]. This technique takes into account a bundle of transmitted rays that may or may not reach the receiver [33]. The accuracy of the model is dependent on the spatial resolution which is determined by the number of rays employed and the terminals location. In short this method considers a comprehensive search of a ray tree taking into account the decomposition of the ray at each planar intersection. Such a model is suited when the details of the geometry is complex, however this method requires more computing power than the image one presented in the next section.

3.2.1.2 The image method

The image method considers the transmitter or the receiver to be mirrored by the reflecting surface. Two and three dimensional models have been reported in the literature [84] [99]. However the majority of the literature presents three dimensional models which are more suitable for indoor environments since reflections from the ceiling and the floor are not negligible when they are not excluded by the antennas radiation patterns.

The accuracy of such a model depends on several parameters like the order of reflection being considered, the assumption of specular or scattered reflection, the potential of diffraction effects and the electrical properties of the surfaces.

The image method is based on the geometrical optics. It considers rays which lay on a plane of incidence and are reflected from a surface.

- The plane of incidence is defined in [100] as *the plane formed by a unit vector normal to the reflecting interface and the vector in the direction of incidence.* The source

point S and the point of reflection O define the vector in the direction of incidence $\vec{SO}$ as illustrated in three-dimensional view in Figure 3-1. The source image I is defined by projecting the spatial coordinate of the source S with respect to the reflecting plane. Therefore the vector $\vec{IS}$ and the unit normal vector to the reflecting surface $\vec{n}$ are colinear. Consequently, the plane of incidence can be defined by the vectors $\vec{IS}$ and $\vec{SO}$. This is the same as considering the vectors $\vec{IS}$ and $\vec{IO}$. The reflected point O is defined as the intersection between the line defined by the receiver point R and the image source I, therefore $\vec{IO}$ and $\vec{IR}$ are colinear. This conclude that the plane of incidence may be defined by the two vectors $\vec{IS}$ and $\vec{IR}$ which is similar as taking into consideration the three points : the source S, the image I and the receiver R.

- The angle of reflection is calculated by the Snell's law of reflection [100]. In ray-tracing the angle between the surface and the incident ray is referred to as the grazing angle and denoted by ψ_i [101].

Figure 3-2 illustrates the two different ways that may be used to trace the ray path in the case of a first order model (i.e. single reflection only) in a two-dimensional sketch. Figure 3-2 (a) demonstrates the ray-tracing concept while using the image of the source. It can be seen that wherever the receiver moves it is possible to compute the path length of the ray (i.e. the distance travelled by the ray) by a simple computer code. The concept remains the same when the receiver image is used as shown in Figure 3-2 (b). When the image source is considered, the method employed is called the forward ray-tracing technique whereas when the receiver image is used it is referred to as the backward ray-tracing method.

The image theory is very useful for modelling indoor environments with low interior structure complexity such as an empty room or corridor. In order to design a complete indoor radio propagation model a knowledge of the principles of electromagnetic wave is introduced in the next section.

3.3 Principles of electromagnetic wave propagation and ray theory

Before introducing the 'ray' concept it is useful to state the difference between 'ray' and 'wave' theories. Huygen defined one of the fundamental principle of physical optics [102] and stated that : *each point on a primary wavefront can be considered to be a new source of a secondary spherical wave and that a secondary wavefront can be constructed as the envelope of these secondary spherical waves.* This principle defines a point to point spherical wave correspondence between two successive positions of a wavefront while geometrical optics theory uses a point to point ray correspondence. Briefly, physical optics involves wavefronts while geometrical optics deals with ray paths [102].

The radiowave propagation mechanism is complex and various. It consists of three basic modes: reflection, diffraction and scattering.

Specular reflection occurs when an electromagnetic wave bounces off an obstacle with large dimensions compared to the wavelength of the radio wave. Depending on the electric properties of the reflecting surface a certain amount of energy, determined by the reflection coefficient, is reflected while the rest is refracted or transmitted through it. Two reflection coefficients are considered; the perpendicular ($\rho_\perp$) and the parallel reflection ($\rho_\parallel$) coefficients . They are often referred to as the Fresnel's equations given by

$$\rho_\perp = \frac{E_r}{E_i} = \frac{\sin\psi_i - \sqrt{\frac{\varepsilon_2}{\varepsilon_1} - \cos^2\psi_i}}{\sin\psi_i + \sqrt{\frac{\varepsilon_2}{\varepsilon_1} - \cos^2\psi_i}} \tag{3.1}$$

$$\rho_\parallel = \frac{E_r}{E_i} = \frac{-\frac{\varepsilon_2}{\varepsilon_1}\sin\psi_i + \sqrt{\frac{\varepsilon_2}{\varepsilon_1} - \cos^2\psi_i}}{\frac{\varepsilon_2}{\varepsilon_1}\sin\psi_i + \sqrt{\frac{\varepsilon_2}{\varepsilon_1} - \cos^2\psi_i}} \tag{3.2}$$

where ε_2 and ε_1 are the permittivity of the two media. In the model developed here, the relative dielectric constant $\frac{\varepsilon_2}{\varepsilon_1}$ is assumed to be a real value. The choice of the reflection coefficient is dependent on the polarization of the electric field which can be vertical or horizontal and the plane of incidence.

Diffraction is experienced when the radio path between both the transmitter and re-

ceiver is obstructed by, for example, a surface with a sharp edge like a roof top. Huygen's principle suggests that the waves originating from all points, propagate into the shadow region. Diffraction is the means by which radio waves may be received in a non line-of-sight (NLOS) scenario such as in urban, rural, and hilly environments. The effect of diffraction becomes less significant when the wavelength becomes smaller [12] [102]. In the model described here therefore diffraction has not been accounted for.

Scattering takes place when the propagating wave impinges upon obstacles of dimensions comparable or smaller to the wavelength. Scattering causes the signal to be reradiated in many different directions. When scattering effects are taken into account in modelling the indoor channel, knowledge of the roughness of the reflecting surfaces is required. It becomes more complicated when working at micro or millimetre frequency bands.

3.4 Development of a three-dimensional ray-tracing tool

An overview of ray-tracing and the concept of image theory has been introduced. A three-dimensional model based on ray-tracing has been developed to assist in interpreting experimental results. The model is of a low complexity in terms of its geometrical description capabilities of indoor environments. The environment is assumed to be as an empty rectangular box where the walls, ceiling, and floor are assumed to be smooth and with the same dielectric constant. It therefore assumes specular reflections only. No diffraction effects have been considered in the model. Nevertheless, the characterisation of the indoor environment, even for a simple empty box, requires a complex ray-tracing algorithm capable of integrating all the reflected rays. For reasons of speed efficiency it was decided to write the codes of the program in C language using Watcom C/C++ ™ compiler. The whole computation was supported by Windows 95 ™ operating system.

The model uses the forward ray-tracing technique. The remainder of this chapter progressively explains the evolution of the model from a single order reflection model to a more complex one considering reflections up to the N^{th} order. Finally the limitations of the model are discussed.

3.4.1 From single to N order two-dimensional reflection model

The case of a first order reflection was previously discussed and illustrated in Figure 3-2 when a single reflection from a wall (wall 1) is considered. When assuming a second wall (wall 2) parallel to the first, as shown in Figure 3-3 a second single reflection occurs. The path length of this second ray can be obtained by considering the single image source 2 which represents the image of the source with respect to wall 2. One can model the indoor environment considering two general cases in terms of the geometrical position of the walls. The first case considers two parallel walls while the other case introduces two adjacent walls being perpendicular to each other.

3.4.1.1 Parallel walls scenario

To develop a second order reflection model, the image source 1 (I_{s1}) is considered acting as a primary source. Therefore when projecting I_{s1} with respect to wall 2 a new image called double image source 1 (I_{d1}) appears as represented in Figure 3-4. A line between I_{d1} and the receiver is drawn. The intersection between this line and wall 2 generates a first point of reflection referred to as A. A second line which connects I_{s1} to A is drawn and a second reflection point B occurs on wall1. Finally, a line, linking B to the source, completes the ray path. It is to be noted that estimating the length of the path is equivalent to calculate the distance from I_{d1} to the receiver.

Following this concept, I_{d1} may be interpreted as a primary source with respect to wall 1 and therefore engender another image called triple image source 1 (I_{t1}). This leads to a third order reflection as illustrated in Figure 3-5. When a higher order reflection is needed then the image of the prior order reflection becomes the primary source. This multi-reflection phenomenon is clearly illustrated when two mirrors are facing each other. It is possible to see an object reflecting itself to infinity.

3.4.1.2 Perpendicular walls scenario

In Figure 3-6, two adjacent walls perpendicular to each other are considered. This case illustrates that, depending on the position of the receiver, the ray-tracing model does not

take into account the same secondary image I_s. Therefore the ray-tracing algorithm develops a routine which generates the correct ray path depending on any three-dimensional position of the receiver. The corner of the Figure 3-6 can be divided into two zones : Zone 1, Zone 2 which are defined by the boundary line (OI_d). In the case of position 1 where the receiver R_1 belongs to Zone 1 as illustrated in Figure 3-6 (a), the first point of intersection A with the line (R_1I_d) and the reflecting surface is on wall 2. Therefore wall 2 becomes the reference surface used by the algorithm for the projection of I_d. When the point I_d is fold back according to the line of reference, a new intersection (point B) occurs with wall 1 and the line A, B, I_{s1} can be drawn. In position 2 (Figure 3-6 (b)), the receiver is moved down from Zone 1 to Zone 2. Therefore wall 1 becomes the new wall of reference to project I_d. Then a new point B occurs on wall 2 and a new raypath R_2, A, B, S is drawn. This is of primary importance since the computation of the grazing angle and consequently the reflection coefficient depends on the choice of the images.

3.4.2 A three dimensional indoor model

For a three-dimensional coordinate, the image rooms can be visualized as boxes placed adjacent to the 6 surfaces of the central primary source room. This defines the first order reflection images with 6 image boxes. For the second order reflections, the double images are within a new layer of boxes placed on the adjacent surfaces of the first layer. There are 18 box images for the second order reflections and 38 triple box images. Generally [86] demonstrated that the number of images added by each order of reflection n is $I_n = 4n^2+2$. In Figure 3-7, an illustration of the image boxes is given for a single order reflection.

3.4.3 Indoor radio wave propagation model

The mathematical representation of the indoor radio channel is often reported to be of the low pass complex impulse response form. In order to introduce this concept into the algorithm, the discrete form of this equation is given by [5]

$$r(t) = \sum_{n=0}^{N} \alpha_n(t) e^{j2\pi f_c \tau_n(t)} s(t - \tau_n(t)) \tag{3.3}$$

where $r(t)$ is the low pass channel response of a low pass signal $s(t)$, $\alpha(t)$ is the attenuation factor of the signal received on the n^{th} path. τ_n is the associated time delay for the n^{th} path and finally f_c is the carrier frequency of the transmitted signal.

In the case of a ray-tracing algorithm, $r(t)$ may be expressed as

$$r(t) = \sum_{n=0}^{N} \alpha_n(t) e^{j\Delta\theta_n(t)} \tag{3.4}$$

where $\Delta\theta_n(t)$ is the phase difference between the nth ray with respect to the line of sight component and is given by :

$$\Delta\theta_n(t) = \frac{2\pi\Delta l(t)}{\lambda} \tag{3.5}$$

where λ is the wavelength and $\Delta l(t)$ is the differential path length of the direct ray and reflected rays and is given by

$$\Delta l(t) = l_{los}(t) - l_n(t) \tag{3.6}$$

where l_{los} is the line of sight path length as shown in Figure 3-3 and l_n is the path length of the n^{th} ray. Figure 3-8 illustrates the equation in the case of a two ray scenario. This shows that for a receiver moving along a straight line, the path length difference Δl varies and hence the phase differential between the two vectors $\vec{E_1}$ and $\vec{E_2}$. Consequently depending on the position of the receiver the two vectors will be adding constructively or destructively. Therefore the magnitude of the resultant vector will experience troughs and peaks with the movement of the receiver.

In a corridor, the differential path length Δl behaves in two different manners.

- When the path length of the n^{th} ray and the line of sight decrease or increase in the same fashion, the change of the differential path length varies at a low rate as the receiver moves away from the transmitter. This results in a large amplitude slow variations in the received signal envelope as previously described in the Chapter 2.

- Whereas, when the line-of-sight path length decreases while the reflected rays path length increases or vice-versa, the rate of change in the path length difference is much larger compared to the distance travelled by the receiver. This causes fast fluctuations in the received signal envelope.

This multipath mechanism is illustrated in the results of Chapter 5 and 6.

3.4.4 Ray tracing algorithm

The ray tracing algorithm considers routines, where first, second and triple order reflections have been developed independently such that higher order reflections may be added to the algorithm in the future. The model takes into account 6 rays for the first order reflection, 18 rays for the second order reflection and 30 for the third order reflection. Although there are 38 possible triple images as explained in section 3.4.2 only 30 are considered to ease the complexity of the model. In the model developed, $\alpha(t)$ of equation 3.4 is dependent on the gain of the antennas and the reflection coefficient. The attenuation of the n^{th} ray and i^{th} reflection is expressed as:

$$\alpha_{n,i}(t) = \frac{G_{T_x n} G_{R_x n} \Gamma_{n,i}}{l_n} \tag{3.7}$$

where l_n is the ray path length, $G_{T_x n}$ and $G_{R_x n}$ are the gain of the transmitting and the receiving antennas respectively for the n^{th} ray. $\Gamma_{n,i}$ is the reflection coefficient of the nth ray with i^{th} reflection and is given by

$$\Gamma_{n,i} = \prod_{j=0}^{i} \Gamma_j \tag{3.8}$$

When $i = 0$, the reflection coefficient is zero. A more complete equation of the reflection coefficient for a spatial three dimensional coordinates will be given in section 3.4.6.

Therefore, the electric field strength is expressed as :

$$E_r(t) = \sum_{n=1,i=0}^{1} \alpha_{n,i}(t)$$

$$+ \sum_{n=1,i=1}^{6} \alpha_{n,i}(t) e^{j\Delta\theta_n(t)}$$
$$+ \sum_{n=1,i=2}^{18} \alpha_{n,i}(t) e^{j\Delta\theta_n(t)}$$
$$+ \sum_{n=1,i=3}^{30} \alpha_{n,i}(t) e^{j\Delta\theta_n(t)} \tag{3.9}$$

and the received N-ray power at the mobile receiver is

$$P_r(t) = |E_r(t)|^2 \tag{3.10}$$

3.4.5 Ray path length

As outlined in section 3.4.1, the distance travelled by the ray l_n is equivalent to the distance between the receiver R and the highest order image source I_n. It is calculated using the three dimensional coordinates and is given by :

$$l_n = \sqrt{(I_{nx} - R_x)^2 + (I_{ny} - R_y)^2 + (I_{nz} - R_z)^2} \tag{3.11}$$

where the receiver position is defined as $\begin{bmatrix} R_x \\ R_y \\ R_z \end{bmatrix}$ and the image coordinates for the n^{th} path as $\begin{bmatrix} I_{nx} \\ I_{ny} \\ I_{nz} \end{bmatrix}$.

3.4.6 Reflection coefficient

It has been explained before that the reflection coefficient is related to the polarization of the electric field and the plane of incidence. When dealing with a three dimensional model the case where the transmitter and the receiver are not at the same height needs to be considered. In such situation the plane of incidence of double reflected rays may not be perpendicular (or parallel) to any of the surfaces of the ideal empty room. Therefore the

use of the two conventional reflection coefficients $\rho_{\parallel}$ and $\rho_{\perp}$ independently is not applicable. This problem can be solved vectorially.

The incident field $\vec{E_i}$ can be characterised vectorially by its tangential $\vec{E_{i\parallel}}$ and orthogonal $\vec{E_{i\perp}}$ components as shown in Figure 3-9 and is given by :

$$\vec{E_i}=\vec{E_{i\parallel}} + \vec{E_{i\perp}} \tag{3.12}$$

where

$$\vec{E_{i\parallel}}= \left|\vec{E_{i\parallel}}\right| . \vec{U_{i\parallel}}= \left(\vec{E_i} . \vec{U_{i\parallel}}\right) \vec{U_{i\parallel}} \tag{3.13}$$

and

$$\vec{E_{i\perp}}= \left|\vec{E_{i\perp}}\right| . \vec{U_{i\perp}}= \left(\vec{E_i} . \vec{U_{i\perp}}\right) \vec{U_{i\perp}} \tag{3.14}$$

Where $\vec{U_{i\parallel}}$ and $\vec{U_{i\perp}}$ are the unit tangential and normal vectors of the plane of incidence as illustrated in Figure 3-10 for an elliptical polarization. In the model, $\vec{U_{i\parallel}}$ and $\vec{U_{i\perp}}$ are determined as follows. $\vec{d_i}$ and $\vec{d_r}$ are the unit vector directions of the incident and the reflected rays respectively and given by :

$$\vec{d_i} = \lambda(\vec{SA}) \tag{3.15}$$

$$\vec{d_r} = \eta(\vec{AR}) \tag{3.16}$$

$$\left|\vec{d_i}\right| = \left|\vec{d_r}\right| = 1 \tag{3.17}$$

where λ and η are proportionality coefficients.

The unit vector normal to the plane of incidence $\vec{U_{i\perp}}$ can be found as :

$$\vec{U_{i\perp}} = \beta(\vec{IA} \times \vec{IS}) \tag{3.18}$$

$$\left|\vec{U_{i\perp}}\right| = 1 \tag{3.19}$$

Consequently the tangential vector $\vec{U_{i\|}}$ is given by the vector product

$$\vec{U_{i\|}}=\vec{U_{i\perp}} \times \vec{d_i} \tag{3.20}$$

Similarly to the expression of $\vec{E_i}$ in the equation 3.12, $\vec{E_r}$ can be written as

$$\vec{E_r}=\vec{E_{r\|}} + \vec{E_{r\perp}} \tag{3.21}$$

The vector $\vec{E_r}$ can be solved by considering its tangential $\vec{E_{r\|}}$ and normal $\vec{E_{r\perp}}$ components separately. The tangential component $\vec{E_{r\|}}$ is given by :

$$\vec{E_{r\|}}= \rho_{\|} \vec{E_{i\|}} \tag{3.22}$$

and

$$\vec{E_{r\perp}}= \rho_{\perp} \vec{E_{i\perp}} \tag{3.23}$$

by substituting $\vec{E_{i\|}}$ as given by equation 3.13, $\vec{E_{r\|}}$ is expressed as

$$\vec{E_{r\|}}= \rho_{\|}(\vec{E_i} \,.\, \vec{U_{i\|}})\, \vec{U_{i\|}} \tag{3.24}$$

similarly, the normal component $\vec{E_{r\perp}}$ is expressed as

$$\vec{E_{r\perp}}= \rho_{\perp}(\vec{E_i} \,.\, \vec{U_{i\perp}})\, \vec{U_{i\perp}} \tag{3.25}$$

In the case of a single reflection, the reflected field vector $\vec{E_r}$ can be deduced from the incident field such as

$$\vec{E_r}= ((\vec{E_i} \,.\, \vec{U_{i\|}}).\rho_{\|})\, \vec{U_{r\|}} +((\vec{E_i} \,.\, \vec{U_{i\perp}}).\rho_{\perp})\, \vec{U_{r\perp}} \tag{3.26}$$

where $\rho_{\|}$ and $\rho_{\perp}$ are the parallel and perpendicular reflection coefficients respectively.

For multiple reflections, the same equation as in 3.26 is used considering the electric field of the reflected ray of a previous reflection as the incident field for the next reflection

as shown in Figure 3-11.

Therefore the algorithm computes the total field for each x, y, z coordinate first and then compute the resultant as :

$$\left|\vec{E_r}\right| = \sqrt{\left|\vec{E_{rx}}\right|^2 + \left|\vec{E_{ry}}\right|^2 + \left|\vec{E_{rz}}\right|^2} \tag{3.27}$$

3.4.7 Antenna parameters

The model considers the real radiation pattern of the antennas used in the measurement presented in the thesis. The radiation patterns of the antennas employed have been measured inside an anechoic chamber. Figure 3-12 shows the different vectors affiliated to the antenna and the ray path. The angle is calculated in three dimension and is given by:

$$\vec{A} \cdot \vec{R} = \left|\vec{A}\right| \cdot \left|\vec{R}\right| \cos\beta \tag{3.28}$$

where $\vec{R}$ is the direction vector of the n^{th} ray and $\vec{A}$ is a reference vector for the antenna pattern.

$$\beta = cos^{-1}\left(\frac{\vec{A} \cdot \vec{R}}{\left|\vec{A}\right| \cdot \left|\vec{R}\right|}\right) \tag{3.29}$$

The gain associated with this angle is then obtained from a look up table which contains the measured data.

3.5 Limitation of the model

In this section, the limitations of the model are outlined. The pros and cons of some assumptions made to simplify the model are also discussed.

- *The dielectric parameters* : The relative dielectric constant ϵ_r of value 3 is assumed to be real. The model assumes the same value of the dielectric constant for all the surfaces. Such assumption influence the depth of the fade only but not the frequency of the amplitude variations. Also it would be too complex

and unrealistic to try to insert precise values for ϵ_r since for a real environment a wall may be made of different materials such as wood, metal and glass.

- *Specular reflection* : It has been reported that predictions obtained from a specular reflection model are in a reasonably good agreement with measured results for indoor propagation [14]. Some research has been undertaken to examine the effects of the surface roughness in sub-urban areas. This may not be significant at 11 GHz, however at 62.4 GHz (of wavelength as small as 4.8 mm) the answer is not of knowledge. Predictions for outdoor environments at millimetre waves have shown that surface roughness may be an important factor in accurately determining the channel characteristics.
- *The reflection order* is limited up to three. It has been shown that the complexity of the model was dependent on the number of reflections. The present model has shown that the third order was already complex. Research in similar field [103] has shown that multiple reflections up to the eighth order could be identified. A channel sounder with a very high time dispersion resolution operating at 1.8 GHz was used. The measurements were made in a corridor of length 7.4 m and width and height of similar dimensions of 2 m. All the surfaces were flat and made of concrete apart from the two end walls which were covered with aluminium sheets.
- *The geometrical description of the real environment.* This is another important factor for the accuracy of the model. For instance, the model assumes walls perfectly parallel or orthogonal which is not the case for a corridor of 40 m length. At millimetre waves and microwave bands, an error of the order of a wavelength (i.e. 0.48 and 2.72 cm respectively) in the estimation of the geometrical description of the environment and locations of terminals can produce significant errors in the computed phases of the rays. Therefore the signal envelope at a specific location can not be accurately predicted.

However such a model is expected to predict similar behaviour to the measurements so that the frequency correlation functions and the coherence bandwidth can be estimated

and the propagation mechanism explained.

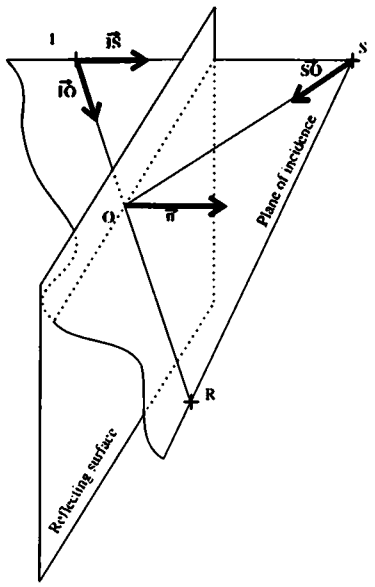

Figure 3-1: 3-D representation of the definition of the plane of incidence

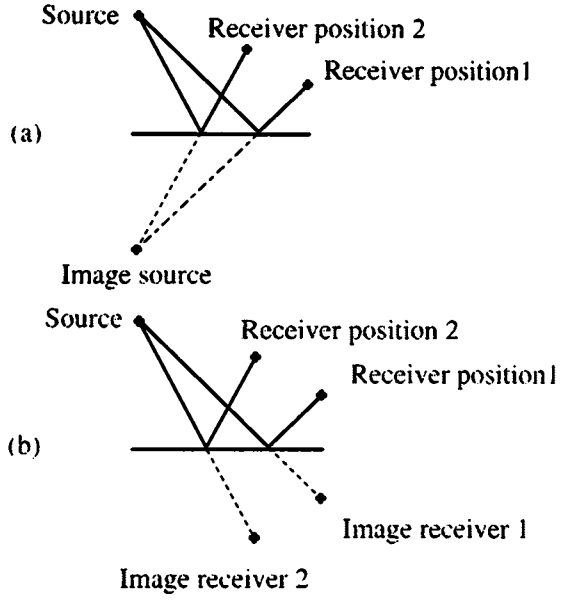

Figure 3-2: Illustration of of the image method using the forward (a) and backward (b) ray-tracing technique

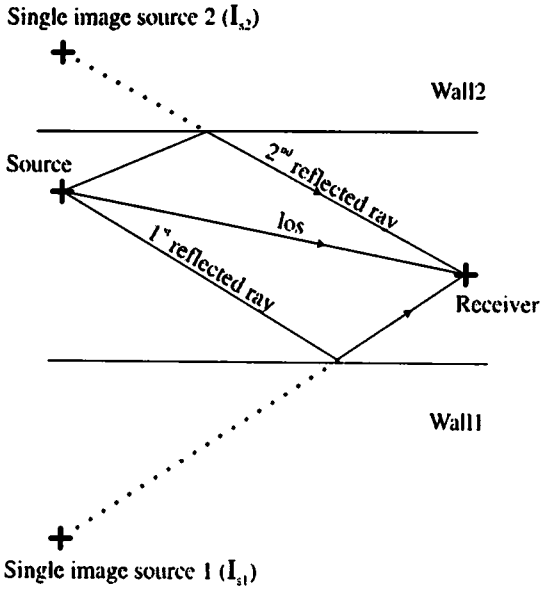

Figure 3-3: First order reflection with two single reflections

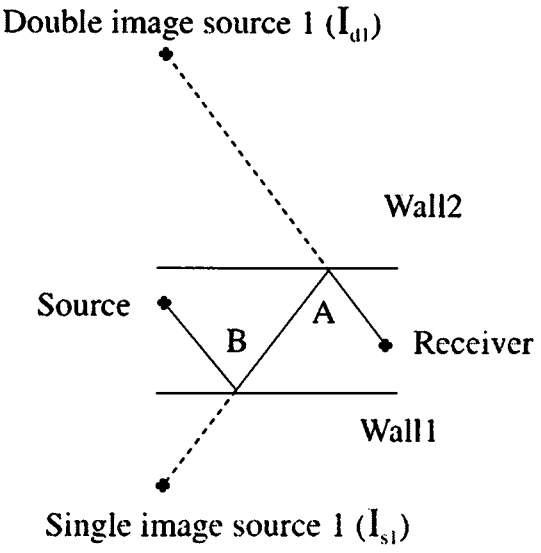

Figure 3-4: A second order reflection ray-tracing model

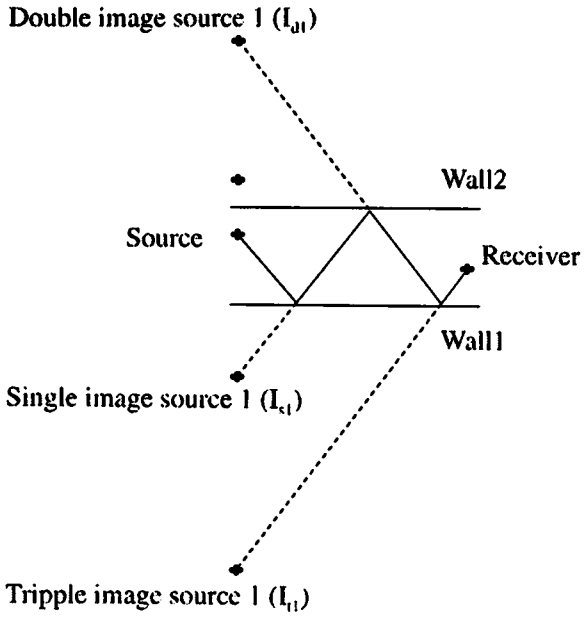

Figure 3-5: A third order reflection ray-tracing model

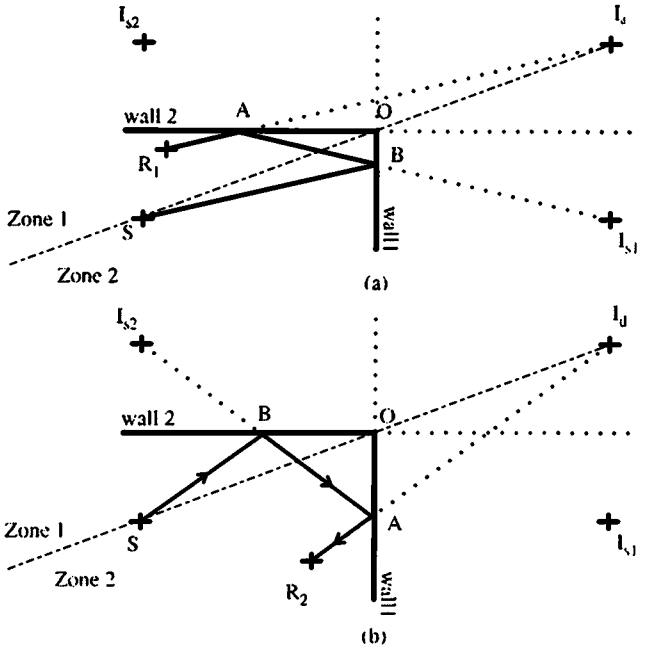

Figure 3-6: Ray-tracing model with two perpendicular walls

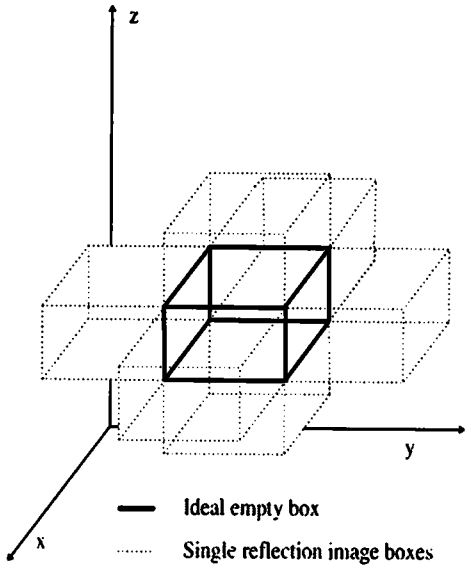

Figure 3-7: Three dimensional representation of the image boxes for a first order layer

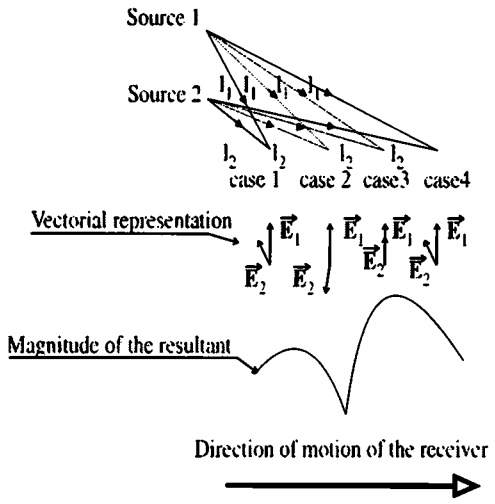

Figure 3-8: Creation of fades in multipath environment

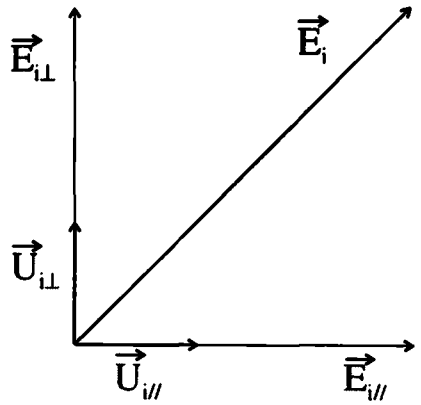

Figure 3-9: Coordinate of the incident field

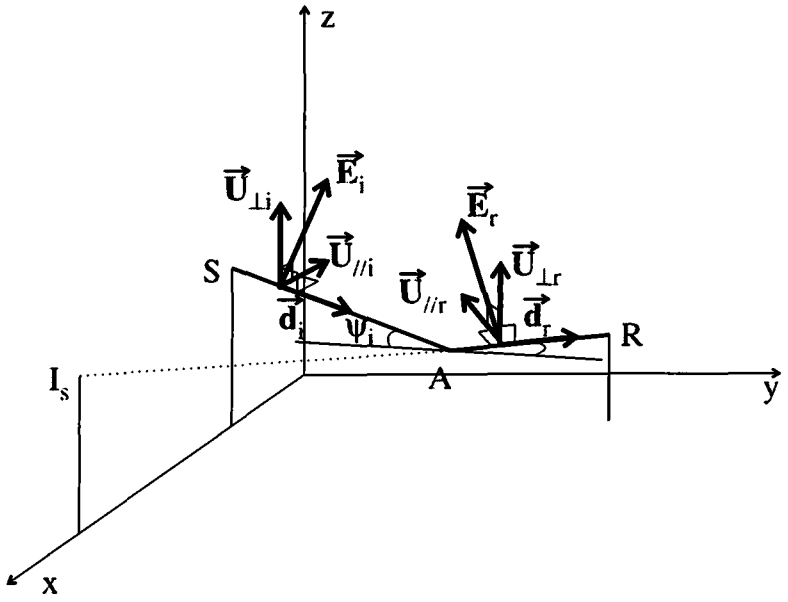

Figure 3-10: Vectorial representation of the electric field E

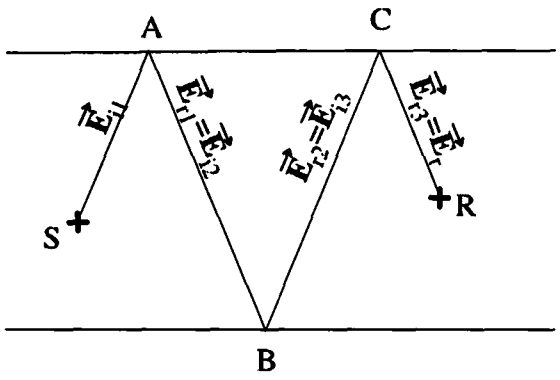

Figure 3-11: Determination of the reflected E field for multireflection scenario

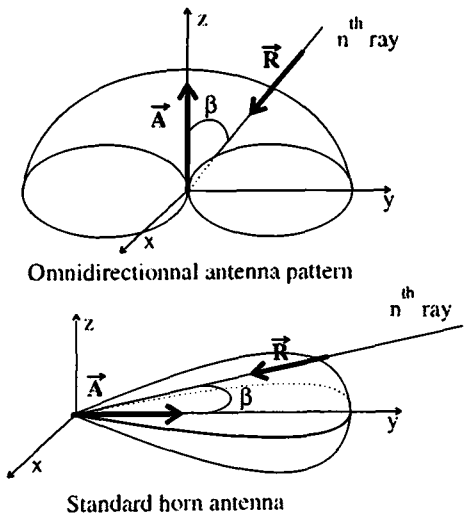

Figure 3-12: Reference vectors for the determination of the gain of the antennas

Chapter 4

Experimental hardware and geometry

4.1 Introduction

Experimental measurements were undertaken to characterise the coherence bandwidth for various indoor radio channels. The estimation of the coherence bandwidth is significant when large bandwidth systems are designed and also when frequency diversity is considered to combat multipath distortion. The knowledge of the coherence bandwidth is valuable in determining the performance of a frequency diversity countermeasure. Experimental results will be supported by predictions obtained from the ray-tracing model described in Chapter 3.

Direct measurement of the coherence bandwidth may be carried out using a two-branch frequency diversity system. A literature survey revealed that the use of such a system has been reported prior to the commencement of this study. Indoors, the use of space and frequency diversity systems has been reported at 1.7 GHz [104] and 900 MHz [105]. [9] proposed a two-branch frequency diversity system used in the measurement of the coherence bandwidth at 55 GHz in a built-up urban area.

In [104] and [105], the measurements were carried out in several rooms and hallways of different sizes varying from 13×13 m^2 to 3.3×3.5 m^2 . Quarter-wavelength monopole

antennas with a ground plane were used. The frequency separation was adjustable from 1 to 20 MHz allowing a dynamic range of 50 dB. Measurements were carried out while people were occupying the rooms. The received envelopes were recorded while the receiving antennas were moved along a circle with a diameter of few wavelengths. This type of measurement provides data for a restricted area only and cannot give an idea of the propagation behavior of the whole room.

In view to the lack of reported measurements of the coherence bandwidth in indoor environments, it was decided to conduct measurements in a room and several corridors at 11 GHz and 62.4 GHz. On the contrary to [9] [104] [105] measurements were made over the entire distance in the microcell in order to estimate the influence of the small scale and the large scale fluctuation of the signal on the coherence bandwidth. Additionally, antennas with different bandwidths were used to establish the effect of the antenna radiation pattern on the coherence bandwidth.

Frequency diversity measurements were conducted by modulating a CW carrier to produce two sidebands symmetrically disposed about it. The diversity branch signal envelopes can be simultaneously recorded. The frequency separation between the sidebands is varied by changing the modulating signal frequency.

This chapter presents the mechanical and electronic apparatus used for undertaking an experimental campaign in a number of indoor environments with the objective of obtaining a direct measurement of the coherence bandwidth. Also description of the different measurement sites together with terminals locations is given.

4.2 The mechanical mobile system

In order to avoid any influence of the human traffic on the received signal, all the measurements were made over several weekends and during the Easter holidays 1997.

For time efficiency, it was decided to equip two trolleys with the necessary equipment. This is to facilitate setting up and storing the equipment quickly. One of the trolleys was left stationary while the other acted as a potential mobile user. A tripod, used to fix the

base station, was left close to the stationary trolley. The elevation of the transmit and receive antennas were chosen to simulate the height of a user of about 1.70 to 1.80 m.

The construction of the mobile system did follow two steps. The first three measurements in the corridor of the 2^{nd} floor of J block (later denoted as corridor J2) were done using a mobile system which was guided by the two parallel side walls with horizontal guiding wheels as illustrated in Figure 4-1. This set up, used at 62.4 GHz, is reported in [51]. Concrete block were placed in the cells of the doors to provide a continuity with the side wall. This method becomes unpractical in the case where the measurements required to move the station along the diagonal of a room.

The second option was to design a rail track which will render measurements possible anywhere along a straight line. The rail track consists of several 2 metre long metal guide of a U shape where a wooden pilot clamped underneath the mobile trolley moves freely into it like a moving tongue in a groove. The total length of the rail track available was 34 m and it was secured on the ground by several concrete block as illustrated in Figure 4-2.

The mobility of the trolley was controlled by a DC motor supplied by a 12 V battery. This results in the trolley to move at a constant speed of 1 ms^{-1}. During the motion of the mobile trolley, its location was recorded by a number of markers positioned along the run. The acceleration and deceleration stages of the trolley at the beginning and the end of the measurements are discarded from the analysis. This mechanical system is an attractive method for three reasons:

- The mobile is in motion free of operators interference.
- Constant speed throughout the measurements.
- One operator is needed only to undertake the measurements.

Pictures of the stationary and mobile trolleys are shown in Figure 4-4 and 4-5 respectively. A description of the complete mechanical system is shown in Figure 4-3.

4.3 The 62.4 GHz system

Characterisation of the coherence bandwidth at millimetre waves is important considering the importance made in the literature of the potential use of the 62.4 GHz band for the MBS European system. For mobility safety measures, the two terminals were enclosed in metal boxes with their antennas mounted on the top.

4.3.1 Transmitter

The transmitter was clamped on the mobile trolley. The 62.4 GHz source transmits a power of 100 mW. It consists of a highly stable CW phase locked loop oscillator with a reference of 100 MHz crystal. The output of the oscillator is connected to an isolator which provides 30 dB of isolation. The oscillator is powered by a 15 V DC supply. A phase lock alarm connected to a voltmeter indicates when the system is in lock. The isolator is connected to the antenna through a bi-phase modulator. The modulator is used to generate two sideband frequencies around the frequency carrier. Due to the response of the modulator, the power of both sideband decreases as the frequency separation increases. This limits the maximum frequency separation to 240 MHz. The 62.4 GHz transmitter block diagram is presented in Figure 4-6. The metal box, where the transmitter was enclosed, and the modulating signal generator were placed on the trolley. The whole system was powered from the mains through a long extension lead.

4.3.2 Receiver

The box where the receiver was housed, was mounted on a tripod and left stationary. It consists of a 61.8GHz phase lock loop oscillator, which converts down the signal to an intermediate frequency (IF) of 600 MHz. The IF is boosted through a low noise amplifier (LNA) which is fed to the input of the two-branch diversity system via a long coaxial cable. The two-branch diversity system was placed on the trolley. Each branch of the diversity system consists of a mixer, a voltage control oscillator (VCO) ranging from 300 to 600 MHz, a narrow band pass filter with a 3 dB bandwidth of 2 MHz, an amplifier with 20 dB gain, and a logarithmic amplifier. The output of the logarithmic amplifier is a DC

voltage which is digitalised for processing by a digital acquisition board. The filters are centred at 170 MHz and 220 MHz. Figure 4-7 provides a block diagram of the two-branch diversity system for the 62.4 GHz measurements.

The diversity system was bench calibrated before the measurements campaign. The noise floor of the two-branch diversity system is limited to -75 dBm by the Log-Amp. This provides a dynamic range of about 50 dB. The two-branch frequency diversity system is tuned manually by selecting the relevant sideband using a spectrum analyser. The main drawback of this system is the intermodulation product at the output of the mixers.

4.3.3 Antennas

For the 62.4 GHz measurements, a combination of an omnidirectional antenna in the azimuth and a horn antenna were used. The antennas were vertically polarized. The omnidirectional antenna has a gain of 6 dBi and an elevation beamwidth of 6.5°. This antenna is of a similar structure to that reported in [106]. It consists of two plates supported by a hollow plastic cylinder. The top plate has a concave shape towards the base plate which has a cone shape.

The standard horn antenna has a gain of 10 dBi with 69° and 55° E and H-plane 3-dB beamwidth respectively. A picture of the omnidirectional antenna and the receiver system is shown in Figure 4-8. The radiation pattern of the omnidirectional antenna for the vertical plane is displayed in Figure 4-9.

4.4 The 11 GHz System

The interest of the 11 GHz in the literature has often been focused to outdoor applications. However a little research has been reported [19] for this band in indoor environments.

4.4.1 Transmitter

The 11 GHz transmitter consists of a 100 mW varactor gunn diode supplied from a 9 VDC power supply. The centre frequency of the oscillator is tuned mechanically. The modulating sinusoidal signal is connected to the varactor input producing two sidebands

signals. The response of the oscillator limits the maximum frequency separation to 190 MHz since the level of the sidebands decrease for large frequency spacings. For indoor environments, the frequency was reasonably stable during the run time of the mobile. An attenuator was connected at the output of the source to avoid saturating the receiver. A block diagram of the 11 GHz transmitter is given in Figure 4-12.

4.4.2 Receiver

The receiver consists on a low noise block (LNB) designed for use in domestic satellite television receivers. The LNB includes a 50 dB amplifier and a 10 GHz local oscillator which down converts the signal to a 1 GHz IF. The LNB is supplied with a 15 V DC through the coaxial cable. An RF choke was connected at the output of the power supply to direct the RF signal to the diversity branch system. Figure 4-13 shows a block diagram of the 11 GHz receiver.

4.4.3 Antennas

Measurements were made using a combination of standard horn antennas and omnidirectional antenna. The measurements were made using vertical polarization. One horn has a gain of 10 dBi and a half power beamwidth of 55°in elevation and 56° in the horizontal while the second one has a gain of 15 dBi with a half power beamwidth of 32°in the elevation and in the horizontal. The omnidirectional antenna was of the type reported in [106]. It was tuned using a short circuit and a coupler to reduce the reflected signal to its minimum in order to give maximum efficiency and greater gain. The resulting gain of the omnidirectional antenna is 5 dBi. The calibration set up is illustrated in Figure 4-14. The radiation pattern in elevation and azimuth was then measured in the anechoic chamber. The elevation radiation pattern of the omnidirectional antenna is displayed in Figure 4-11. A picture of the antenna mounted on the mobile trolley is displayed in Figure 4-10.

4.5 The data acquisition system

The received signal strength was measured using logarithmic amplifiers. The DC values from the Log-Amps were digitalised using a portable data acquisition unit mounted on the stationary trolley. This data acquisition system is linked to a laptop where the data was stored. From the computer, a user friendly software controls the board using Testpoint© language. This software also allows to display the signal for a certain distance after each run to check that the signal is properly recorded. Three channels are used to record simultaneously the two envelopes separated in frequency and the position of the trolley. The sampling rate was 6 KHz for all the 62.4 GHz measurements. For the 11 GHz experiments, the sampling rate was 2.5 KHz for the corridor J2 and was changed to 6 KHz for the rest of the measurements to avoid confusion. The sampling was chosen to be high enough in order to record all the components of the received signal envelope. Previous research [25] [55] has shown that the maximum frequency present in a signal envelope is equal to twice the maximum Doppler shift effect i.e.

$$f_{max} \leq \frac{2v}{\lambda} \tag{4.1}$$

where v is the speed of the mobile, and λ is the wavelength.

4.6 Description of the indoor environment

Measurements were made in a number of environments inside the University campus. Environments such as rooms and corridors were preferred to workshops since furniture (if present) would be easy to empty and therefore to compare with predictions obtained from the model. The choice of the environment was also limited by the antenna radiation pattern. Rooms and corridors where it was not possible to measure the effect of multipath fading over a large distance were precluded in the selection. Measurements were made using two different operating frequencies. Depending on the schedule, two sets of measurement at 11 and 62.4 GHz were undertaken in the environment labelled corridor J2 and the room B68. The 11 GHz system was also used in the corridor H and the corridor

J3.

4.6.1 J Block corridor 2^{nd}floor : corridor J2

Corridor J2 was located on the 2^{nd} floor of the Department of Electronics and Information Technology of the University Of Glamorgan. A picture of the corridor is given in Figure 4-16. Corridor J2 is a long narrow corridor of 41 m long, 1.92 wide and 2.68 high. This corridor presents various types of wall materials. Also neon lamp, windows in alcoves and one metal heater are present. The outer surface of the walls is made of three different layers i.e. 1 mm metallic sheet, 10 mm plasterboard and a thin layer of foil. The inner part of the structure is made of metal pillar. The two ends of the corridor are made of wooden doors. Wall C has a number of doors leading off to different laboratories as sketch in Figure 4-15. The floor is covered with vinyl plastic tiles and the ceiling with polystyrene tiles and with neon lamps positioned across the corridor. Any obstacles like fire extinguisher hooked to the wall and metal bins were removed from the corridor when the measurements took place. Results from corridor J2 could be compared with results from measurements undertaken in corridors without windows such as corridor J3 and corridor H. Another advantage was that corridor J2 was close to the microwave research lab. This facilitated the set up of the equipments.

4.6.2 J Block corridor 3^{nd}floor : corridor J3

Corridor J3 is located on the top floor of J block and is 41 m long, 1.59 m wide and 2.68 m high. This corridor is in the center of the building, therefore there is no windows as displayed in Figure 4-18. The walls are of the same nature as these for corridor J2 i.e. mainly metal. Offices doors and glass covered display boards are present on the wall A and B along the whole corridor. The floor and the ceiling are of the same type as for corridor J2. The neon lamp are disposed across the corridor. A cornice which leads to other rooms was used to place the stationary trolley apart and to leave the tripod, the motor and the mobile trolley in the corridor as illustrated in Figure 4-17. This corridor presents similar dimensions to corridor J2 with similar material for Wall A and C.

4.6.3 H Block corridor : corridor H

Corridor H is on the first floor of the Business Department which is adjacent to J block. This corridor leads to the Electronics Department which eased the transfer of the equipment. This corridor is smaller in length and narrower than corridor J2 (25.66 m $\times$ 1.66 m $\times$ 3.03 m). The floor is carpeted and the ceiling is made of polystyrene tiles. The neon lamp are disposed along the corridor. Walls A and C are not smooth and exhibit doors in alcoves all along the corridor on both side as shown in Figure 4-20. These walls are metal like in corridor J2. Wall B is made of metal whereas Wall C is made of wood. The two end walls have wooden doors. The corridor crosses another one forming a T junction which permits storage of the stationary trolley. Therefore only the mobile trolley, the motor and the tripod were in the propagation channel. Figures 4-20 and 4-19 display a picture of the corridor and the lay out of the measurement set up respectively.

4.6.4 B 68

A literature survey indicates that the propagation behaviour in corridors and rooms was different. Therefore, it was decided to extend the measurements campaign to rooms. A 12.8 m long, 6.92 m wide and 2.6 m high room was chosen. It is a relatively new building type with thick walls made of bricks and concrete blocks. The floor was carpeted and the ceiling was made from polystyrene tiles. Cubic electric metallic heaters were located on wall C (see Figure 4-22). Wall D had a metal fire door with two white boards. Wall B was smooth and free of any fixtures. Walls A and C had windows in cells. Figures 4-21 and 4-23 represent the main lay out of the room, position of the stations and the rail track for an empty and furnished room respectively. Figure 4-24 shows the lay out of the room when it was furnished. It was decided to undertake measurements at two different frequencies for a room when it was empty and later when furnished. The tables, originally present in this room, were arranged in order to simulate an office furniture. In view to the time needed to set up the environment i.e. emptying the room, setting the furniture back, installing the rail track, a time slot of a week was considered. The period of Easter holidays was ideal and the room B68 was chosen.

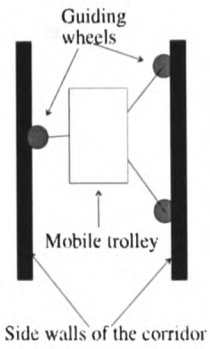

Figure 4-1: First setup : Detail of the horizontal guiding wheels

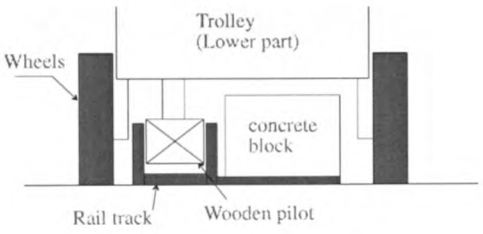

Figure 4-2: Second setup : Detail of the rail track design

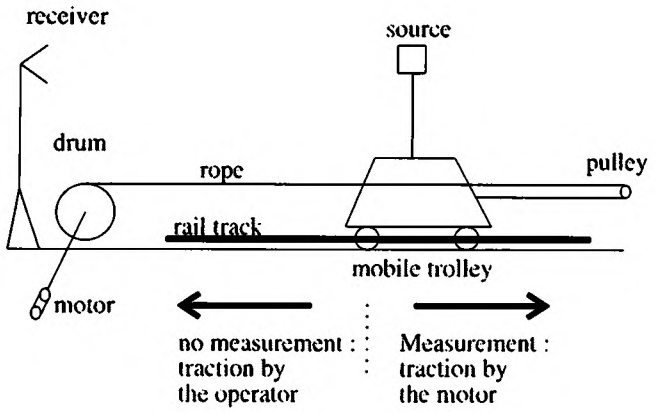

Figure 4-3: Description of the finalised mechanical set up

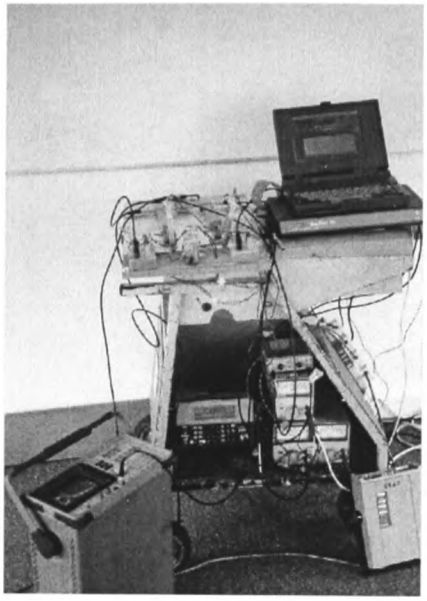

Figure 4-4: Stationary trolley fully equiped

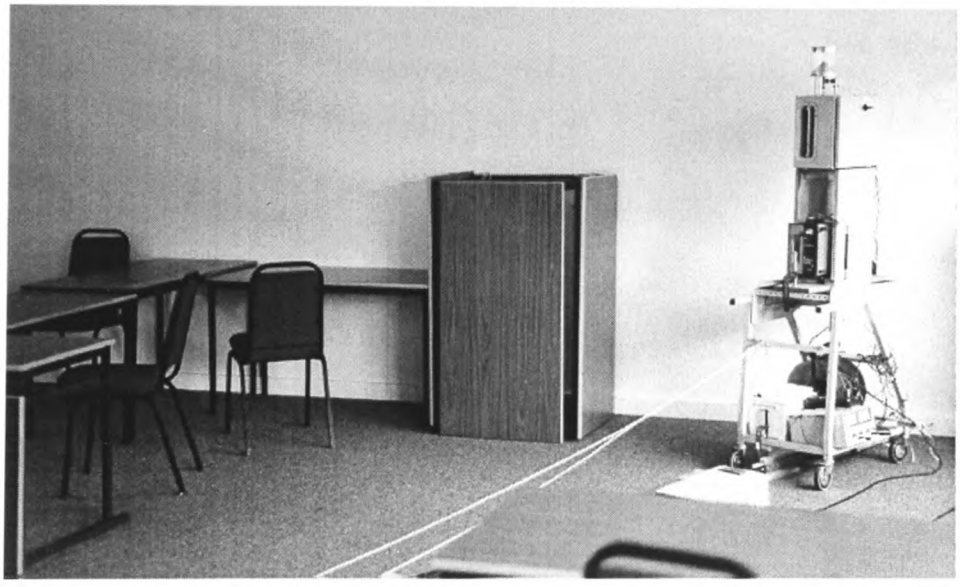

Figure 4-5: Mobile trolley equiped with the 62.4 GHz system

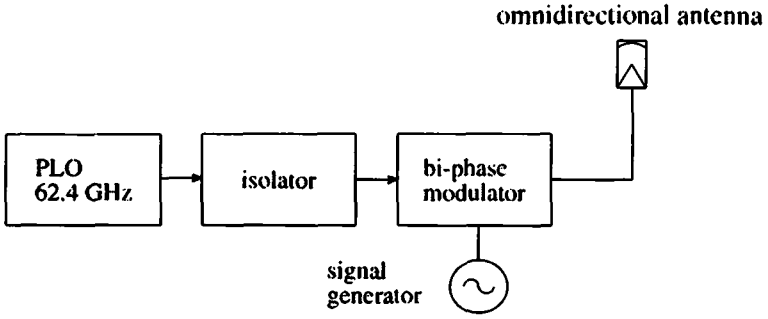

Figure 4-6: Block diagram of the transmitter at 62.4 GHz

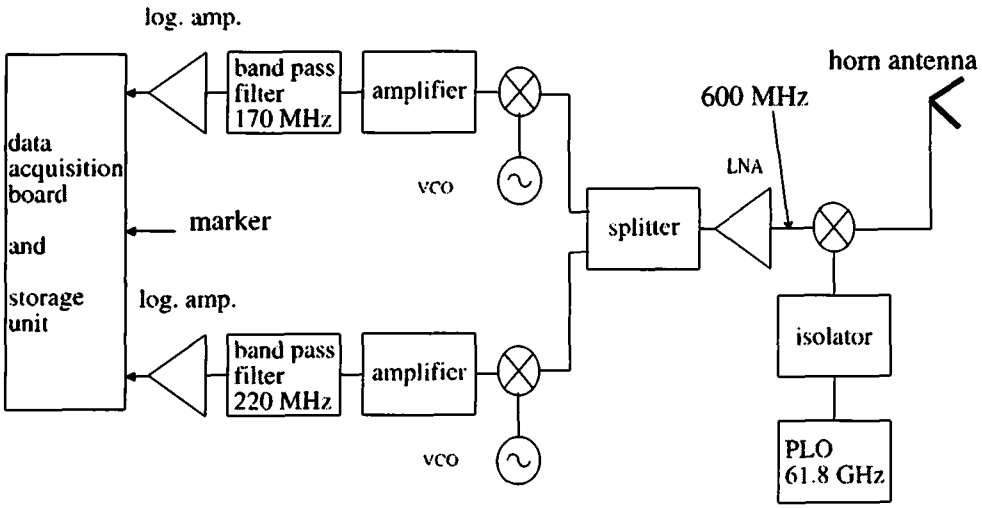

Figure 4-7: Block diagram of the receiver at 62.4 GHz and the two-branch diversity system

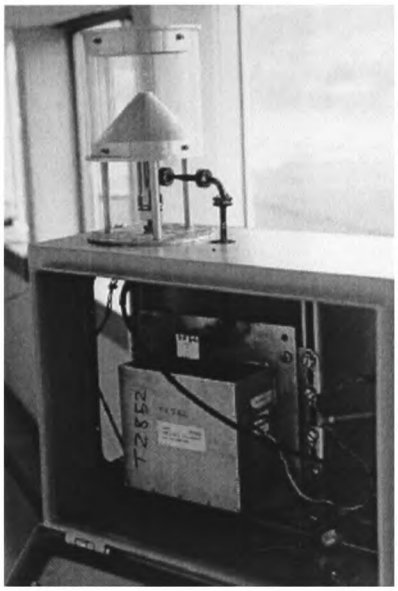

Figure 4-8: Omnidirectional antenna and the transmitter at 62.4 GHz

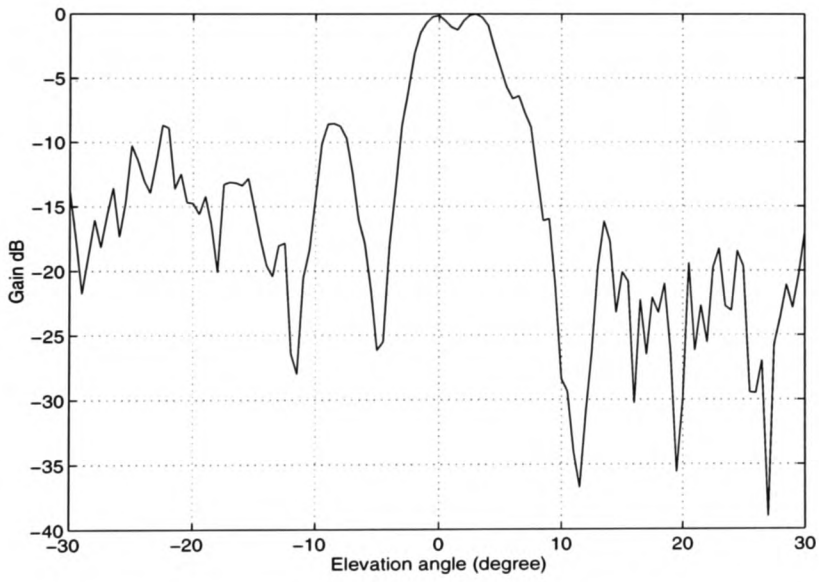

Figure 4-9: Radiation pattern in elevation of the omnidirectional antenna at 62.4 GHz

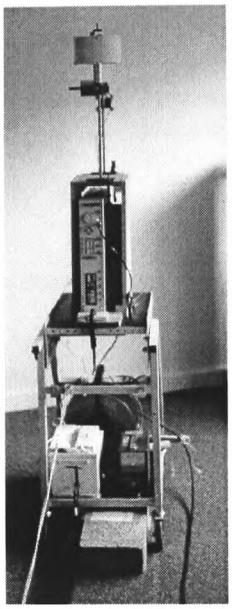

Figure 4-10: Omnidirectional antenna mounted on the mobile trolley for measurements at 11 GHz

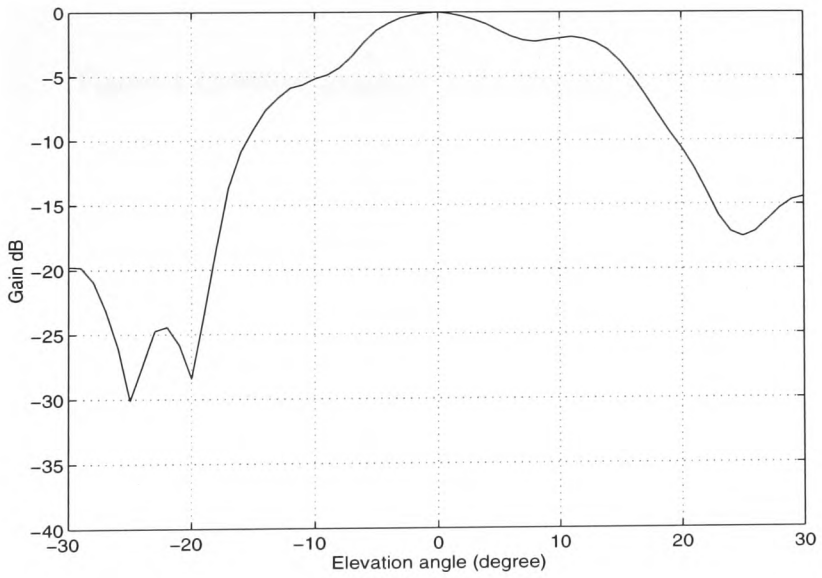

Figure 4-11: Radiation pattern in elevation of the omnidirectional antenna at 11 GHz

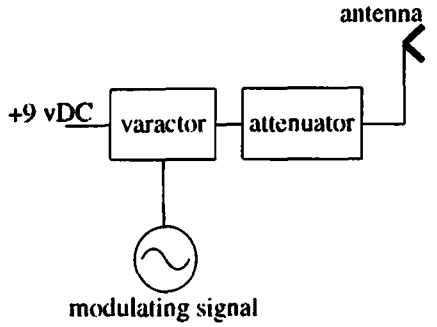

Figure 4-12: Block diagram of the transmitter at 11.0 GHz

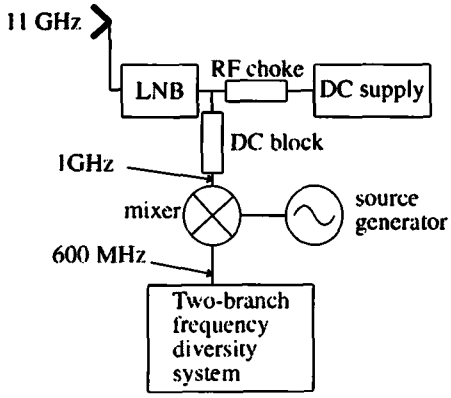

Figure 4-13: Block diagram of the receiver at 11 GHz

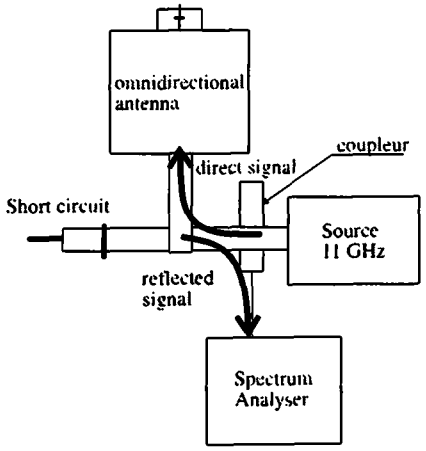

Figure 4-14: Calibration setup of the omnidirectional antenna at 11 GHz

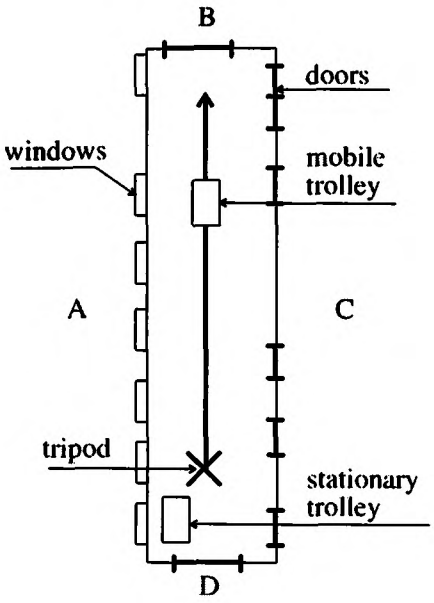

Figure 4-15: Lay out of the measurement set up for corridor J2 (not to scale)

Figure 4-16: Corridor J2, view of wall B

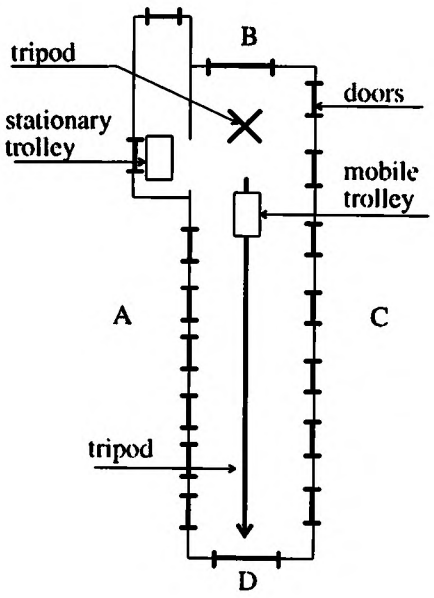

Figure 4-17: lay out of the measurement set up for corridor J3 (not to scale)

Figure 4-18: Corridor J3, view of wall B

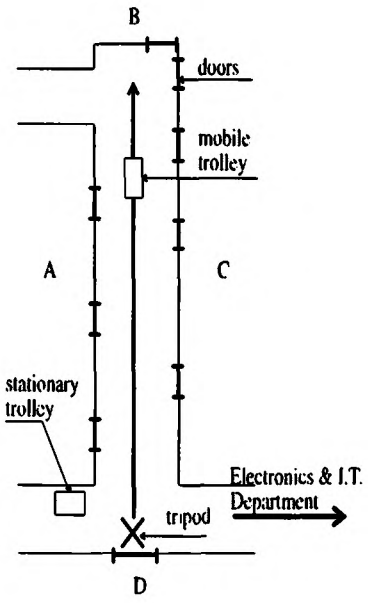

Figure 4-19: Lay out of the measurement set up for the corridor H (not to scale)

Figure 4-20: Corridor H, view of wall D

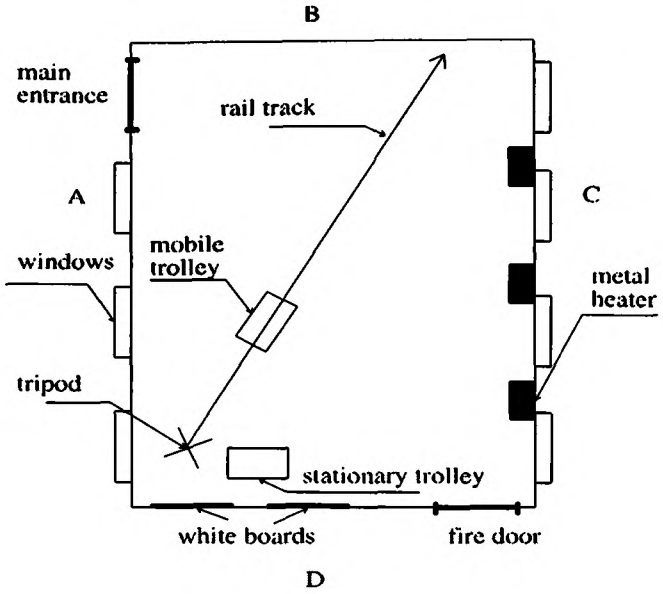

Figure 4-21: Lay out of the measurement set up of the room B68 without furniture (not to scale)

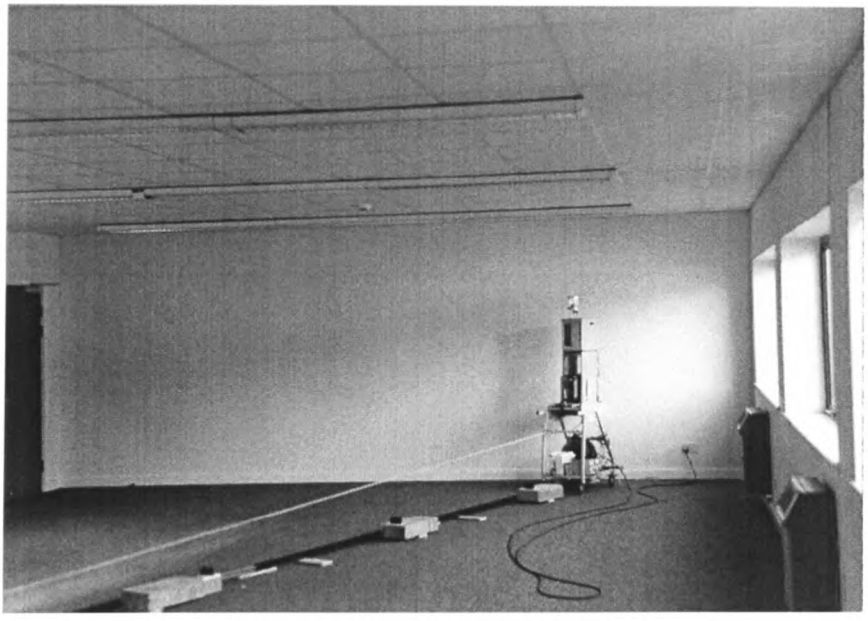

Figure 4-22: Room B68 with the 62.4 GHz system, view of the wall B

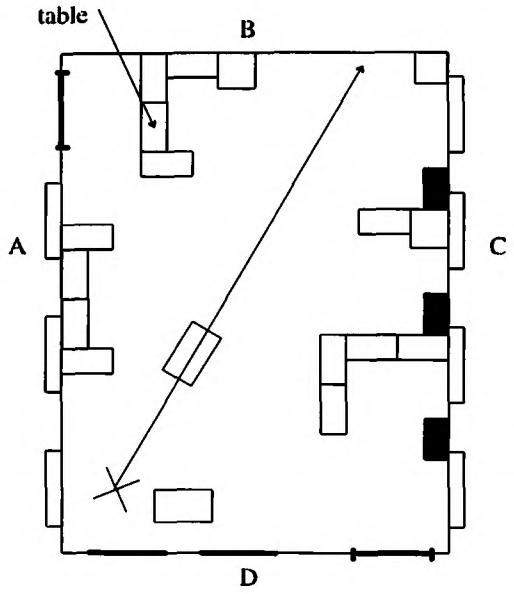

Figure 4-23: lay out of the measurement set up for the room B68 with furniture (not to scale)

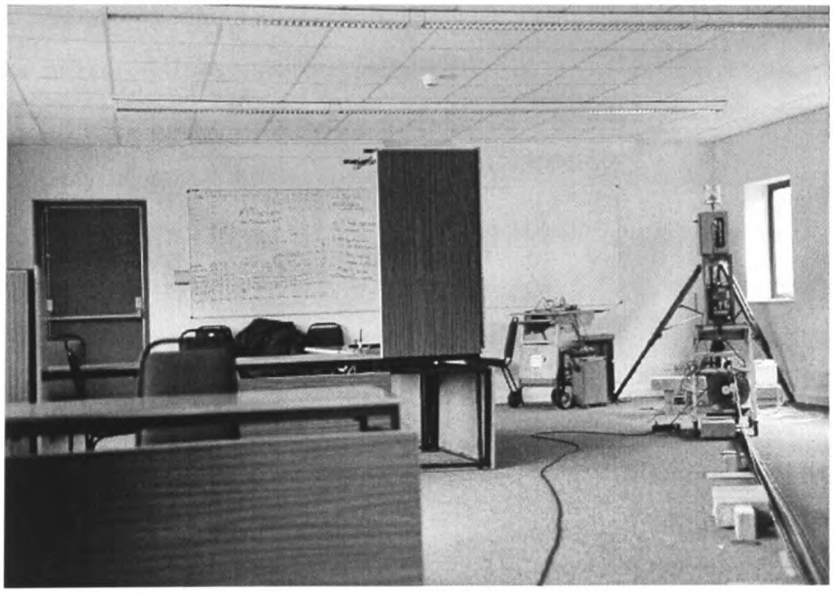

Figure 4-24: Room B68 with furniture, view of the wall D

Chapter 5

Characterisation of the indoor mobile radio channel and its coherence bandwidth at 11 GHz

5.1 Introduction

This chapter presents results for the measurement campaign undertaken at 11 GHz in various indoor microcells. Results are reported for 3 corridors and a room as described in details in Chapter 4. The correlation level between the signal envelopes separated in frequency has been measured and expressed as a function of mobile position in the microcell. The coherence bandwidth for correlation levels of 0.5, 0.7 and 0.9 has been computed from the frequency correlation functions. Experimental results are compared with theoretical predictions obtained using the ray-tracing algorithm described in Chapter 3. The algorithm is also used to assist in interpreting experimental results. The effects of the microcell dimension and structure on the value of the coherence bandwidth has also been examined. The influence of the antennas radiation patterns on the coherence bandwidth has been investigated by using a combination of different antennas. In additions, measurements with the presence of furniture have been analysed to examine their effects on the coherence bandwidth.

5.2 Experimental and theoretical characterisation using horn to omnidirectional antenna

This section describes results of experiments made at 11 GHz in several indoor environments using a 10 dBi horn antenna at the stationary receiver and an omnidirectional antenna at the mobile transmitter.

5.2.1 Corridor J2

A full description of the corridor J2 has been presented in section 4.6.1. This is a long narrow corridor of dimension 41 m × 1.92 m × 2.68 m. Its main characteristic is that, Wall A as depicted in Figure 4-15 (Chapter 4) is mainly composed of windows in alcoves whereas Wall C is made from metal surfaces with doors leading off. The measurements were made over a distance of 29 m. The receiver, with its antenna set at a height of 1.55 m above the ground, was left stationary and located at 1.12 m from wall A and 6.91 m from wall D. The transmitter, with its antenna set at a height of 1.60 m, was moved 2.43 m away from the receiver along a line at 1.17 m from Wall A. Owing to the frequency response of the modulator, the maximum frequency separation that can be used was 158 MHz. In order to record the distance travelled by the mobile station, 7 markers were used and placed at 3, 10, 15, 20, 25, 30 and 32 m from the receiver. Two software packages were used to process the data, i.e. Matlab^{TM} and Watcom^{TM} C++ version 10.6 compiler. Matlab^{TM} offers statistical tools such as Fast Fourier Transform Algorithm and Watcom^{TM} provides fast executable code for long processing.

5.2.1.1 Received signal envelopes

The received signal envelopes obtained when the transmitter moved from 2.43 m to 31.43 m away from the receiver, with the signal envelopes separated by 5 MHz, are shown in Figure 5-1. Each envelope is normalised with respect to its maximum value. It is shown that both signal envelopes exhibit strong amplitude fluctuations and exhibit fades as low as about 30 dB below the mean power of the signal envelopes. The amplitude variations are caused primarily by interference between the direct ray and reflections from the walls,

the floor and ceiling when the receive antenna radiation pattern does not exclude them. Reflections from the ceiling start occurring at a distance of 12.5 m between terminals, whereas the terminals need to be 17.8 m apart for the first reflection from the floor to occur. The measured mean level decays, with a path loss exponent of n = 1.4, as the transmitter moves away from the receiver. This value of n is smaller than that of the free space exponent value of two. This indicates that, at 11 GHz, the reflected rays are strong and the corridor behaves as a wave guide maintaining a high signal level. Predicted envelopes obtained using up to third order reflections with a frequency separation of 5 MHz are presented in Figure 5-2. Signal envelopes with frequency separations up to 310 MHz have been computed using identical geometry to that used in the measurements.

The power spectra of the measured envelopes are calculated using a Fast Fourier Transform routine to examine the frequency of the amplitude variations. The calculations are made over a window length of 40λ to ensure that the signal is stationary and the number of points is large enough to provide a good estimate of the signal statistics [62]. Figure 5-3 shows the power spectra of the received signal envelope measured at different positions of the mobile station. The frequency spectrum exhibits two distinctive frequency regions. The low frequency components are mainly caused by interactions between the direct component and sidewalls reflections as well as reflections from the floor and ceiling. As explained in Chapter 3, such reflections experience a small rate of change in their differential path lengths with respect to the direct ray as the transmitter moves away from the receiver. Higher frequency components, with a maximum frequency of $\frac{2v}{\lambda}$, twice the maximum Doppler shift, are caused by reflections from ahead of the transmitter. Those reflections have a faster rate of change in their relative path lengths with respect to the direct ray as the distance increases, and become more significant as the transmitter approaches the endwall of the corridor as reported in [25]. The predicted frequency spectrum presented in Figure 5-5 exhibits two distinctive frequency regions similar to that measured under similar conditions and given in Figure 5-4. However, it is to be noted that less frequency components are present in the predicted spectrum compared to the measured one, which implies that the number of rays in the model is not sufficient to predict similar amplitude variations. The number of reflections that contribute to the received signal is

an important factor in determining the value of the coherence bandwidth.

The number and amplitude of rays that contribute to the received signal strength are also significant factors in determining the theoretical value of the power ratio of the line of sight to that in the reflected rays (k-parameter of the Rice distribution). The cumulative distribution functions of the received signal envelopes have been computed over a window length of 40λ which is being moved every 20λ. The value of the k-parameter that provides the best fit to the measured distribution has then been computed and plotted as a function of distance from the receiver as shown in Figure 5-6. This figure shows that values of k varies from 0, corresponding to a distribution near to Rayleigh, to larger values with a maximum of 14.

In order to combat the multipath effect which occurs in the propagation channel, frequency diversity techniques may be attractive at micro and millimetre wave bands because of the wide signal bandwidth available in comparison with the UHF band. This technique consists of transmitting the same information using two carrier frequencies with a separation large enough to ensure decorrelated signal envelopes. The coherence bandwidth is defined [55] as *the maximum frequency difference for which the signals are still strongly correlated.*

The value of the coherence bandwidth is dependent on the number and amplitude of rays and the time delay associated with them. The low frequency part of the frequency spectrum is caused by sidewall reflections with small differential time delays relative to the direct component. However, reflections with longer time delays, such as those from the wall opposite the receiver cause fast fading. When considering a two-ray model, as shown in Figure 5-7, with time delays of τ_1 and τ_2, the differential time delay may be expressed as

$$\Delta\tau = \tau_2 - \tau_1 \tag{5.1}$$

The two signals add constructively when

$$\omega_1(\tau_2 - \tau_1) = \omega_1\Delta\tau = 2\pi n \tag{5.2}$$

and destructively when

$$\omega_1(\tau_2 - \tau_1) = \omega_1 \Delta\tau = (2n+1)\pi \tag{5.3}$$

in the case where $n = 0$

$$\omega_1 \tau - \omega_2 \tau = \pi \tag{5.4}$$

$$2\pi(f_1 - f_2)\Delta\tau = 2\pi\Delta f \Delta\tau = \pi \tag{5.5}$$

$$\Delta f = \frac{1}{2\Delta\tau} \tag{5.6}$$

This indicates that rays with small differential time delays require large frequency separations Δf to decorrelate, whereas components with long differential time delays require smaller Δf. In the corridor environment, the situation is a lot more complex since the frequency spectrum of the signal envelope exhibits two distinctive regions caused by components with small and long time delays respectively.

5.2.1.2 Correlation coefficient as a function of distance

A method similar to the moving average, referred to as moving correlation, has been developed and reported in [107]. The correlation between the measured signal envelopes is expressed as a function of the mobile transmitter position by calculating the correlation coefficient over a window of 40λ which is moved by 10λ. The correlation versus distance, computed with the envelopes separated in frequency by 5 MHz, 40 MHz and 132 MHz, are shown in Figure 5-8 to Figure 5-10 respectively. It can be seen that the correlation values fluctuate significantly between -1 and 1 with the location of the transmitter. When comparing the three figures, it can be seen that the correlation coefficient values, as expected, decrease with increasing frequency separation. Predicted results shown in Figure 5-11, 5-12 and 5-13 for frequency separations of 5 MHz, 40 MHz and 130 MHz respectively demonstrate similar behaviour. Additionally, the predicted results differ from the measured ones in the sense that the fluctuation in the correlation values becomes faster at larger frequency separations.

Considering the complexity of the correlation coefficient behaviour, two methods have been developed to interpret and characterise the coherence bandwidth. The first method

consists of constructing the frequency correlation functions by determining the level of correlation below which the measured values stay for a certain percentage of time. This method is based on considering all the values of the correlation coefficient. The second method is based on determining the frequency correlation function at each position of the mobile terminal in the microcell. Using this technique the coherence bandwidth can be expressed as a function of distance between terminals.

5.2.1.3 Method 1 : Characterisation of the coherence bandwidth using the microcell frequency correlation function

Because of the difficulty in getting a single correlation value for a particular frequency separation, the cumulative distributions of the correlation coefficients have been calculated, Figure 5-14, and the level of correlation below which the measured values stay for a certain percentage of time is computed. The distributions show that the correlation values decrease with increasing frequency separation. This behaviour is similar to the predicted results as displayed in Figure 5-15.

The frequency correlation functions are generated from the cumulative distribution functions by computing the level below which the correlation stays for 70%, 80%, 90%, 95% and 99% of the time. Then these values are plotted against the frequency separation as shown in Figure 5-16. The solid lines represent the best fit of the measured values to a function of the form $\rho = \frac{1}{(1+c\Delta f^n)}$ where ρ is the correlation coefficient, Δf is the frequency separation in MHz and c and n are constants. The values of c and n are given in Table 5.1.

The 0.5, 0.7 and 0.9 coherence bandwidths obtained from these frequency correlation

	c	n
70%	0.119	0.685
80%	0.089	0.680
90%	0.062	0.675
95%	0.043	0.706
99%	0.029	0.711

Table 5.1: coefficients of the best fit function $\rho = 1/(1 + c\Delta f^n)$

functions are given in Table 5.2. As is evident in this table a frequency spacing equal to or larger than 18.3 MHz for example, will ensure a correlation level below 0.7 for 90% of the time.

In such environment, it is interesting to note that to ensure a correlation level below 0.9 for 99% of the time a frequency separation of 3.9 MHz is needed compared to a frequency spacing of 1.3 MHz to ensure the same level of correlation but for 70% of the time. The frequency separation required to achieve this degree of correlation for larger percentages of time increases progressively. However, in the case where a correlation level below 0.5 is needed, larger separations are required, and the rate of change in the value of frequency spacing with the percentage of time is rapid. For instance, 33.7 MHz is necessary to achieve a level of correlation below 0.5 for 70% of time compared to 131.0 MHz for 99% of the time.

Additionally, the results of Table 5.2 indicate that the degree of decorrelation required to estimate the coherence bandwidth is significant since much larger frequency separations are needed to achieve low correlation levels.

The predicted signal envelopes have been processed in a similar manner and results are given in Figure 5-17 and Table 5.3. The predicted frequency correlation function shows, as expected, lower values of correlation for larger frequency spacings. These results are in a qualitative agreement with the measured ones given in Figure 5-16 and Table 5.2. The values of the coherence bandwidth obtained from the model are much larger than the measured ones. This may be due to the simplicity of the model which considers reflections up to the third order only. Later in this thesis, it will be shown that the number of rays considered in the ray-tracing model is a crucial factor in determining the value of the coherence bandwidth.

5.2.1.4 Method 2 : Coherence bandwidth characterisation using the frequency correlation function at each position

The first technique deduces the coherence bandwidth from the frequency correlation function calculated using all the measured correlation values over the whole run. Another way

to characterise the coherence bandwidth would be to measure the frequency correlation function at each position of the terminal in motion and to examine the variation of the coherence bandwidth with the position of the mobile station.

Figures 5-18, 5-19 and 5-20 show the frequency correlation functions measured when the terminals were 0.8 m, 12 m and 23.2 m apart respectively. It can be seen that the frequency correlation functions are not expected to be monotonously decreasing with frequency separation. Figure 5-19 shows that frequency separations of 2.6 MHz, 25.9 MHz and 33.8 MHz provide a correlation value of 0.7 when the terminals are 12 m apart. This means that a frequency separation larger than 2.6 MHz does no necessarily achieve a level of correlation below 0.7. It is clearly seen that frequency separations between 25.9 MHz and 33.8 MHz result in larger correlation levels. Similarly, when the terminals are 23.2 m apart, as shown in Figure 5-20, frequency separations of 1.5 MHz, 11.9 MHz and 19.5 MHz give the same correlation value of 0.7. In this case, one frequency separation gives 0.9 correlation while 5 frequency separations may be used to obtain 0.5 correlation level. Nevertheless the coherence bandwidth is defined as the minimum frequency separation required to achieve a certain correlation level. These results show that the frequency correlation function is therefore not a monotonously decreasing one.

Using this method, the coherence bandwidth is expressed as a function of distance by computing, for each transmitter position, the frequency spacing at which the correlation drops to a certain value [83]. Results obtained for correlation levels of 0.5, 0.7, 0.9 are plotted in Figure 5-21. It is shown that the coherence bandwidth is highly variable with distance. It also indicates that the coherence bandwidth increases when a lower level of correlation is sought.

Due to the difficulty in interpreting the variation of the coherence bandwidth with distance the cumulative distribution functions of the coherence bandwidth are calculated and the values of the coherence bandwidth for 70%, 80%, 90%, 95% and 99% of transmitter locations, obtained from the distributions are given in Table 5.4. It can be seen that the coherence bandwidth for 99% of transmitter locations in the microcell, corresponding to a correlation level of 0.7, is below 18.5 MHz.

Theoretical results obtained using this second method are shown in Figure 5-22 with the values of the coherence bandwidth for different correlation levels given in Table 5.5. It is evident that the coherence bandwidth behaviour with the location of the transmitter in the microcell is similar to the measured one. However, the values predicted for the coherence bandwidth are significantly larger.

The coherence bandwidth values calculated using the first method (Table 5.2) are larger than those obtained from the second one as is evident in Table 5.4 particularly for lower correlation degrees. The reason behind this is the fact that the correlation versus frequency spacing at each transmitter position in the microcell is not necessarily a monotonously decreasing function. This fact is taken into account in the first method where all correlation values measured at all transmitter positions are used to estimate the coherence bandwidth. However, estimates obtained from the second method are based on computing the smallest frequency spacing at which the correlation drops to a certain level without taking into account the fact that the same or a higher correlation level is reached again at larger frequency separations as it is illustrated in Figures 5-18, 5-19 and 5-20. A frequency spacing larger than the value of the coherence bandwidth calculated from the second method does not ensure that the correlation will stay at the level specified for a given percentage of transmitter locations. It is therefore, pointless to use this technique to estimate the coherence bandwidth.

The differences between measured values using both methods become less significant at high correlation values. This is because it is unlikely that the frequency correlation function at each transmitter location, despite not being monotonous, will reach those high correlation values again at larger frequency spacings. These results are in agreement with the theoretical predictions obtained using both methods as shown in Figure 5-17 (Table 5.3) and Figure 5-22 (Table 5.5).

5.2.1.5 Theoretical investigation of the relationship between the coherence bandwidth and RMS delay spread

In conventional mobile radio theory, it is shown that the coherence bandwidth is inversely proportional to the RMS delay spread as explained in section 2.2.5. Using the ray-tracing,

the RMS delay spread has been computed and expressed as a function of distance. Figure 5-23 shows that the RMS delay describes a "Bell" shape with distance. Therefore, the coherence bandwidth is expected to be large when the two terminals are close to each other, then the value of the coherence bandwidth should decrease at larger distances between terminals to eventually increase again when the transmitter reaches the end of the corridor. Ray-tracing using up to the third order reflection has also been used in the previous section to predict the coherence bandwidth as a function of distance as is given in Figure 5-22. It is therefore possible to plot the coherence bandwidth as a function of the RMS delay spread as given in Figure 5-24. The coherence bandwidth in this figure corresponds to the smallest frequency separation giving a correlation level of 0.7. This result represents a scatter diagram and does not show any clear relationship between the coherence bandwidth and RMS delay spread.

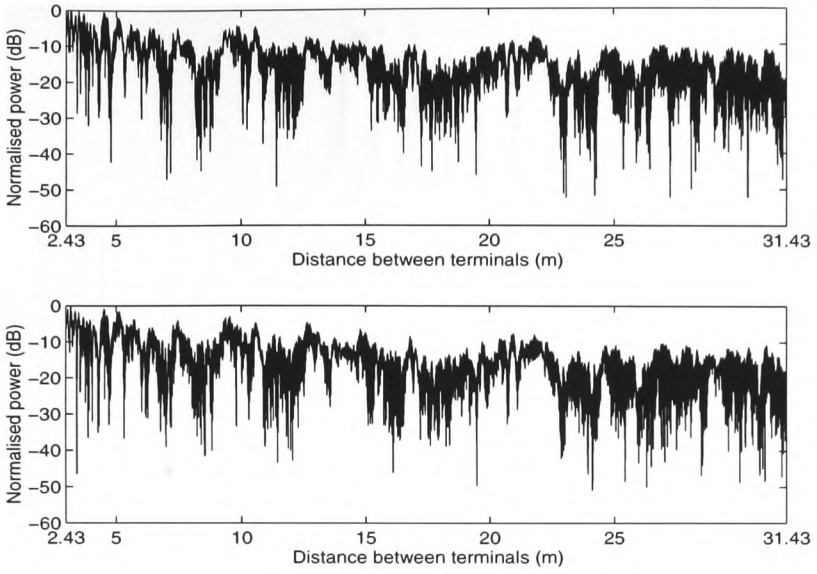

Figure 5-1: Received envelopes for a frequency spacing of 5 MHz in corridor J2 using a horn to omnidirectional antenna at 11 GHz

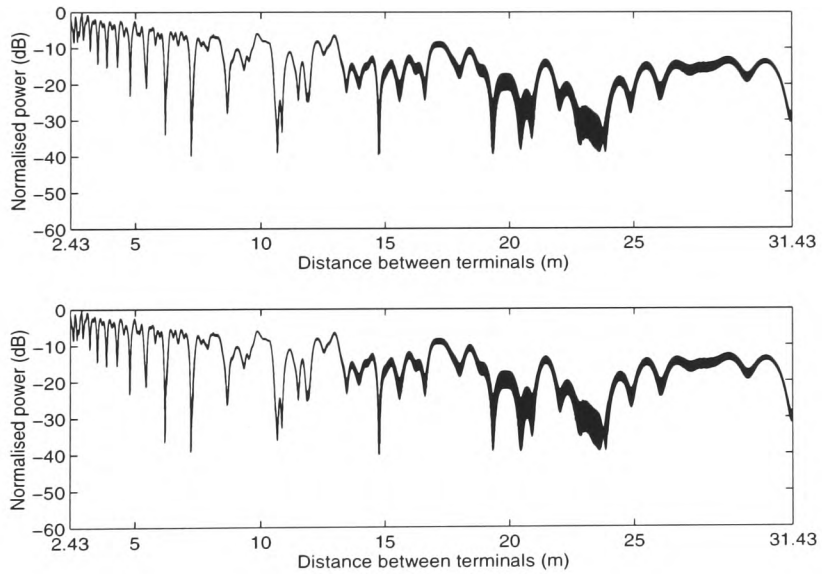

Figure 5-2: Predicted envelopes using a third order ray-tracing model computed for a frequency spacing of 5 MHz in corridor J2 using a horn to omidirectional antenna at 11 GHz

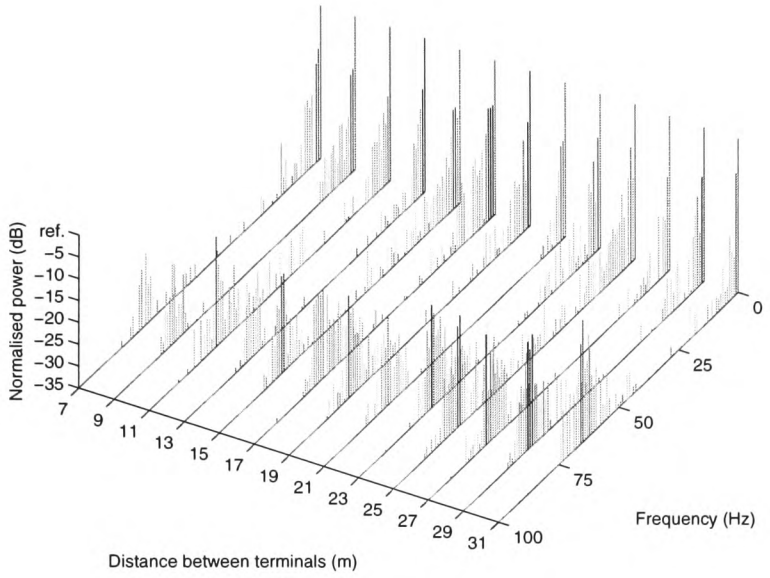

Figure 5-3: Power spectra of the signal envelope received as function of distance between terminals in corridor J2 using a horn to omnidirectional antenna at 11 GHz

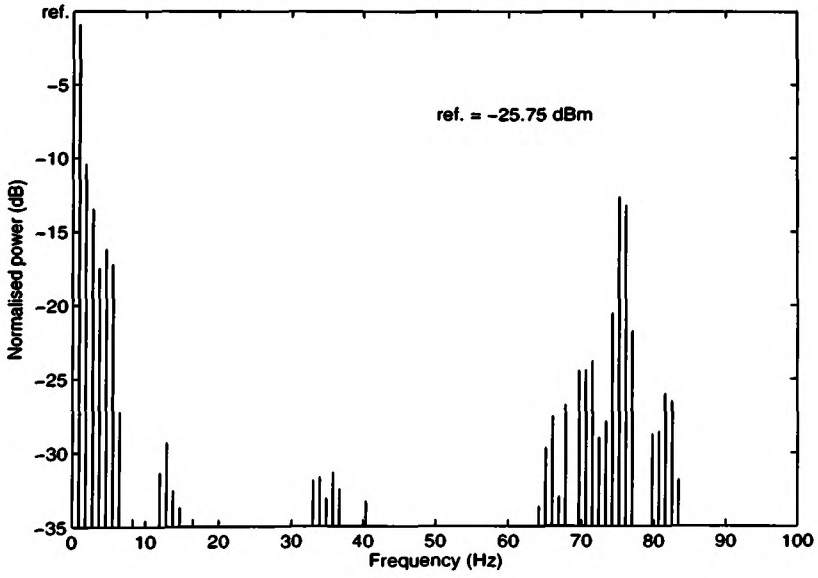

Figure 5-4: Power spectrum of the received signal envelope with the terminals 20 m apart in corridor J2 using a horn to omnidirectional antenna at 11 GHz

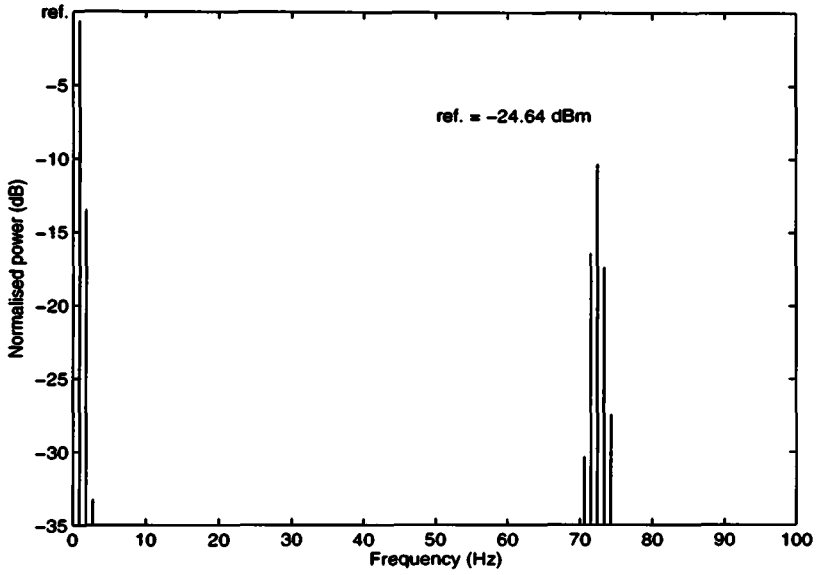

Figure 5-5: Power spectrum of the predicted signal envelope with the terminals 20 m apart in corridor J2 using a horn to omnidirectional antenna at 11 GHz

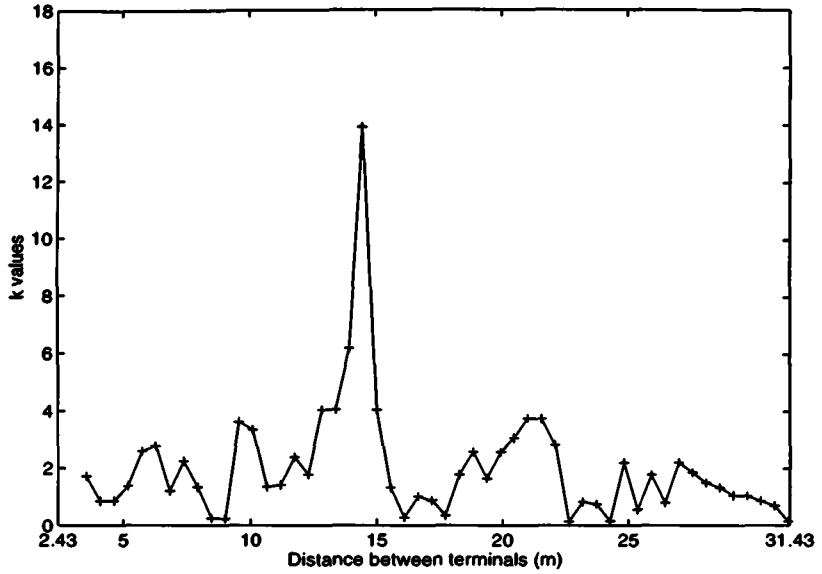

Figure 5-6: K-parameter in the Rice distribution as function of distance between terminals in corridor J2 using a horn to omnidirectional antenna at 11 GHz

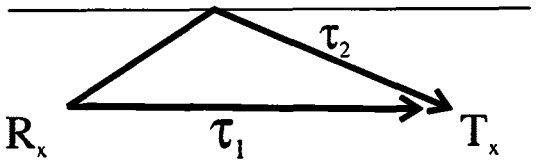

Figure 5-7: Time delay for a two-ray model

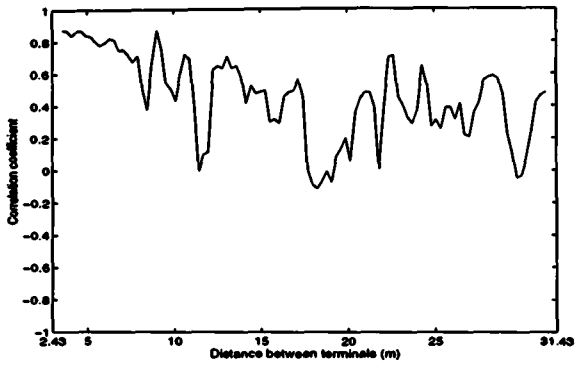

Figure 5-8: Correlation between the envelopes separated by 5 MHz versus distance between terminals

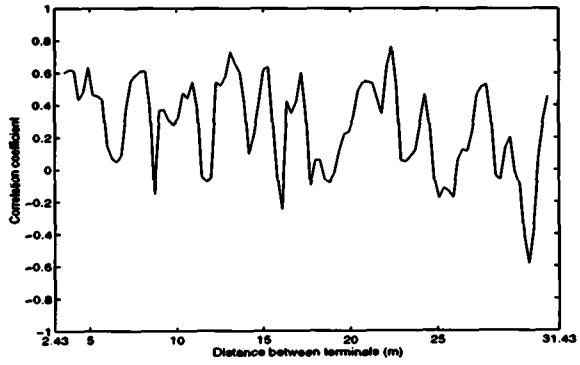

Figure 5-9: Correlation between the envelopes separated by 40 MHz versus distance between terminals

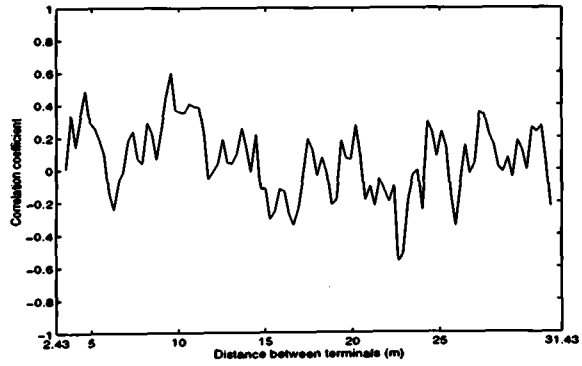

Figure 5-10: Correlation between the envelopes separated by 132 MHz versus distance between terminals

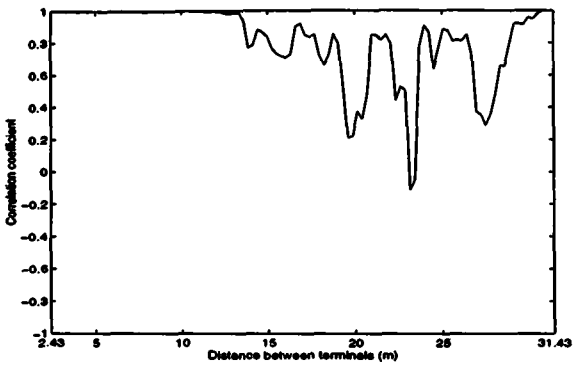

Figure 5-11: Correlation between the predicted envelopes separated by 5 MHz versus distance between terminals

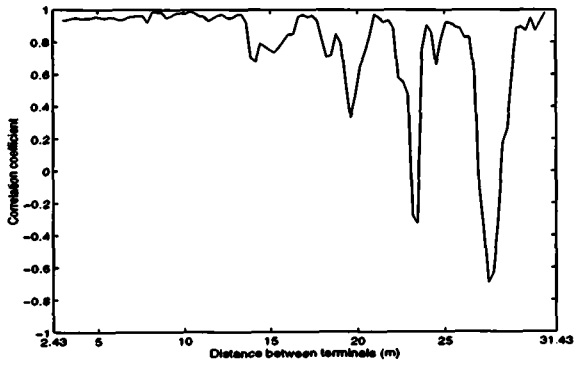

Figure 5-12: Correlation between the predicted envelopes separated by 40 MHz versus distance between terminals

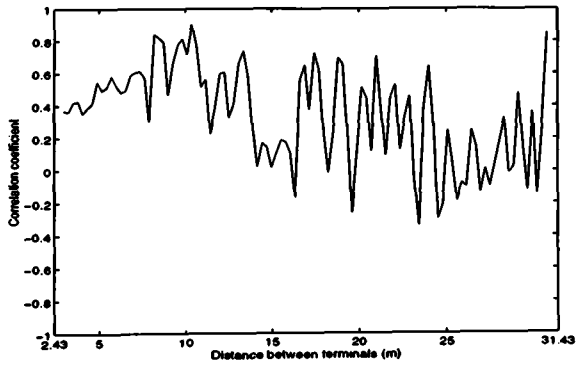

Figure 5-13: Correlation between the predicted envelopes separated by 130 MHz versus distance between terminals

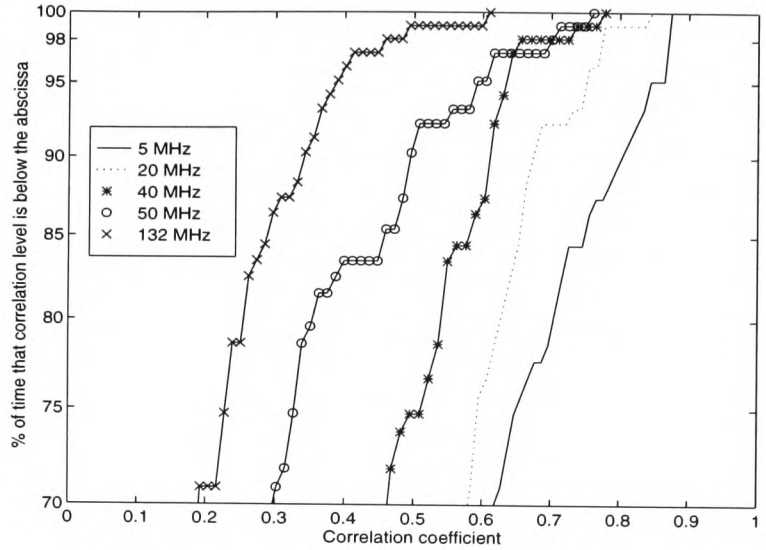

Figure 5-14: Cumulative distribution functions of the correlation coefficient for different frequency spacings in corridor J2 using a horn to omnidirectional antenna at 11 GHz

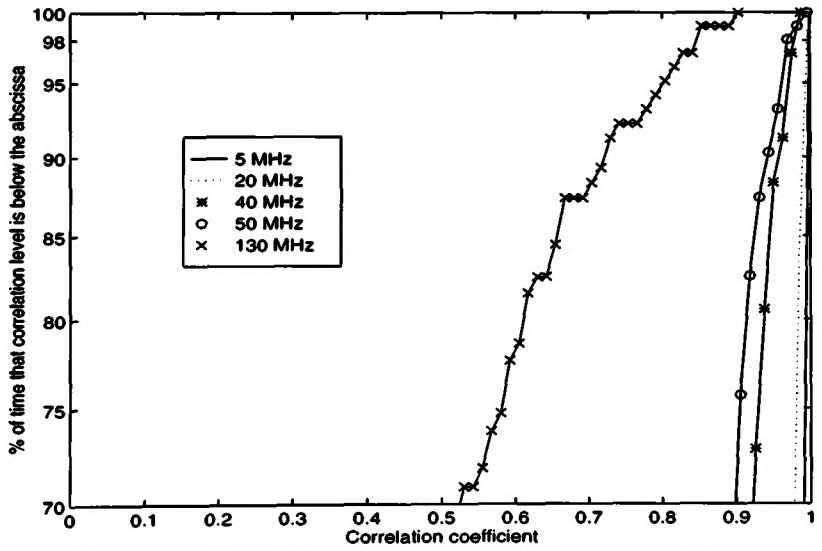

Figure 5-15: Cumulative distribution functions of the predicted correlation coefficient for different frequency spacings in corridor J2 using a horn to omnidirectional antenna at 11 GHz

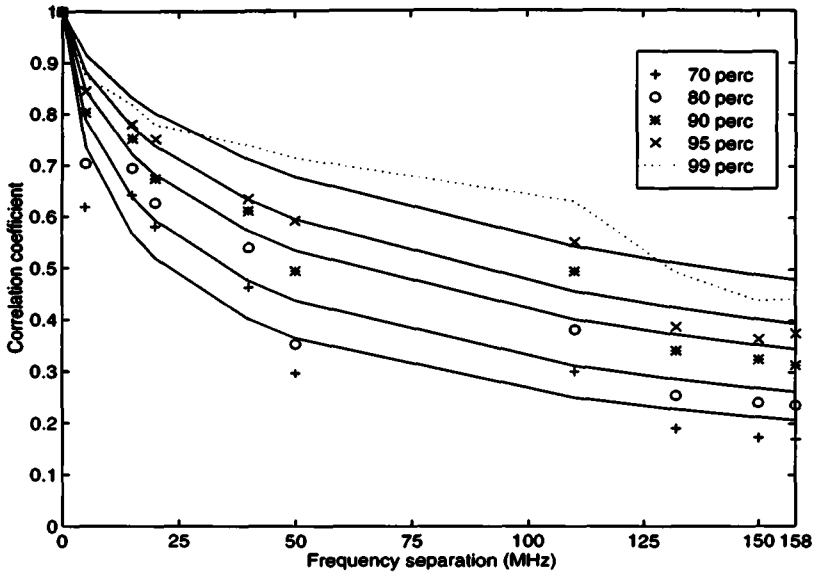

Figure 5-16: Frequency correlation functions measured in corridor J2 using a horn to omnidirectional antenna at 11 GHz

	Percentage of time				
Coherence bandwidth (MHz)	70%	80%	90%	95%	99%
$B_{0.9}$	1.3	1.7	2.5	3.2	3.9
$B_{0.7}$	3.9	8.6	18.3	28.7	59.6
$B_{0.5}$	33.7	42.1	49.5	117.0	131.0

Table 5.2: Coherence bandwidth for 0.5 ($B_{0.5}$), 0.7 ($B_{0.7}$) and 0.9 ($B_{0.9}$) correlation levels computed from the above frequency correlation functions

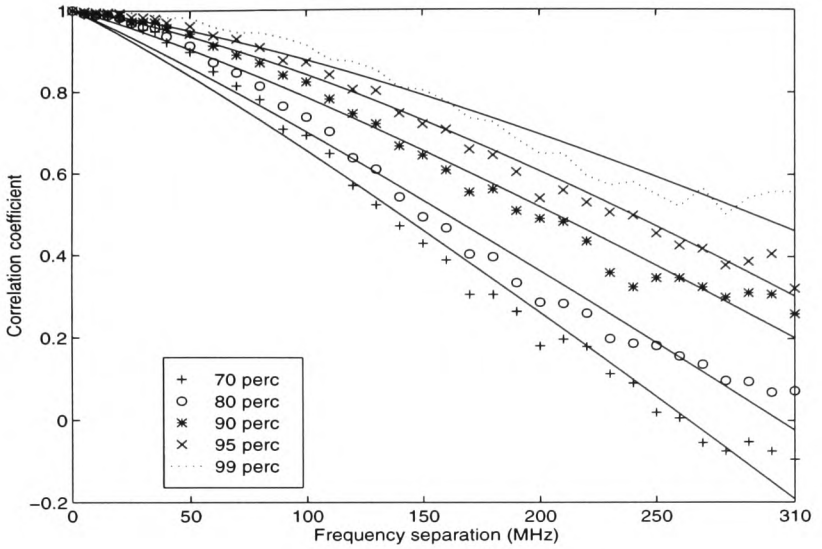

Figure 5-17: Frequency correlation functions predicted in corridor J2 using a horn to omnidirectional antenna at 11 GHz

	Percentage of time				
Coherence bandwidth (MHz)	70%	80%	90%	95%	99%
$B_{0.9}$	49.3	53.3	65.7	82.7	104.0
$B_{0.7}$	95.2	110.3	133.9	161.7	186.5
$B_{0.5}$	134.8	148.9	195.8	240.0	>310

Table 5.3: Coherence bandwidth for 0.5 ($B_{0.5}$), 0.7 ($B_{0.7}$) and 0.9 ($B_{0.9}$) correlation levels computed from the above predicted frequency correlation functions

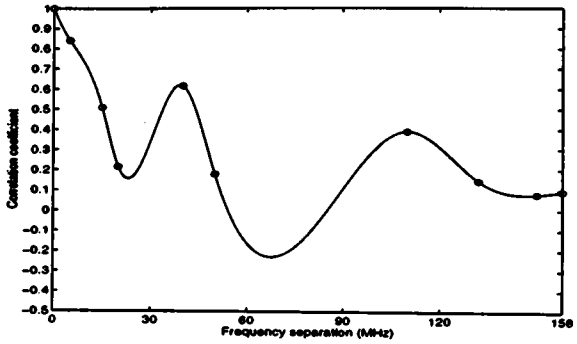

Figure 5-18: Frequency correlation function measured at a distance of 0.8 m from the receiver in corridor J2 using a horn to omnidirectional at 11 GHz

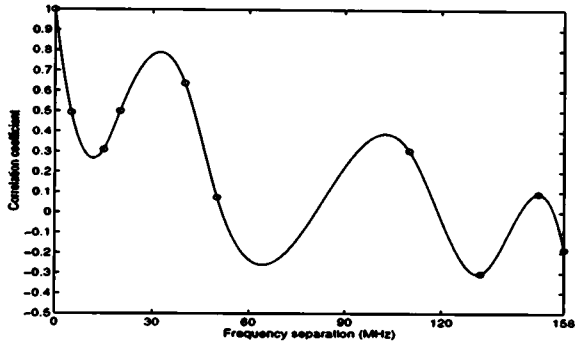

Figure 5-19: Frequency correlation function measured at a distance of 12 m from the receiver in corridor J2 using a horn to omnidirectional at 11 GHz

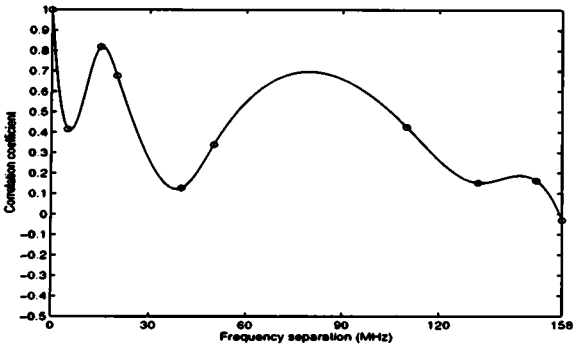

Figure 5-20: Frequency correlation function measured at a distance of 23.2 m from the receiver in corridor J2 using a horn to omnidirectional at 11 GHz

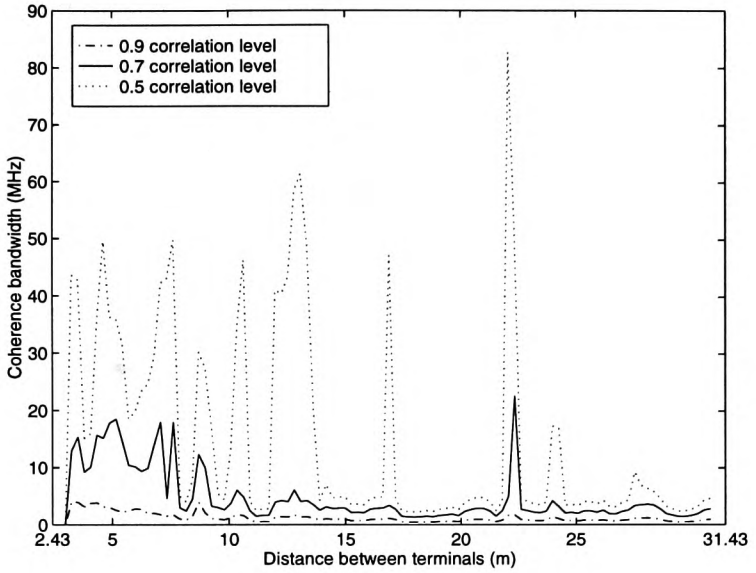

Figure 5-21: Coherence bandwidth for three correlation levels as a function of distance between terminals in corridor J2 using a horn to onmnidirectional antenna at 11 GHz

	Percentage of time				
Coherence bandwidth (MHz)	70%	80%	90%	95%	99%
$B_{0.9}$	1.3	1.7	2.5	3.1	3.9
$B_{0.7}$	3.8	5.9	13.0	15.8	18.5
$B_{0.5}$	16.8	31.8	43.5	49.3	62.0

Table 5.4: Coherence bandwidth for 0.5 ($B_{0.5}$), 0.7 ($B_{0.7}$) and 0.9 ($B_{0.9}$) correlation levels computed from the above coherence bandwidth function

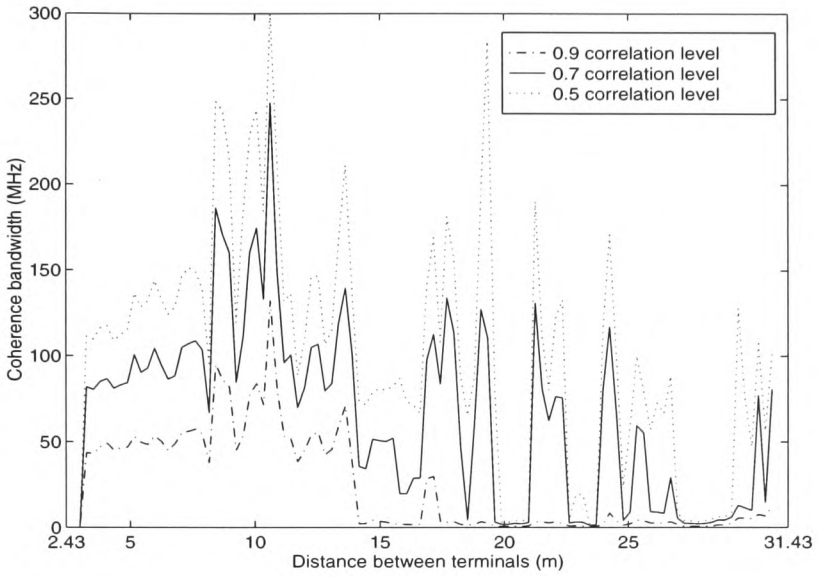

Figure 5-22: Predicted coherence bandwidth for three correlation levels as a function of distance between terminals in corridor J2 using a horn to omnidirectional antenna at 11 GHz

	Percentage of time				
Coherence bandwidth (MHz)	70%	80%	90%	95%	99%
$B_{0.9}$	45.6	52.0	57.7	80.4	96.4
$B_{0.7}$	94.2	106.7	130.4	159.5	188.1
$B_{0.5}$	132.2	146.4	191.1	230.5	284.9

Table 5.5: Coherence bandwidth for 0.5 ($B_{0.5}$), 0.7 ($B_{0.7}$) and 0.9 ($B_{0.9}$) correlation levels computed from the above predicted coherence bandwidth function

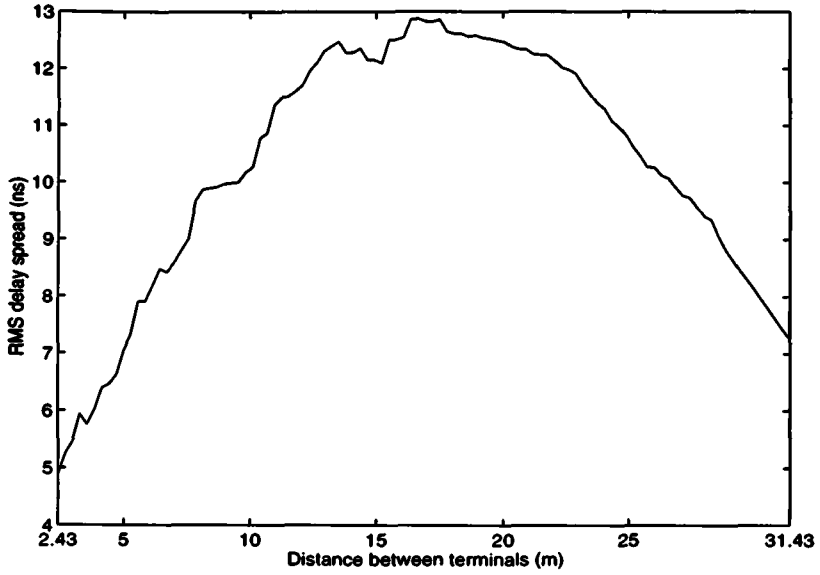

Figure 5-23: Predicted RMS delay spread versus distance between terminals

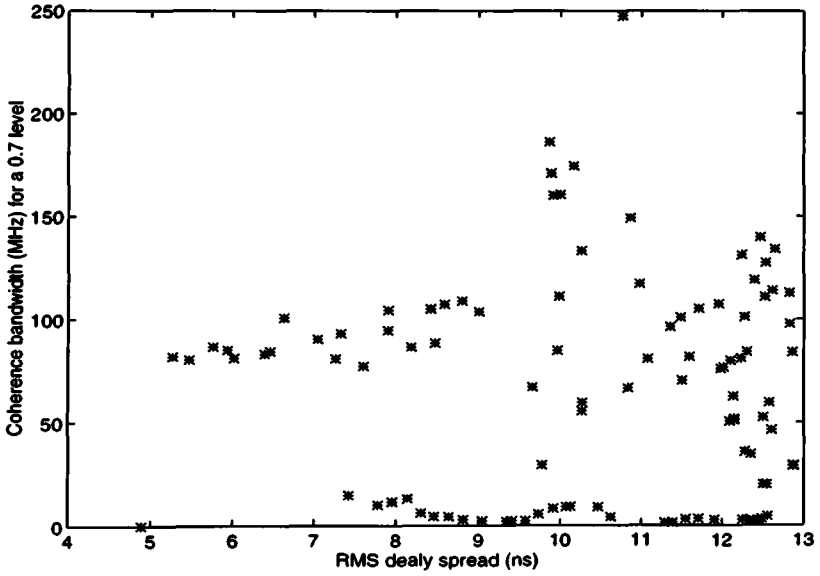

Figure 5-24: Coherence bandwidth for a 0.7 correlation level versus RMS delay spread

5.2.2 Corridor J3

In corridor J3, the measurement campaign considers several frequency separations ranging from 0 to 80 MHz. The received signal envelopes are measured as the transmitter moved 31 m. The receiver, with its antenna set at a height of 1.74 m, was stationary at 0.78 m from wall C as depicted in Figure 4-17 (see section 4.6.2) and 3.66 m from wall B. The transmitter, with its antenna set at a similar height, was located at 0.78 m from wall C and started the run at 5.83 m away from the receiver. This corridor (45 m $\times$ 1.59 m $\times$ 2.69 m) is a little narrower than corridor J2. The principal difference between corridor J2 and corridor J3 is that one of the sidewalls of J2 is mainly made of glass windows while in corridor J3 both sidewalls are made of the same material which is mainly metal as already discussed in section 4.6.2.

In this corridor, ground reflections start when the transmitter is at 18.9 m from the receiver. However, ceiling reflections start when the terminals are 11.6 m apart. The metal surfaces provide strong reflected components which maintain a high signal level. This type of corridor may be assimilated to a waveguide which guide all the power to the receiver with a smaller mean power loss compared to that reported for corridor J2. This phenomena has been well understood and explained in [17] [18]. In this corridor the mean power level of the received signal envelopes, shown in Figure 5-25, decays with an exponent of 1.0.

For an ideal environment, the predicted signal envelopes are calculated over the same distances as the measured ones using the coordinates of the terminals outlined in the above paragraph. The predicted signal envelopes, with a frequency separation of 5 MHz, are shown in Figure 5-26. The frequency spectra of the measured envelopes are presented as a function of distance between the terminals and given in Figure 5-27. The low frequency part of the spectra measured in corridor J3 , Figure 5-27, exhibit additional low frequency components compared to that obtained in corridor J2. This is due to the presence of the metal sidewalls giving rise to multiple reflections. Also the proportion of fast fading measured in corridor J3 is larger because of strong reflections coming from the endwall of the corridor after being reflected from the sidewalls.

The value of the k-factor in the Rice distribution measured as a function of distance between the terminals is shown in Figure 5-28 and varies from about 0.2 to maximum value of 4.

The frequency correlation function measured using all the correlation values obtained along the transmitter route is given in Figure 5-29. The best fit indicates that the correlation levels decrease with increasing frequency spacings in the same manner to the results of corridor J2. Values of the coherence bandwidth obtained from Figure 5-29, for different levels of correlation, are given in Table 5.6. This table shows that the coherence bandwidth values are smaller than those measured in corridor J2 (see Table 5.2). For instance, the coherence bandwidth required to achieve a level of correlation below 0.7 for 95 % of the time in corridor J3 is 11.7 MHz, whereas in corridor J2 a coherence bandwidth of 28.7 MHz is needed to achieve the same level of correlation. The reason of these lower values is the presence of the metal walls giving rise to additional multiple sidewalls reflections as explained earlier.

The coherence bandwidth, corresponding to various correlation levels, has also been computed as a function of distance. Results for a correlation level of 0.9 are given in Figure 5-30. Values of the coherence bandwidth obtained from this second method are given in Table 5.7. These results exhibit similar behaviour to those described for corridor J2. The general trend confirms a larger coherence bandwidth at small distances between terminals.

The predicted frequency correlation function obtain for this corridor is given in Figure 5-31, with the values of the coherence bandwidth given in Table 5.8. It is evident that, when compared to results shown in Figure 5-17 and Table 5.3 for corridor J2, the correlation levels for corridor J3 are higher than those computed for corridor J2. This results in larger values of the coherence bandwidth. This is explained by the fact that in the wider corridor (corridor J2), reflections off the sidewalls have longer differential time delays with respect to the direct component than those in the narrower corridor (corridor J3). Therefore, the frequency separations required to decorrelate these signals will be smaller. The difference between the measured and the simulated results is due to the fact

that the model does not take into account the presence of different partition materials and reflections higher than the 3^{rd} order are not considered.

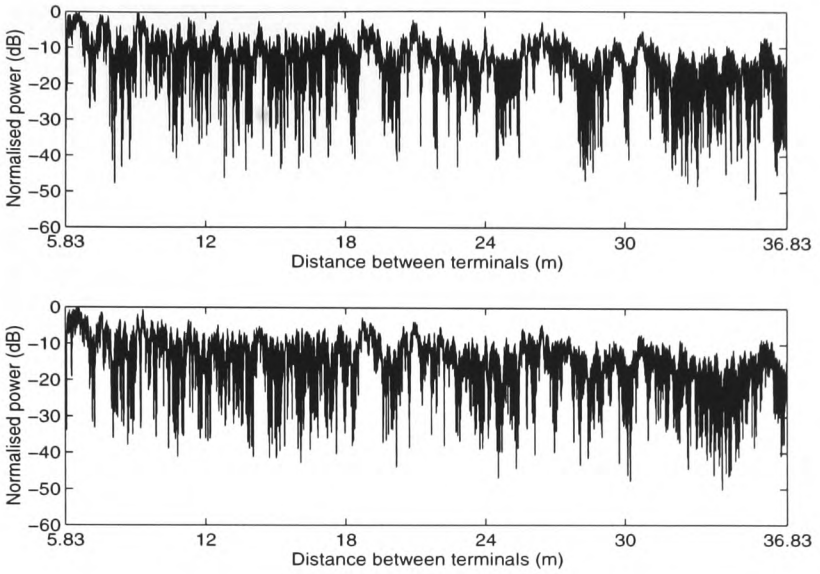

Figure 5-25: Received envelopes for a frequency spacing of 5 MHz in corridor J3 using a horn to omnidirectional antenna at 11 GHz

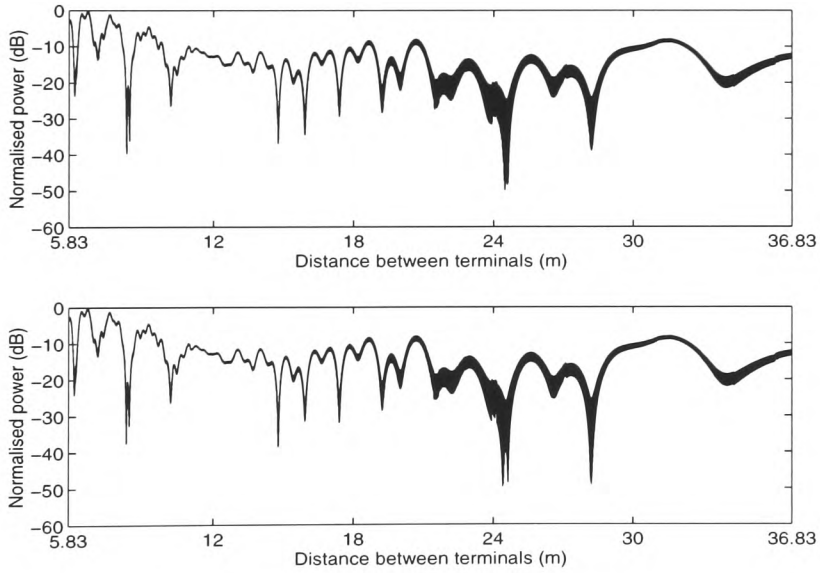

Figure 5-26: Predicted envelopes using a third order ray-tracing model computed with a frequency spacing of 5 MHz in corridor J3 using a horn to omidirectional antenna at 11 GHz

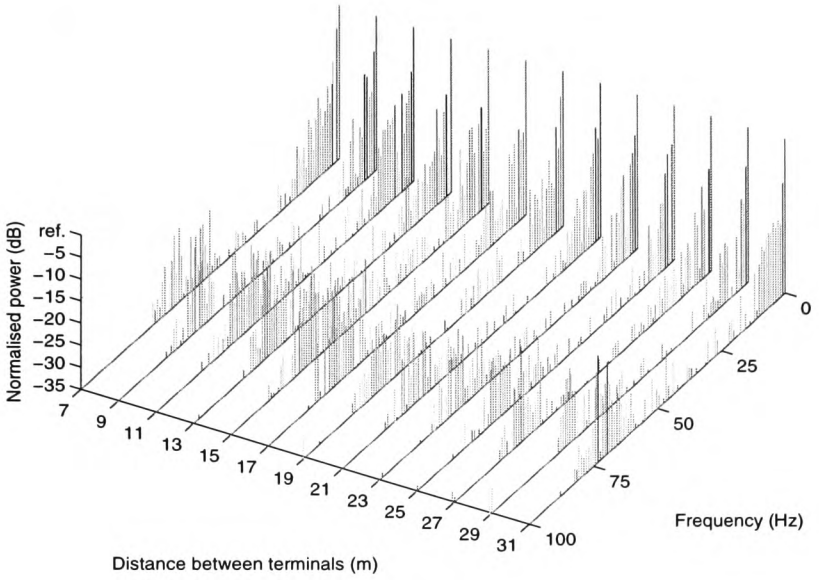

Figure 5-27: Power spectra of the signal envelope as function of distance between terminals in corridor J3 using a horn to omnidirectional antenna at 11 GHz

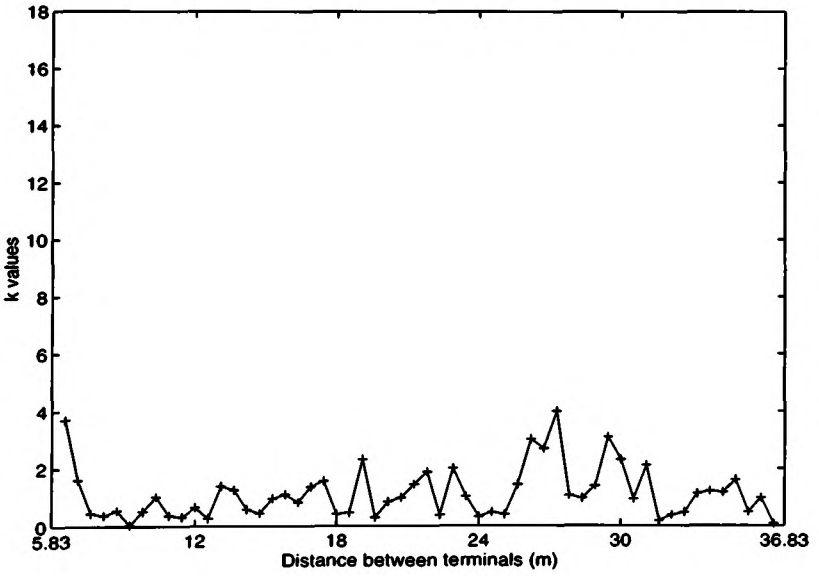

Figure 5-28: K factor in the Rice distribution as function of distance between terminals in corridor J3 using a horn to onmidirectional antenna at 11 GHz

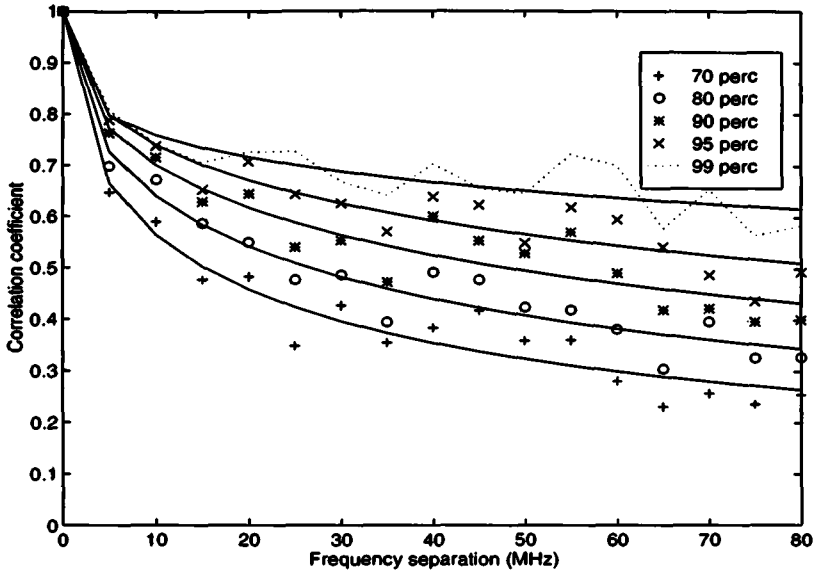

Figure 5-29: Frequency correlation functions measured in corridor J3 using a horn to omnidirectional antenna at 11 GHz

	Percentage of time				
Coherence bandwidth (MHz)	70%	80%	90%	95%	99%
$B_{0.9}$	1.3	1.5	1.9	2.2	2.5
$B_{0.7}$	3.8	4.6	9.9	11.7	12.4
$B_{0.5}$	10.2	28.3	47.6	65.8	>80

Table 5.6: Coherence bandwidth for 0.5 ($B_{0.5}$), 0.7 ($B_{0.7}$) and 0.9 ($B_{0.9}$) correlation levels computed from the above frequency correlation functions

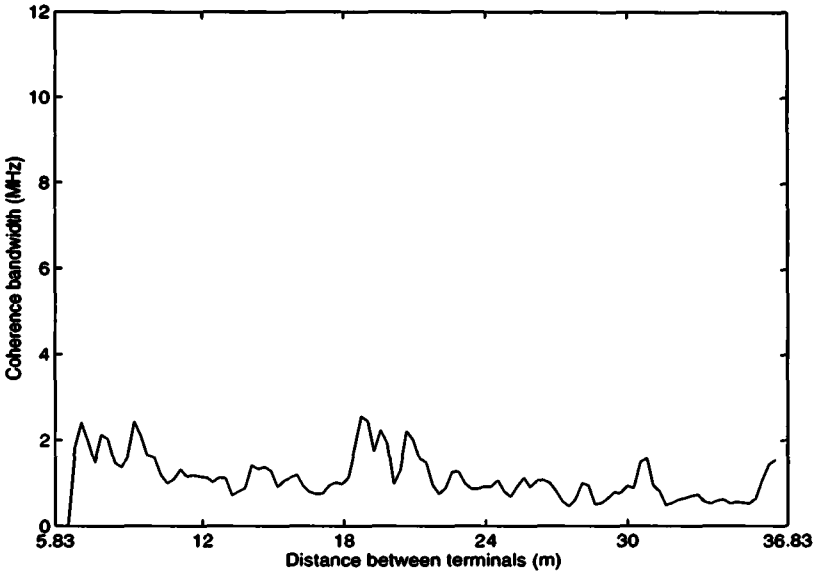

Figure 5-30: Coherence bandwidth for a correlation level of 0.9 versus distance between terminals in corridor J3 at 11 GHz

	Percentage of time				
Coherence bandwidth (MHz)	70%	80%	90%	95%	99%
$B_{0.9}$	1.3	1.5	1.9	2.2	2.5
$B_{0.7}$	3.8	4.5	7.5	11.2	12.2
$B_{0.5}$	8.7	11.6	23.9	34.1	58.9

Table 5.7: Coherence bandwidth for 0.5 ($B_{0.5}$), 0.7 ($B_{0.7}$) and 0.9 ($B_{0.9}$) correlation levels for the corridor J3 using a horn to omnidirectional antenna configuration at 11 GHz

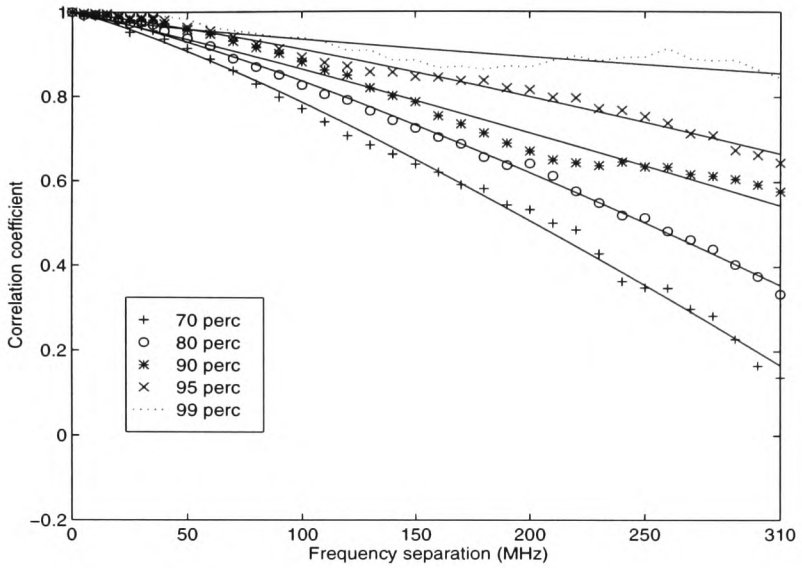

Figure 5-31: Frequency correlation functions predicted in corridor J3 using a horn to omnidirectional antenna at 11 GHz

	Percentage of time				
Coherence bandwidth (MHz)	70%	80%	90%	95%	99%
$B_{0.9}$	53.7	65.8	92.8	123.1	307.8
$B_{0.7}$	122.9	169.9	269.2	>310	>310
$B_{0.5}$	268.6	>310	>310	>310	>310

Table 5.8: Coherence bandwidth for 0.5 ($B_{0.5}$), 0.7 ($B_{0.7}$) and 0.9 ($B_{0.9}$) correlation levels computed from the above predicted frequency correlation functions

5.2.3 Corridor H

In this microcell, the frequency separations used during the measurement campaign were ranging from 0 to 110 MHz. The received envelopes are measured over a distance of 21 m. The receiver, with its antenna set at a height of 1.71, was located at 0.85 m from wall A and 0.6 m from wall D as depicted in Figure 4-19 (see section 4.6.3). The transmitter, with its antenna set at the same height as the receiver, was located at 0.86 m from Wall A and started the run at 2.22 m away from the receiver. This corridor is the smallest in length of the three corridors under consideration (25.66 m $\times$ 1.66 m $\times$ 3.03 m). The sidewalls of this corridor are made of metal as in corridor J3 and the endwall (Wall B) is made of wood, as already discussed in section 4.6.3.

Due to the fact that the transmitter was moved along a straight line positioned in the middle of the corridor reflections from both sidewalls start occurring when the terminals are about 3.2 m apart. Ground and ceiling reflections start contibuting to the received signal when the terminals are 19.4 m and 14.9 m apart respectively. In this corridor the mean power level decays with an exponent of 1.2.

The measured and predicted received envelopes, with a frequency separation of 5 MHz, are shown in Figure 5-32 and Figure 5-33 respectively. In this corridor, because of its shortest length compared to the other two corridors, the proportion of fast fading is larger. The frequency spectra, depicted in Figure 5-34, show extra low frequency and high frequency components when compared to the frequency spectra of corridor J2 (Figure 5-3). The predicted envelopes also illustrate that fast variations are predominant in the envelopes at an earlier stage than the predicted ones in the two previous corridors.

The value of the k-factor in the Rice distribution measured as a function of distance between the terminals is shown in Figure 5-35. The value of k varies from about 0.2 to a maximum value of 7.

Figure 5-36 represents the frequency correlation functions of the measured envelopes for a separation ranging from 0 to 110 MHz. Values of the coherence bandwidth, estimated from this figure for different levels of correlation, are summarised in Table 5.9. This table indicates that the coherence bandwidth values are smaller than those measured in corridor

J2 (see Table 5.2) but higher than the results of corridor J3 (see Table 5.6). It is interesting to note that some values obtained in the corridor H and corridor J3 for correlation levels of 0.9 and 0.7 at low percentages of time are similar. In both corridors, the coherence bandwidth required to achieve a level of correlation below 0.7 is 3.8 MHz and 4.6 MHz for 70% and 80% of the time respectively, and for a correlation below 0.9, the coherence bandwidth decreases to 1.3 MHz and 1.5 MHz respectively. However for a more severe percentage of time, for instance 99%, the coherence bandwidth required to achieve a correlation below 0.9 is 3.1 MHz for corridor H, 2.5 MHz for corridor J3 and 3.9 MHz for corridor J2. In general, when considering the 95 % of time criteria, this microcell requires a coherence bandwidth of 20.6 MHz to achieve a correlation below 0.7 whereas a smaller value of 11.7 MHz is needed in corridor J3 and a larger value of 28.7 MHz is required in corridor J2.

The coherence bandwidth measured, for a correlation level of 0.9, as a function of distance is shown in Figure 5-37. Results computed using this second method are summarised in Table 5.10. The coherence bandwidth exhibits fluctuations over distance ranging from 0.5 to 3 MHz.

The predicted frequency correlation function in this corridor is shown in Figure 5-38 with the values of the coherence bandwidth given in Table 5.11. The value of the coherence bandwidth giving a correlation below 0.5 at 99 % of the time could not be deduced because its value is larger than the maximum frequency separation used in the simulation. The lower values of correlation for this corridor H , compared to those computed for corridor J3, is because corridor H is slightly wider than corridor J3. Consequently as explained in section 5.2.2 reflections off the sidewalls have longer differential time delays with respect to the direct component. Additionally, the contribution of reflections off the endwall, which require smaller frequency separation to decorrelate, is more important. The combination of these two mechanisms results in a smaller coherence bandwidth for corridor H than corridor J3.

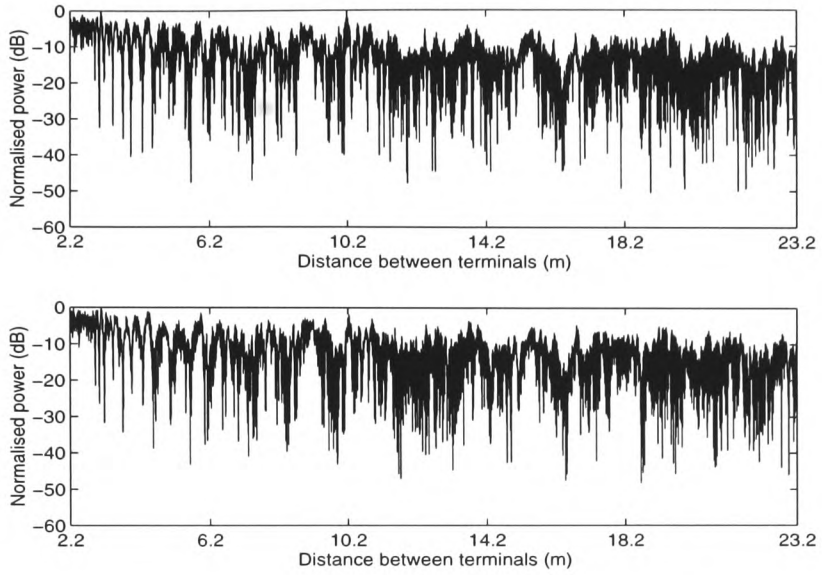

Figure 5-32: Received envelopes for a frequency spacing of 5 MHz in corridor H using a horn to omnidirectional antenna at 11 GHz

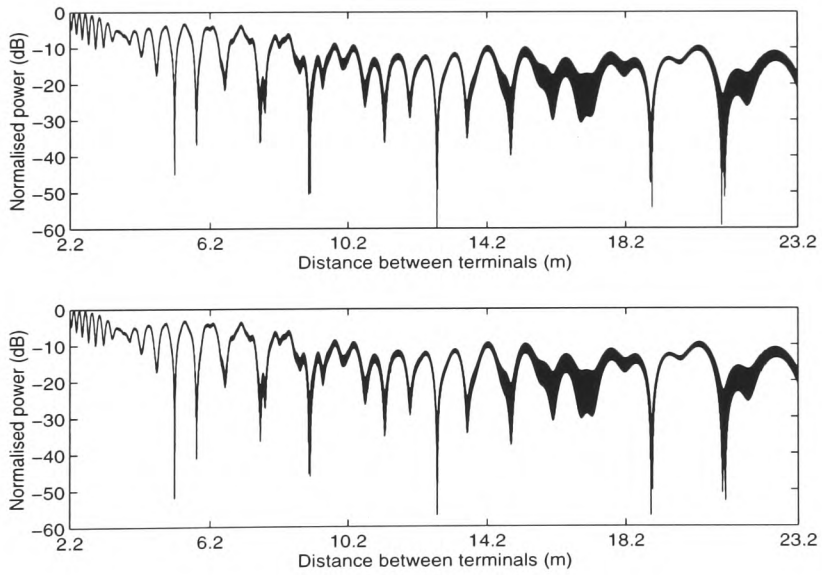

Figure 5-33: Predicted envelopes using a third order ray-tracing model computed with a frequency spacing of 5 MHz in corridor H using a horn to omidirectional at 11 GHz

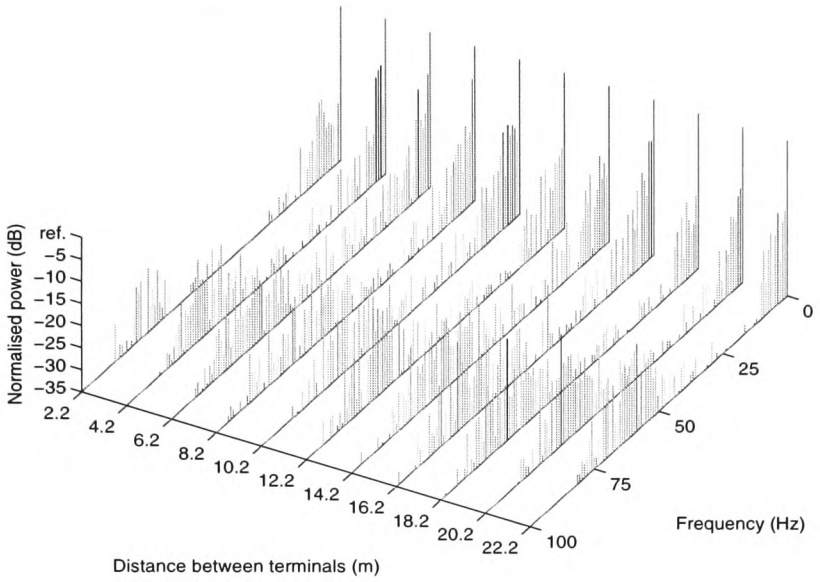

Figure 5-34: Power spectra of the signal envelope as a function of distance between terminals in corridor H using a horn to omnidirectional antenna at 11 GHz

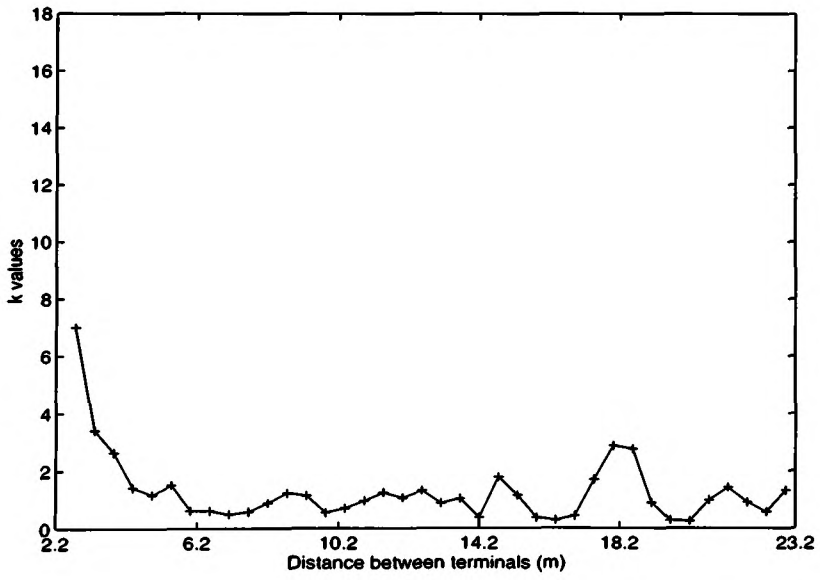

Figure 5-35: K factor in the Rice distribution as a function of distance between terminals in corridor H using a horn to omnidirectional antenna at 11 GHz

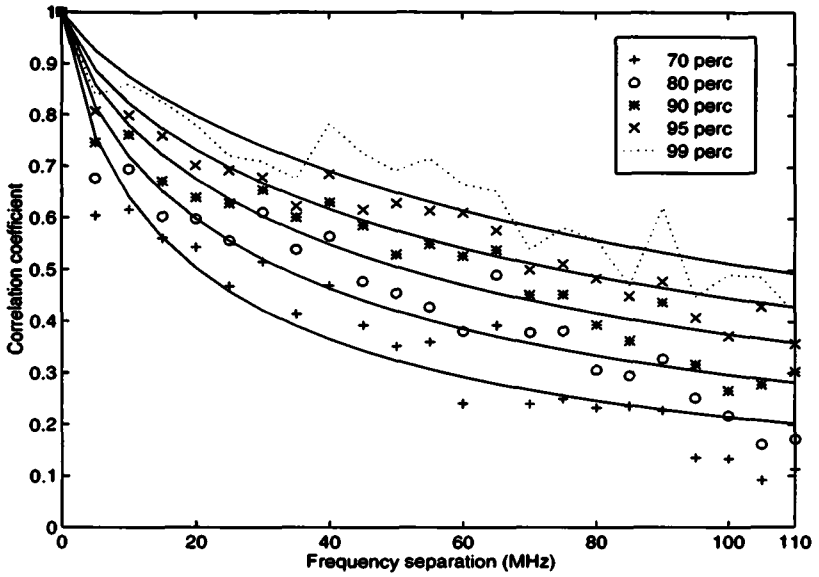

Figure 5-36: Frequency correlation function measured in corridor H using the horn to omnidirectional antenna at 11 GHz

	Percentage of time				
Coherence bandwidth (MHz)	70%	80%	90%	95%	99%
$B_{0.9}$	1.3	1.5	1.9	2.6	3.1
$B_{0.7}$	3.8	4.6	13.4	20.6	31.4
$B_{0.5}$	22.8	43.7	67.3	77.2	83.4

Table 5.9: Coherence bandwidth for 0.5 ($B_{0.5}$), 0.7 ($B_{0.7}$) and 0.9 ($B_{0.9}$) correlation levels computed from the above frequency correlation functions

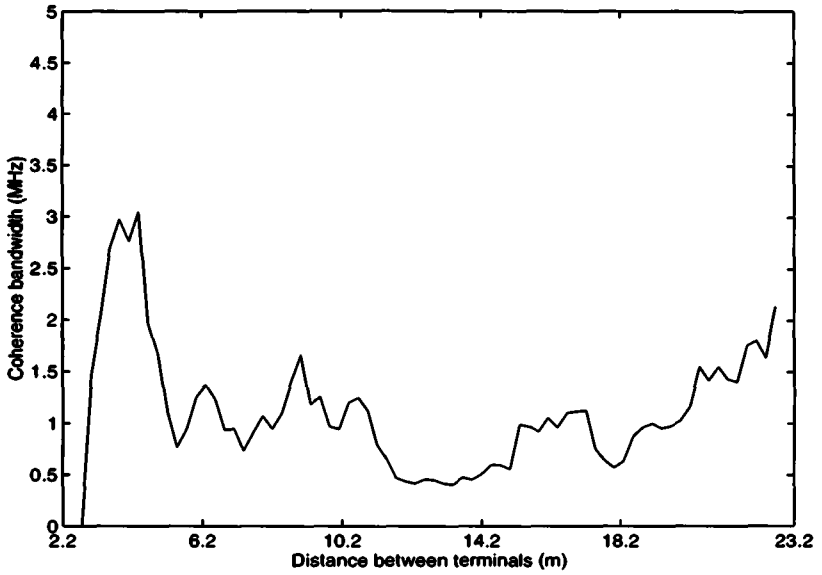

Figure 5-37: Coherence bandwidth at a correlation level of 0.9 versus distance between terminals in corridor H at 11 GHz

	Percentage of time				
Coherence bandwidth (MHz)	70%	80%	90%	95%	99%
$B_{0.9}$	1.2	1.4	1.8	2.6	3.0
$B_{0.7}$	3.8	4.4	6.2	18.1	23.2
$B_{0.5}$	9.2	14.0	43.4	67.2	76.5

Table 5.10: Coherence bandwidth for 0.5 ($B_{0.5}$), 0.7 ($B_{0.7}$) and 0.9 ($B_{0.9}$) correlation levels computed fron the coherence bandwidth functions in corridor H using a horn to omnidirectional antenna at 11 GHz

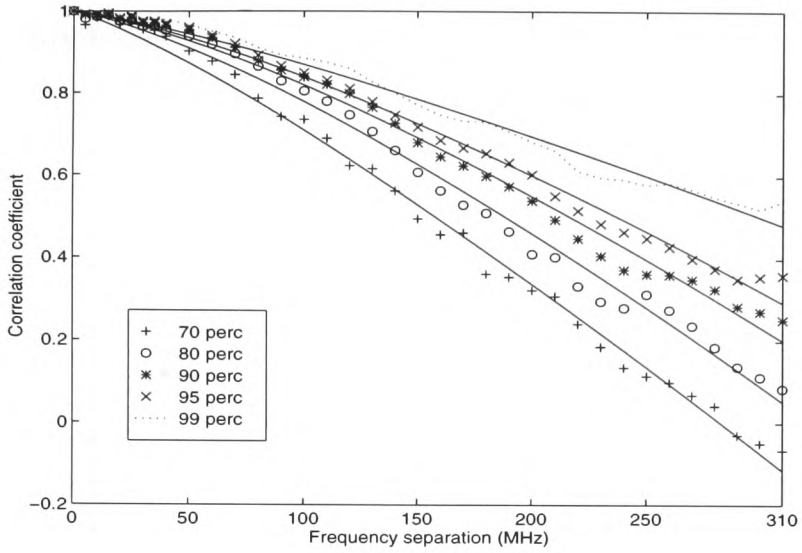

Figure 5-38: Frequency correlation function predicted in corridor H using the horn to omnidirectional antenna at 11 GHz

	Percentage of time				
Coherence bandwidth (MHz)	70%	80%	90%	95%	99%
$B_{0.9}$	50.8	68.0	73.2	77.2	85.9
$B_{0.7}$	107.9	131.7	145.9	155.9	193.4
$B_{0.5}$	149.4	182.4	208.9	225.4	>310

Table 5.11: Coherence bandwidth for 0.5 ($B_{0.5}$), 0.7 ($B_{0.7}$) and 0.9 ($B_{0.9}$) correlation levels from the above predicted frequency correlation functions

5.2.4 Interim summary

Measurements in long narrow corridors have shown that the amplitude variations of the received signal envelope are caused by reflections from all surfaces of the enclosed environment. The low frequency variation is caused by reflections from the sidewalls, floor and ceiling whereas reflections coming from surfaces ahead of the transmitter cause fast variations. The distributions of the signal envelopes are found to be Rician with the value of the power ratio of the line-of-sight to that in the reflected ray varying significantly with the distance between terminals

The coherence bandwidth measured in a long narrow corridor with metal sidewalls is lower than that obtained in a corridor of similar dimensions but with metal and glass sidewalls. This is due to the additional multiple sidewall reflections and larger proportion of fast fading measured in the corridor with metal sidewalls.

Measurements made under identical conditions, but in a shorter corridor with metal sidewalls have shown larger coherence bandwidth compared to that obtained in the longer corridor with similar sidewalls material. This is due to the lower time delays associated with rays in the shorter corridor.

5.2.5 Room B68

The characteristic of the room (12.8 m $\times$ 6.92 m $\times$ 2.6 m) has been described in details in section 4.6.4. The receiver,with its antenna set at a height of 1.73 m, was located at 0.41 m from wall A and 0.87 m from wall D. The transmitter, with its antenna set at the same height as the receiving one, was moved along a diagonal which made an angle of 22.59° with wall A. The received envelopes were recorded over a distance of 8 m. The starting point of the mobile station was at 1.81 m and 3.86 m from wall A and D respectively. This is equivalent to a distance between terminals of 3.3 m. The measurements described here were made with the room empty of furniture. Wall B presents a smooth surface made of plaster whereas its adjacent wall, Wall C, is composed of windows in alcoves and electrical metal heaters.

Only one set of antennas is used and the horn to omnidirectional antenna configuration

was chosen. The use of the horn antenna at the stationary receiver suppresses single reflections from wall A, C and D as depicted in Figure 4-21. However higher order reflections from Wall C start occurring at 6.4 m from Wall B. Double reflections from wall D-B and B-C add to the received signal strength. Due to the beamwidth of the omnidirectional antenna there are no reflections coming from the ground and the ceiling. The measured received envelopes, with a frequency separation of 5 MHz, are displayed in Figure 5-39. It can be seen that the signal envelopes exhibit a low frequency component superimposed on which is a higher amplitude variation. In comparison to the envelopes shown for the three corridors, it can clearly be seen that the geometry of this microcell and terminals location result in less severe multipath fading. Figure 5-40 represents the predicted signal envelopes computed for a frequency separation of 5 MHz.

The power spectra of the received signal envelopes have been computed and expressed as a function of distance between the terminals as given in Figure 5-41. These spectra are somewhat different to those measured in the corridor. This suggests that the angle of arrivals of the rays are different. The spectra show that high frequency components become significant when the transmitter is moved away from the receiver. This is because single reflections from Wall B become stronger as this wall is approached. The low frequency part of the spectra is due to double reflections from Walls D-B. The highest frequency parts are caused by single reflections off Wall B and double reflections off Wall B after being reflected from Wall C. It is noted that no frequency components are found above twice the maximum Doppler frequency (73 Hz).

The value of the k-factor in the Rice distribution measured as a function of distance between the terminals is shown in Figure 5-42. The behaviour of this function has a trend different to that measured in the corridors. It can be clearly seen that, at smaller distances, the envelope is Rician and becomes Rayleigh as the distance between terminals increases. This is explained by the fact that, at the beginning, a strong direct ray with weak reflections contribute to the signal envelope, while at larger distances rays become more significant resulting in a near Rayleigh distribution.

The frequency correlation function obtained at various percentages of time is shown

in Figure 5-43 with the values of the coherence bandwidth given in Table 5.12. The frequency correlation functions in the room are somewhat different to those measured in the three corridor. The most significant of these results is that the actual measured correlation values exhibit strong fluctuation with frequency separation and do not exhibit a monotonously decreasing trend. This behaviour is similar to that obtained from the ray-tracing predictions as shown in Figure 5-45. Values of the predicted coherence bandwidth are given in Table 5.12. All the values of coherence bandwidth measured in the room are smaller than those obtained for corridor J2. However, when compared to corridor J3 and H, no consistent conclusions may be drawn, although in general, the values for the room are much smaller. It may be noted that the coherence bandwidth required to achieve a level of correlation below 0.7 for 95 % of the time in the room is 7 MHz while it is 11.7 MHz and 20.6 MHz for corridor J3 and corridor H respectively.

The coherence bandwidth measured, as a function of distance, is given in Figure 5-44 with the values of the coherence bandwidth given in Table 5.13. On the contrary to the results in the corridors, the coherence bandwidth does not experience large fluctuations and may be characterised as a 'flat' function of distance.

It can be seen that the values of the coherence bandwidth obtained using this second method are not significantly different to those computed from the frequency correlation functions (see Table 5.12). This is because the frequency correlation function in such microcell is not a monotonously decreasing one. As in the previous environments, the predicted coherence bandwidth values are larger than the measured ones.

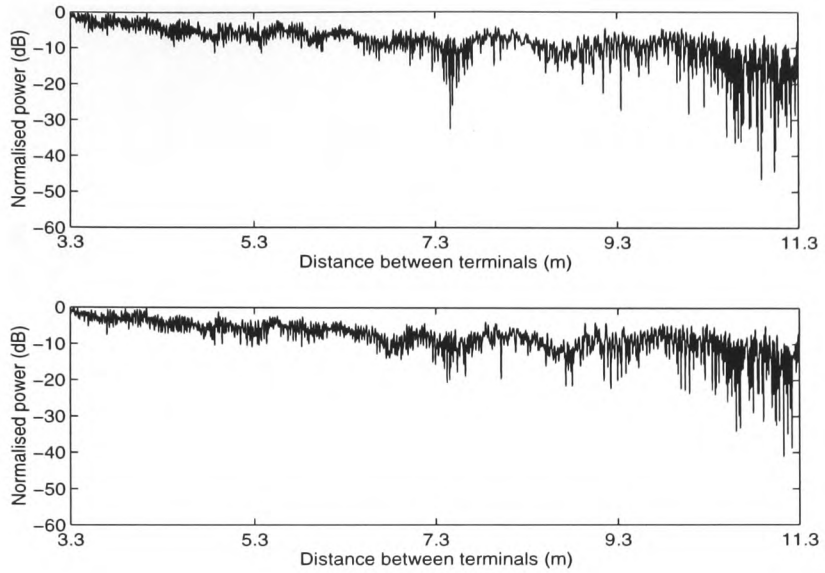

Figure 5-39: Received envelopes for a frequency spacing of 5 MHz in room B68 empty using a horn to omnidirectional antenna at 11 GHz

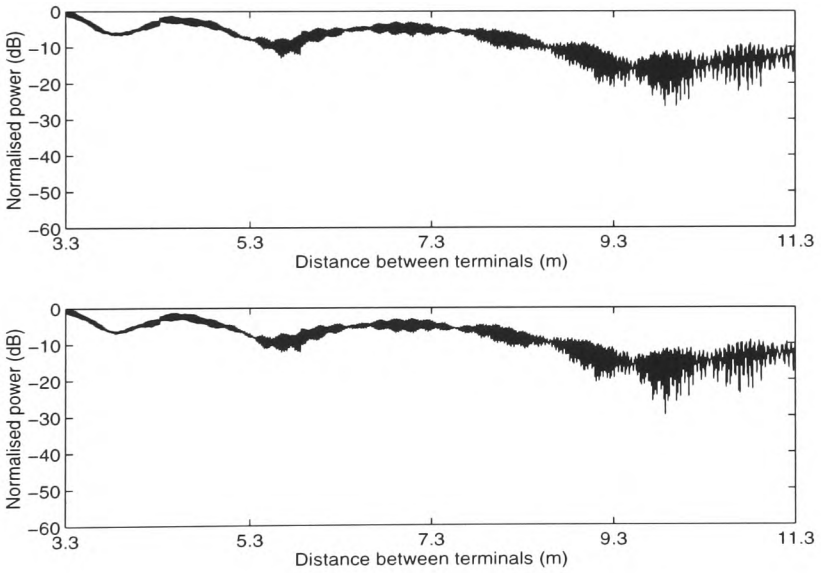

Figure 5-40: Predicted envelopes using a third order ray-tracing model computed using a frequency separation of 5 MHz for the room B68 using a horn/omidirectional configuration at 11 GHz

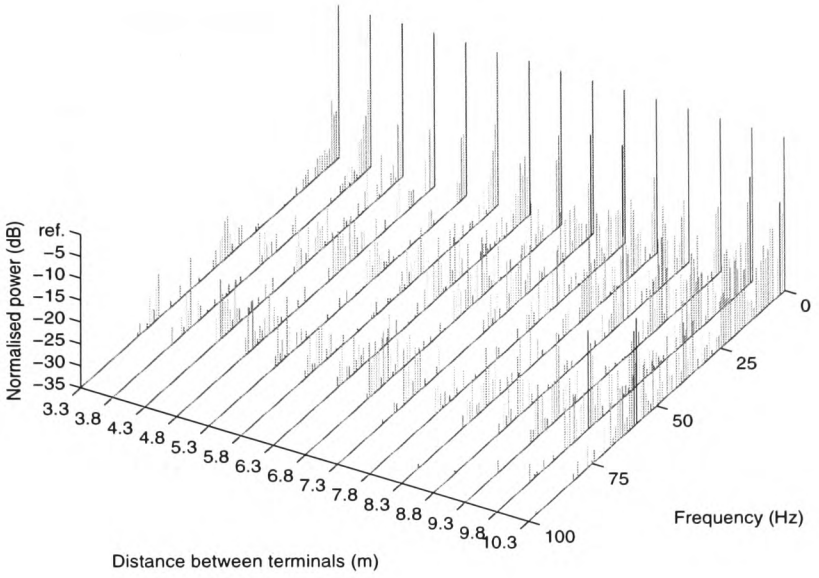

Figure 5-41: Power spectra of the signal envelopes as function of distance for B68 empty using a horn to omnidirectional antenna configuration

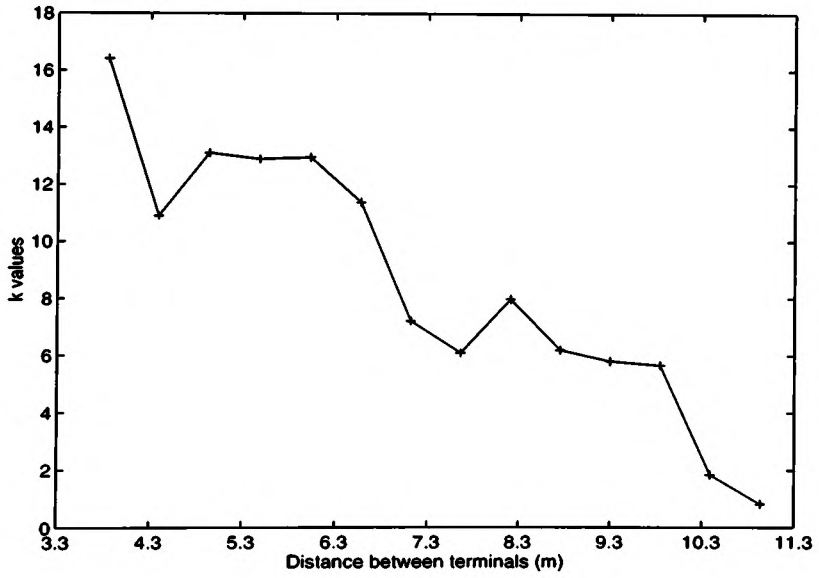

Figure 5-42: K factor in the Rice distribution with distance for B68 empty at 11 GHz using a horn to omnidirectional antenna configuration

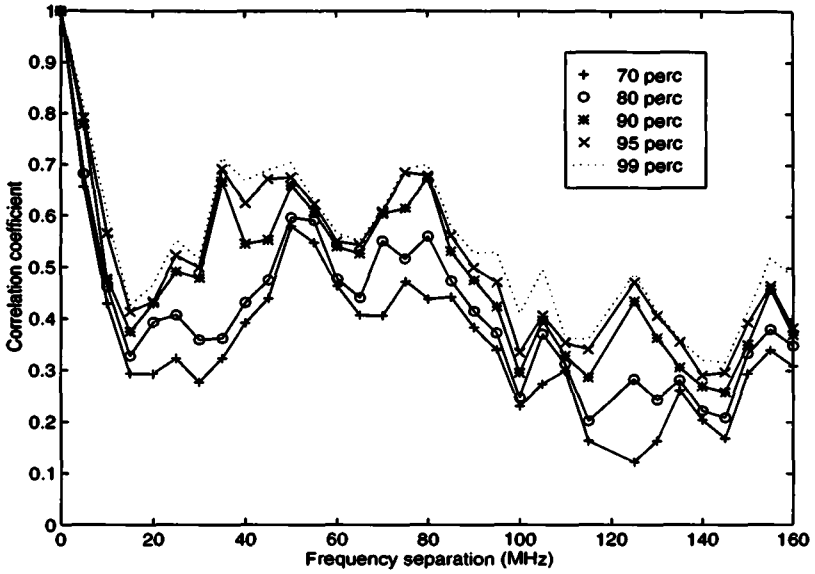

Figure 5-43: Frequency correlation function for different percentage of time for the room B68 empty using a horn to omnidirectional antenna configuration at 11 GHz

	Percentage of time				
Coherence bandwidth (MHz)	70%	80%	90%	95%	99%
$B_{0.9}$	1.4	1.6	2.2	2.4	2.7
$B_{0.7}$	4.3	4.7	6.3	7.0	7.7
$B_{0.5}$	8.4	9.1	9.6	12.1	12.9

Table 5.12: Coherence bandwidth for 0.5 ($B_{0.5}$), 0.7 ($B_{0.7}$) and 0.9 ($B_{0.9}$) correlation levels for the room B68 empty using a horn to omnidirectional antenna configuration at 11 GHz

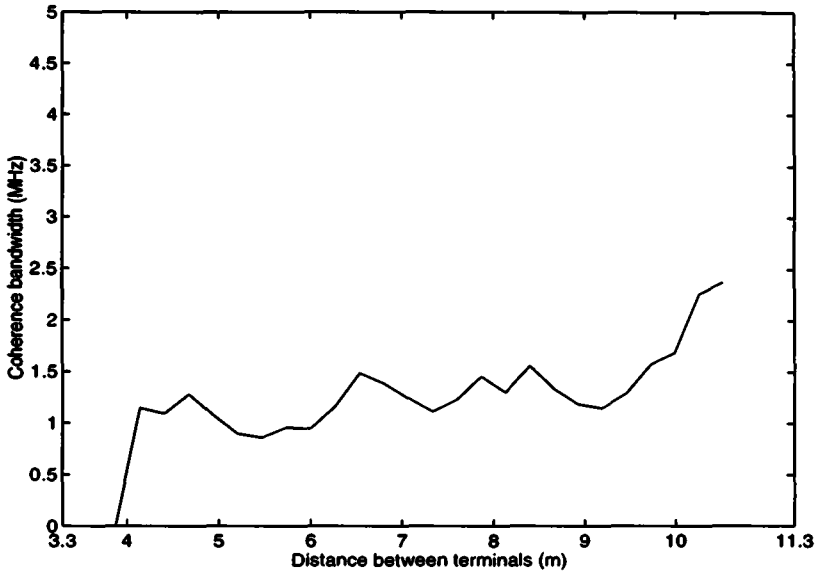

Figure 5-44: Coherence bandwidth at a correlation level of 0.9 versus distance between the terminals using a horn to omnidirectional antenna configuration for the room B68 empty at 11 GHz

	Percentage of time				
Coherence bandwidth (MHz)	70%	80%	90%	95%	99%
$B_{0.9}$	1.4	1.5	1.7	2.3	2.4
$B_{0.7}$	4.1	4.4	5.0	6.3	6.9
$B_{0.5}$	7.3	8.2	9.3	9.4	12.1

Table 5.13: Coherence bandwidth for 0.5 ($B_{0.5}$), 0.7 ($B_{0.7}$) and 0.9 ($B_{0.9}$) correlation levels for the room B68 empty using a horn to omnidirectional antenna configuration at 11 GHz

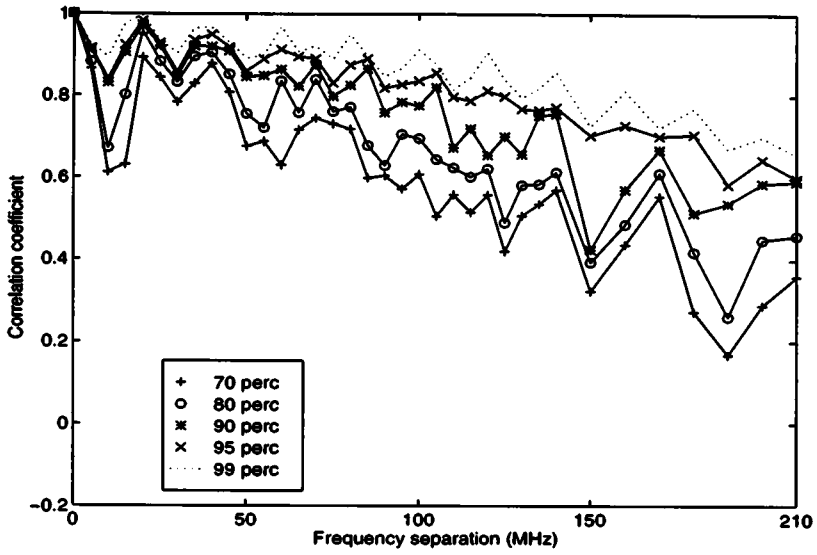

Figure 5-45: Predicted frequency correlation function for different percentage of time for the room B68 empty using a horn to omnidirectional antenna configuration

	Percentage of time				
Coherence bandwidth (MHz)	70%	80%	90%	95%	99%
$B_{0.9}$	9.9	19.6	35.3	53.2	77.4
$B_{0.7}$	56.4	82.9	124.7	168.4	200.4
$B_{0.5}$	126.7	162.4	>210	>210	>210

Table 5.14: Coherence bandwidth for 0.5 ($B_{0.5}$), 0.7 ($B_{0.7}$) and 0.9 ($B_{0.9}$) correlation levels from the prediction for the room B68 using a horn to omnidirectional antenna configuration at 11 GHz

5.3 Effects of the antennas radiation patterns on coherence bandwidth

This section describes results of experiments made under identical conditions in the same three corridors but with the omnidirectional antenna at the transmitter replaced by a 15 dBi horn antenna. This has been made in order to examine the effect of the antennas radiation pattern on the coherence bandwidth.

5.3.1 Corridor J2

The use of the 15 dBi horn antenna at the mobile transmitter suppresses reflections coming from Wall B (Figure 4-15). This has the effect of reducing the amount of fast variations present in the signal envelopes.

The half power beamwidth of the 15 dBi horn antenna is narrower than the 10 dBi one. Using horn to horn antennas, ground and ceiling reflections start occurring when the terminals are about 11 and 7.7 m apart respectively. Reflections on Wall A and C start when the terminals are 8 m and 5.4 m apart respectively. The measured and predicted received signal envelopes, with a frequency separation of 5 MHz, are shown in Figure 5-46 and Figure 5-47 respectively. The predicted envelopes, because reflections of the endwall opposite the receiver are completely suppressed, do not exhibit any fast variations.

The power spectra, plotted as a function of distance between terminals, as shown in Figure 5-48 exhibit less high frequency components compared to those measured under identical conditions but using horn and omnidirectional antennas as in Figure 5-3. Also it is to be noted that the low frequency components occupy a small bandwidth at the beginning the run. This is due to the narrow half power beamwidth of the horn antenna radiation which causes reflections off sidewalls to occur at longer distances as described in the above paragraph.

The value of the k-factor in the Rice distribution, measured as a function of distance between the terminals, is shown in Figure 5-49 for the two set of antenna configurations. It can be seen that using two different sets of antennas alter the statistical distribution of

the signal envelope. The use of two horns provides higher values of k. This is due to the smaller number of significant components of the received signal.

The frequency correlation function has been constructed for various percentages of time and given in Figure 5-50 for 70 % and 95 % of the time together with the functions obtained under identical conditions but using horn and omnidirectional antennas. Values of the coherence bandwidth obtained from Figure 5-50 for different levels of correlation are given in Table 5.15. This table shows that the coherence bandwidth values are much higher when two horn antennas are used. For instance, the coherence bandwidth required to achieve a level of correlation below 0.7 for 95 % of the time is 28.7 MHz with a horn to omnidirectional antenna configuration and 154.7 MHz with a horn to horn antenna configuration.

The coherence bandwidth, corresponding to a correlation level of 0.9, as a function of distance for the two sets of antenna configurations is shown in Figure 5-51. Table 5.16 shows the values of the coherence bandwidth for different levels of correlation. It can be seen that the coherence bandwidth using two horn antennas experiences larger variation with distance.

The signal envelopes have been predicted using two horn antennas at the transmitter and receiver similar to those used in the measurements. The frequency correlation functions obtained by considering the level below which the correlation stays for 70 % and 95 % of the time are given in Figure 5-52. The frequency correlation functions obtained under similar conditions but using a horn and omnidirectional antenna are also given in Figure 5-52. These results clearly show higher correlation levels when two horns are used and therefore larger coherence bandwidths. This is mainly due to the fact, that reflections from the endwall of the corridor with long time delays, are suppressed. For instance, the coherence bandwidth required to achieve a level of correlation below 0.7 for 90 % of the time is 192.0 MHz with a horn to horn antenna and 133.9 MHz using a horn to omnidirectional antenna.

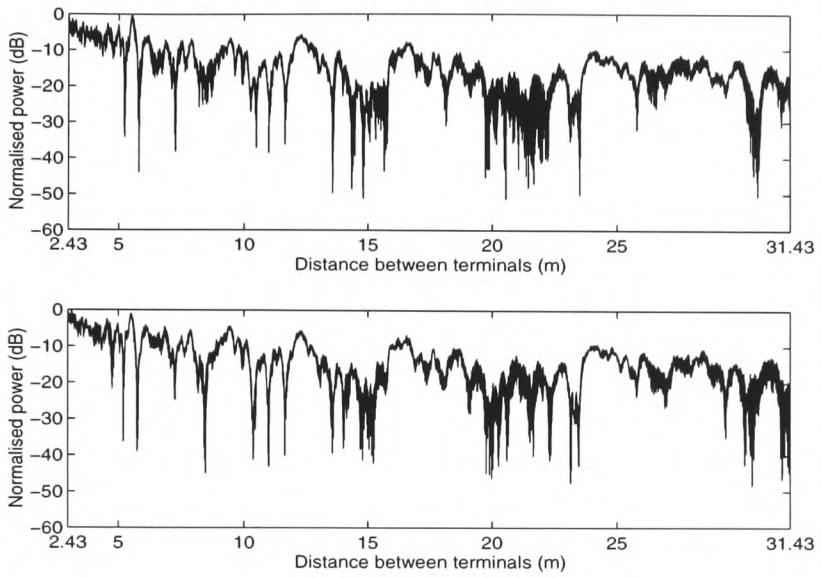

Figure 5-46: Received envelopes for a frequency spacing of 5 MHz in corridor J2 using a horn to horn configuration at 11 GHz

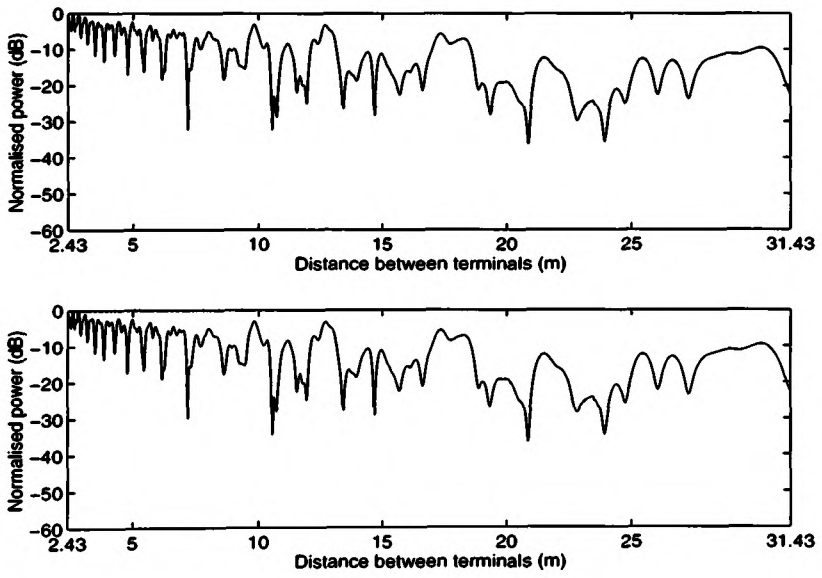

Figure 5-47: Predicted envelopes using a third order ray-tracing model computed with a frequency spacing of 5 MHz in corridor J2 using a horn to horn antenna at 11 GHz

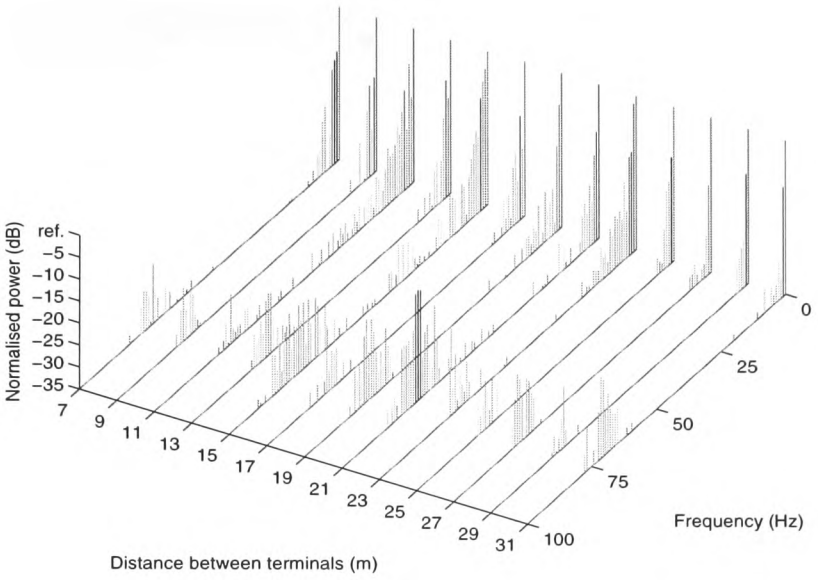

Figure 5-48: Power spectra of the signal envelope received as function of distance between terminals in corridor J2 using a horn to horn antenna at 11 GHz

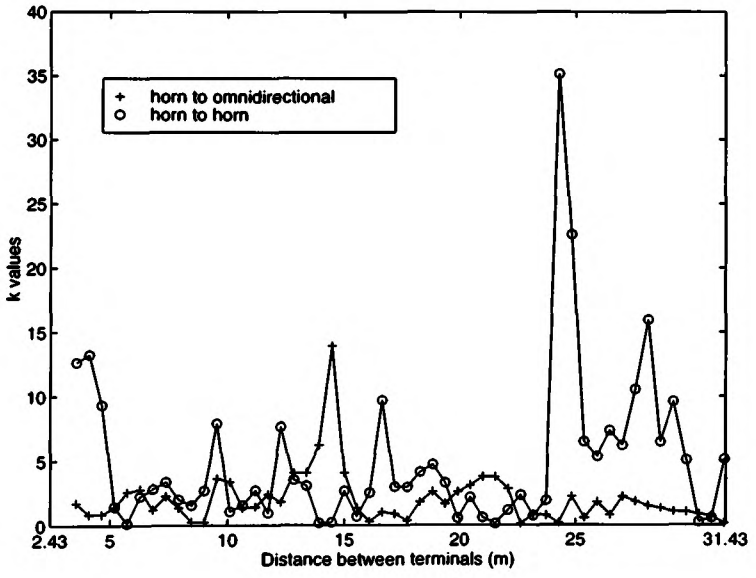

Figure 5-49: K factor in the Rice distribution as function of distance between terminals in corridor J2 using a horn to horn and a horn to omnidirectional antenna at 11 GHz

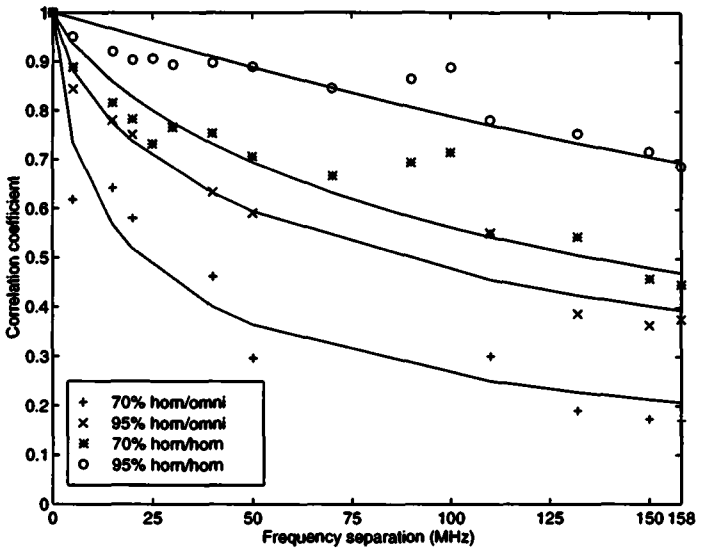

Figure 5-50: Frequency correlation functions measured in corridor J2 for 70 and 95 % of the time using a horn to horn and a horn to omnidirectional antenna at 11 GHz

	Percentage of time			
Coherence bandwidth (MHz)	70%		95%	
antennas	horn/horn	horn/omni	horn/horn	horn/omni
$B_{0.9}$	4.5	1.3	27.6	3.2
$B_{0.7}$	53.3	3.9	154.7	28.7
$B_{0.5}$	141.3	33.7	>190	117.0

Table 5.15: Coherence bandwidth for 0.5 ($B_{0.5}$), 0.7 ($B_{0.7}$) and 0.9 ($B_{0.9}$) correlation levels computed from the above frequency correlation fuctions

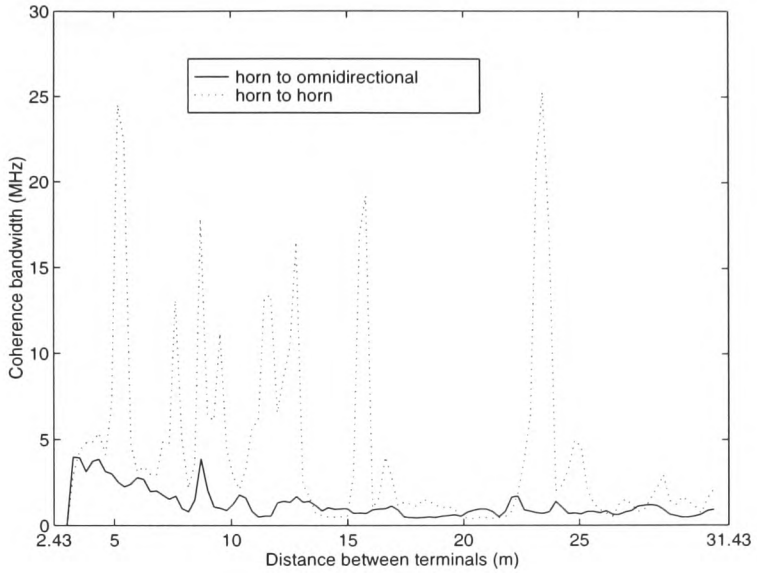

Figure 5-51: Coherence bandwidth for correlation level of 0.9 versus distance between terminals in corridor J2 using a horn to horn and a horn to omnidirectional antenna at 11 GHz

	Percentage of time			
Coherence bandwidth (MHz)	70%		95%	
antennas	horn/horn	horn/omni	horn/horn	horn/omni
$B_{0.9}$	4.6	1.3	17.9	3.1
$B_{0.7}$	27.3	3.8	128.5	15.8
$B_{0.5}$	104.1	16.8	182.7	49.3

Table 5.16: Coherence bandwidth for 0.5 ($B_{0.5}$), 0.7 ($B_{0.7}$) and 0.9 ($B_{0.9}$) correlation levels in corridor J2 computed from the coherence bandwidth functions for 70 and 95 using horn to horn and horn to omnidirectional antenna at 11 GHz

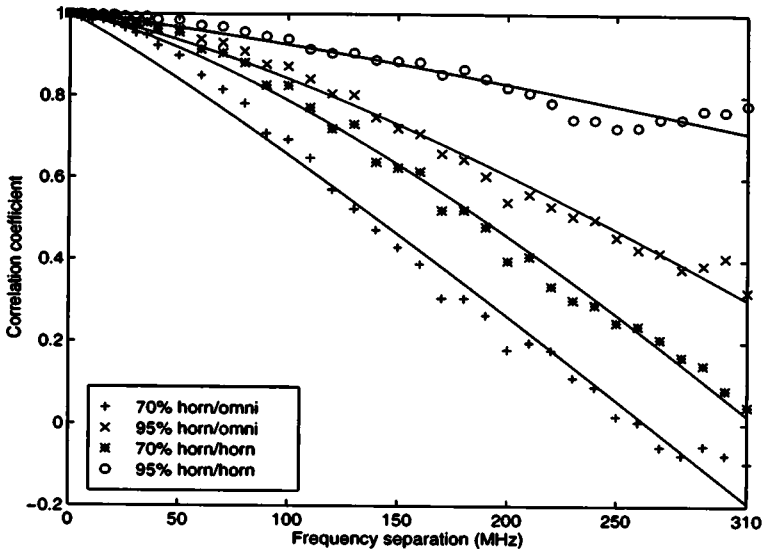

Figure 5-52: Frequency correlation function predicted in corridor J2 for 70 and 95 % of the time using a horn to horn and a horn to omnidirectional antenna at 11 GHz

	Percentage of time			
Coherence bandwidth (MHz)	70%		95%	
antennas	horn/horn	horn/omni	horn/horn	horn/omni
$B_{0.9}$	71.8	45.6	132.8	80.4
$B_{0.7}$	133.3	94.2	>310	159.5
$B_{0.5}$	185.5	132.2	>310	230.5

Table 5.17: Coherence bandwidth for 0.5 ($B_{0.5}$), 0.7 ($B_{0.7}$) and 0.9 ($B_{0.9}$) correlation levels computed from the above predicted frequency correlation functions

5.3.2 Corridor J3

In this corridor and when two horn antennas are used reflections from Wall C and Wall A start occurring when the terminals are 6.7 m and 4.4 m apart respectively. Ground reflections start when the distance between the terminals is 11.6 m and 7.1 m for the ceiling reflections.

The power spectra as a function of distance between the terminal are shown in Figure 5-53. It can be seen that the proportion of fast fading has been greatly reduced when two horn antennas are used. The value of the k-factor in the Rice distribution measured as a function of distance between the terminals for this corridor is shown in Figure 5-54 for the two sets of antenna configurations. The values of k vary with distance from 0 to a maximum value of 28. It can be seen that the use of a horn to horn antenna configuration causes the value of k to be higher than for a horn to omnidirectional antenna configuration. These results are in agreement with those obtained in corridor J2.

The frequency correlation function is given in Figure 5-55 for 70 % and 95 % of the time when the two horns and a horn and omnidirectional antennas are used. Values of the coherence bandwidth obtained from Figure 5-55 are shown in Table 5.18. This table shows that the coherence bandwidth values are much higher using a horn to horn antenna configuration. For instance, the coherence bandwidth required to achieve a level of correlation below 0.7 for 95 % of the time is 106.6 MHz for a horn to horn configuration and only 11.7 MHz for the second antenna configuration.

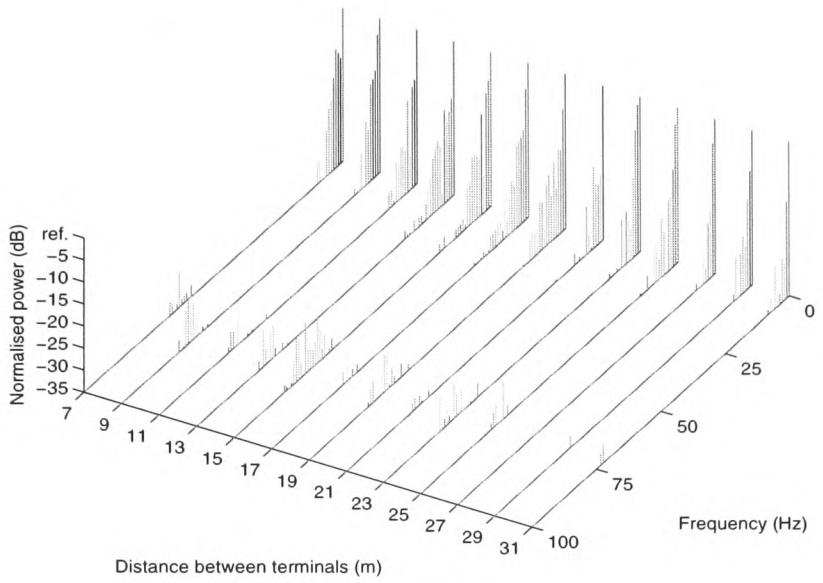

Figure 5-53: Power spectra of the signal envelope received as a function of distance between terminals in corridor J3 using a horn to horn antenna at 11 GHz

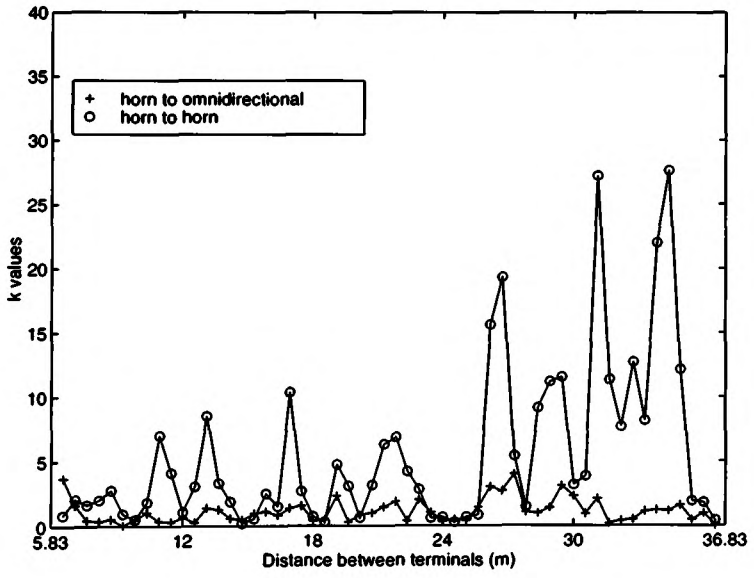

Figure 5-54: K factor in the Rice distribution as a function of distance between terminals in corridor J3 using a horn to horn and a horn to omnidirectional antenna at 11 GHz

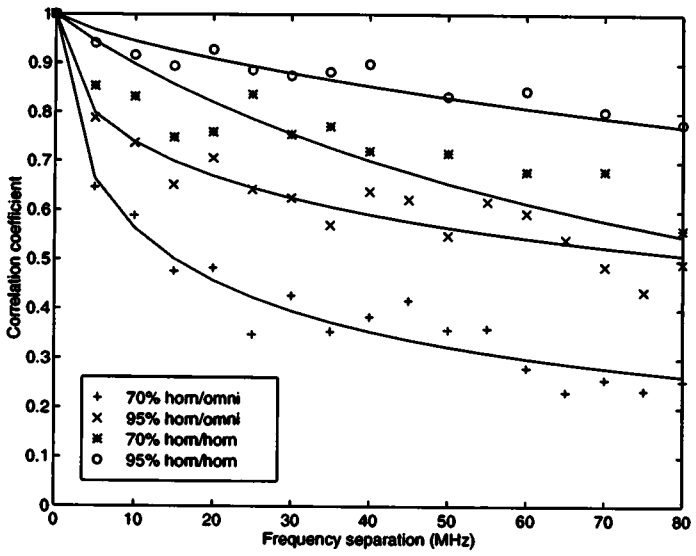

Figure 5-55: Frequency correlation function measured in corridor J3 for 70 and 95 % of the time using a horn to horn and a horn to omnidirectional antenna at 11 GHz

	Percentage of time			
Coherence bandwidth (MHz)	70%		95%	
antennas	horn/horn	horn/omni	horn/horn	horn/omni
$B_{0.9}$	3.4	1.3	13.7	2.2
$B_{0.7}$	54.8	3.8	106.6	11.7
$B_{0.5}$	93.7	10.2	>150	65.8

Table 5.18: Coherence bandwidth for 0.5 ($B_{0.5}$), 0.7 ($B_{0.7}$) and 0.9 ($B_{0.9}$) correlation levels computed from the above frequency correlation functions

5.3.3 Corridor H

With two horn antennas, reflections off Wall A and Wall C occur when the terminals are approximately 5.9 m apart. Ground and ceiling reflections occur when the transmitter is about 12 m and 9.2 m away from the receiver respectively.

The power spectra of the received envelopes are given in Figure 5-56. The high frequency components are evident in this corridor although two horn antennas are used. This is because strong reflections coming from behind the transmitter are not completely eliminated but suppressed by the front-to-back ratio of the horn antenna.

The value of the k-factor in the Rice distribution, measured as a function of distance between the terminals, is shown in Figure 5-57 for the two sets of antennas. These results are in agreement with the measurements made in corridor J2 and corridor J3.

The frequency correlation function, obtained for 70 % and 95 % of the time, using the two sets of antennas are given in Figure 5-58 with the coherence bandwidth given in Table 5.19. It can be seen that the coherence bandwidth with a horn to horn antenna is much higher than for a horn to omnidirectional antenna. For instance, the coherence bandwidth required to achieve a level of correlation below 0.7 for 95 % of the time is 43.8 MHz for a horn to horn configuration and 20.6 MHz when an omnidirectional antenna is used.

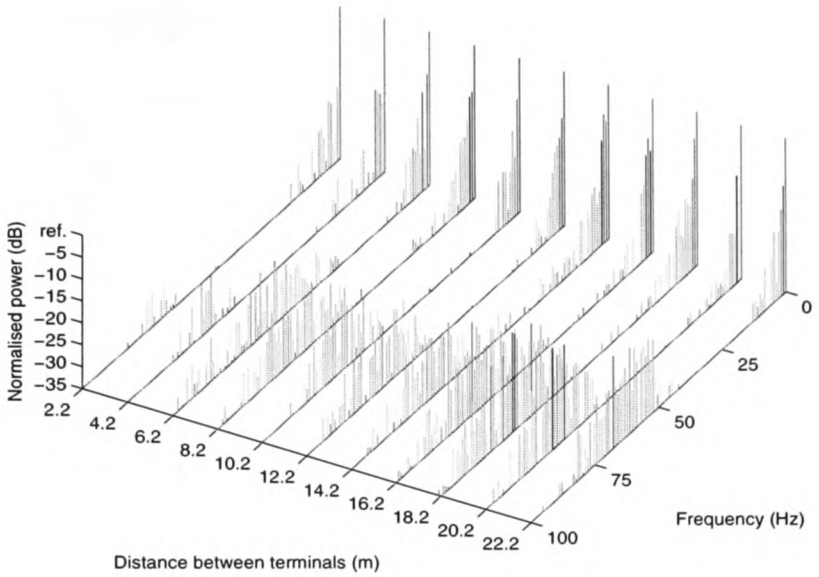

Figure 5-56: Power spectra of the signal envelope as a function of distance between terminals in corridor H using a horn to horn antenna at 11 GHz

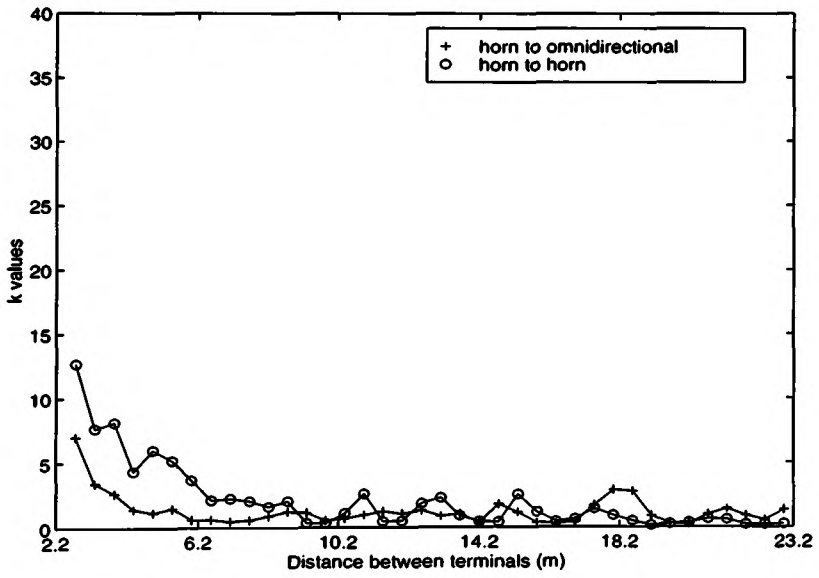

Figure 5-57: K factor in the Rice distribution with distance between terminals in corridor H using a horn to horn and a horn to omnidirectional antenna at 11 GHz

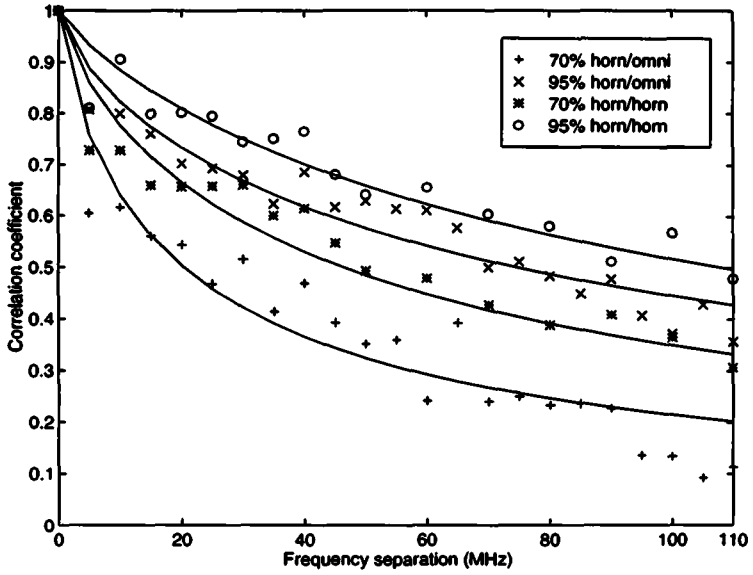

Figure 5-58: Frequency correlation function measured in corridor H for 70 % and 95 % of the time using a horn to horn and a horn to omnidirectional antenna at 11 GHz

	Percentage of time			
Coherence bandwidth (MHz)	70%		95%	
antennas	horn/horn	horn/omni	horn/horn	horn/omni
$B_{0.9}$	1.8	1.3	2.6	2.6
$B_{0.7}$	11.9	3.8	43.8	20.6
$B_{0.5}$	49.5	22.8	107.6	77.2

Table 5.19: Coherence bandwidth for 0.5 ($B_{0.5}$), 0.7 ($B_{0.7}$) and 0.9 ($B_{0.9}$) correlation levels computed from the above frequency correlation function

5.3.4 Interim summary

Influence of the radiation patterns on the coherence bandwidth has been investigated. It has been shown that when a horn antenna is used instead of an omnidirectional at the transmitter, larger values of coherence bandwidth have been measured. This is due to the fact that components with a long time delays, coming from the surfaces ahead of the transmitter, are attenuated by the front-to-back ratio of the antenna radiation pattern.

5.4 Effects of furniture in room B68

Measurement under identical conditions were made in the room but with the presence of furniture to examine the influence of furniture on the coherence bandwidth. The lay out of the furniture is depicted in Figure 4-23 of section 4.6.4. It is supposed to represent an office with tables, cupboards and chairs. The cupboards were realised by positioning tables up side down as shown in Figure 4-24. The horn antenna was mounted on the stationary receiver whereas the omnidirectional antenna was used with the mobile transmitter.

The received signal envelopes, obtained with a frequency separation of 5 MHz, are shown in Figure 5-59 with the power spectra plotted as a function of distance given in Figure 5-60. In general there are no specific changes in the frequency spectra.

The value of the k-factor in the Rice distribution versus distance measured with and without furniture is shown in Figure 5-61. It can be seen that the values of k obtained when the room was empty are higher.

The frequency correlation functions obtained for 70 % and 95 % of the time when the room is furnished and unfurnished are given in Figure 5-62. Values of the coherence bandwidth are shown in Table 5.20. It can be seen from these results that the coherence bandwidth is almost similar which indicates that the present lay out of the furniture did not influence the coherence bandwidth. For instance, the coherence bandwidth required to achieve a level of correlation below 0.7 for 95 % of the time is 6.2 MHz for the furnished room and 7.0 MHz for the empty room.

The coherence bandwidth equivalent to a correlation level of 0.9 is presented in Figure

5-63 as a function of distance between the terminals for the furnished and empty room, with the values of the coherence bandwidth given in Table 5.21. There is no significant difference between the two results.

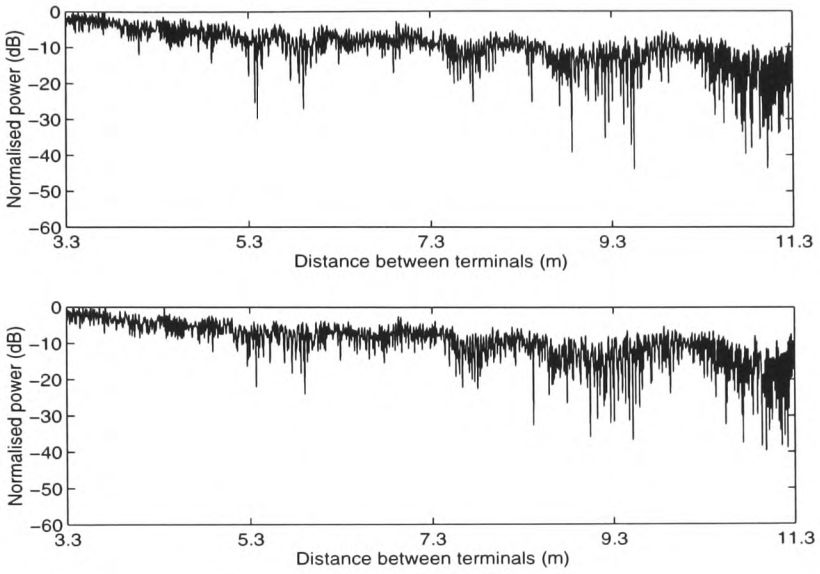

Figure 5-59: Received envelopes for a frequency spacing of 5 MHz in room B68 furnished using a horn to omnidirectional antenna at 11 GHz

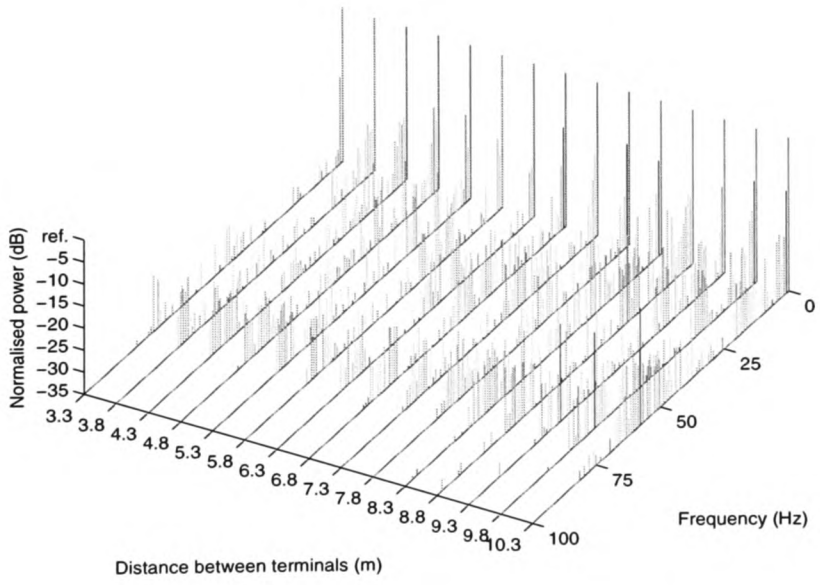

Figure 5-60: Power spectra of the signal envelope as a function of distance between terminals in room B68 furnished using a horn to omnidirectional antenna at 11GHz

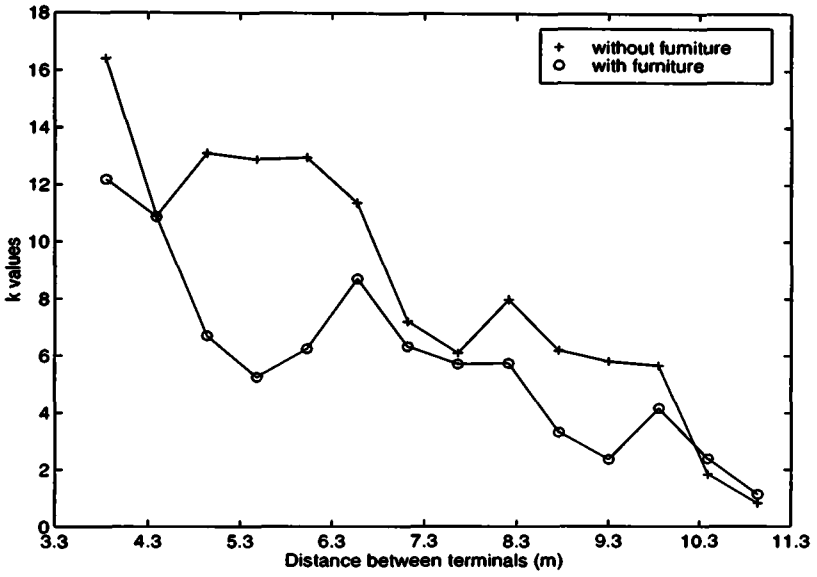

Figure 5-61: K factor in the Rice distribution with distance between terminals in B68 empty and furnished using a horn to omnidirectional antenna at 11 GHz

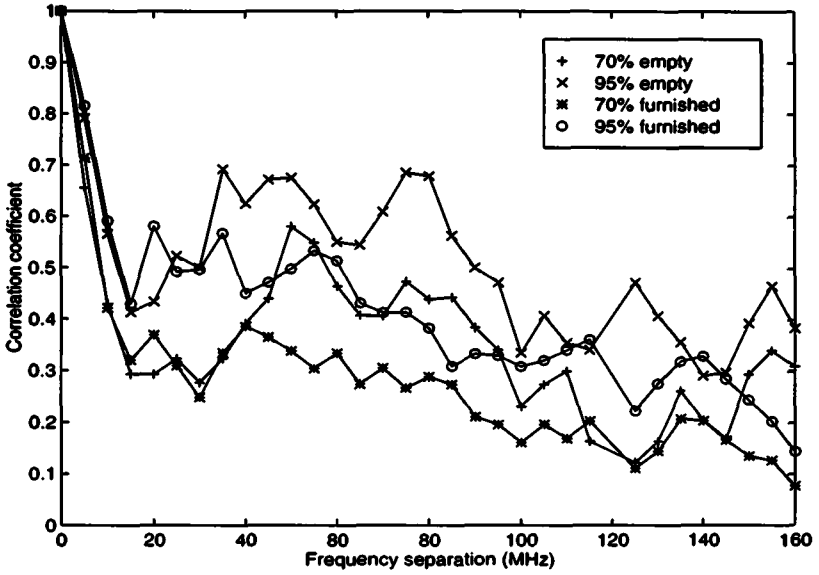

Figure 5-62: Frequency correlation function measured fro 70 % and 95 % of the time in room B68 furnished using a horn to omnidirectional antenna at 11 GHz

	Percentage of time			
Coherence bandwidth (MHz)	70%		95%	
room	empty	furnished	empty	furnished
$B_{0.9}$	1.4	1.7	2.4	2.7
$B_{0.7}$	4.3	5.2	7.0	7.6
$B_{0.5}$	8.4	8.6	12.1	12.8

Table 5.20: Coherence bandwidth for 0.5 ($B_{0.5}$), 0.7 ($B_{0.7}$) and 0.9 ($B_{0.9}$) correlation levels computed from the above frequency correlation functions

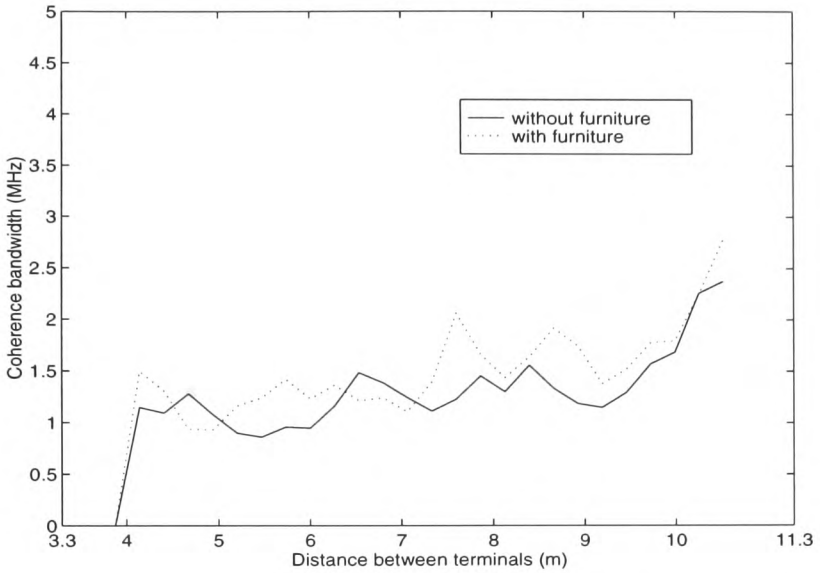

Figure 5-63: Coherence bandwidth at a correlation level of 0.9 in room B68 with and without furniture using a horn to omnidirectional antenna at 11 GHz

	Percentage of time			
Coherence bandwidth (MHz)	70%		95%	
room	empty	furnished	empty	furnished
$B_{0.9}$	1.4	1.7	2.3	2.3
$B_{0.7}$	4.1	4.9	6.3	6.2
$B_{0.5}$	7.3	8.2	9.4	11.1

Table 5.21: Coherence bandwidth for 0.5 ($B_{0.5}$), 0.7 ($B_{0.7}$) and 0.9 ($B_{0.9}$) correlation levels computed from the coherence bandwidth functions in room B68 with and without furniture for 70 and 95 % of the time using a horn to omnidirectional antenna at 11 GHz

Chapter 6

Coherence bandwidth characterisation at 62.4 GHz and comparison with results at 11 GHz

6.1 Introduction

This chapter presents results of experiments made in the same indoor microcells and under identical conditions to those reported in Chapter 5 but at 62.4 GHz. Results are given for corridor J2 and the room using a 10 dBi horn antenna at the receiver and an omnidirectional transmit antenna. A comparison of the frequency correlation functions and the coherence bandwidth with results obtained at 11 GHz is presented. The effect of furniture on the value of the coherence bandwidth has also been demonstrated at 62.4 GHz. The model is also used to interpret the influence of the order of reflection on the accuracy of the predicted results.

6.2 Corridor J2

Using the 62.4 GHz system in corridor J2 (41 m $\times$ 1.92 m $\times$ 2.68 m), measurements were conducted using frequency separations ranging from 0 to 240 MHz. The measurement geometry is identical to that explained in section 5.2.1 but with small differences in the

locations of terminals and their heights. The transmitter, with its antenna set at a height of 1.73 m, was moved along a straight line at a distance of 1.19 m from Wall A starting at 2.43 m from the receiver. The receiver, with its antenna set at a height of 1.68 m above the ground, was left stationary and placed at 1.22 m and 6.91 m from Wall A and Wall D respectively.

Sidewall reflections start occurring when the terminals are 3.5 m and 2.1 m apart for Wall A and Wall C respectively. Due to the narrow elevation beamwidth of the antenna, there are no reflections occuring from the ground and ceiling. These reflections start occurring at large separations between the terminals because the omnidirectional antenna has a narrow half power elevation beamwidth of 6 °. The received signal envelopes, obtained with a frequency separation of 5 MHz, are shown in Figure 6-1. The measured mean level decays with an exponent of 1.6. This is larger than that obtained at 11 GHz but smaller than the free space exponent. The predicted signal envelopes, using up to third order reflections with a frequency separation of 5 MHz, are shown in Figure 6-2. The signal envelopes, due to the smaller wavelength at 62.4 GHz, experience faster amplitude variations compared to those measured at 11 GHz.

The frequency spectra of the measured signal envelopes are presented in Figure 6-3. The spectra exhibit similar characteristics to those previously described at 11 GHz for such indoor microcell.

The distribution of the received signal envelopes have also been modeled as Rician and the value of k is expressed as a function of distance between terminals as shown in Figure 6-4. Results given in this figure show more fluctuations in comparison with those obtained at 11 GHz (Figure 5-6 of section 5.2.1).

The correlation between the measured signal envelopes, separated by 5 MHz, is expressed as a function of distance between the terminals and shown in Figure 6-5. The correlation values fluctuate significantly from -1 to 1 at a faster rate than those of Figure 5-8 obtained at 11 GHz. The frequency correlation function, obtained by considering all the correlation values measured in the microcell for different percentages of time, is given in Figure 6-6. The solid line represents the best fit of the measured values to a function

of the form $\rho = \frac{1}{(1+c\Delta f^n)}$ with the values of the coefficients c and n given in Table 6.1.

It can be seen that the value of correlation decreases with increasing frequency separation in a similar manner to that at 11 GHz. The coherence bandwidth values estimated from this figure for different levels of correlation are summarised in Table 6.2.

It can be seen that frequency separations larger than 240 MHz are required in order to ensure a level of correlation below 0.5 for high percentages of time. To achieve this corelation degree for 90 % of the time a frequency spacing of 191.2 MHz is needed.

A comparison between the frequency correlation functions measured in this corridor at 11 GHz and 62.4 GHz for 90 % of the time is given in Figure 6-7. Values of the coherence bandwidth at both frequencies and for various levels of correlation are given in Table 6.3. These results show that larger frequency separations are required at 62.4 GHz to achieve low correlation levels for the majority of time compared to those needed at 11 GHz. This is due to the narrower elevation beamwidth of the 62.4 GHz omnidirectional antenna which precludes reflections from the ceiling, ground and those from the endwall of the corridor opposite the receiver after being reflected from these surfaces.

The 62.4 GHz coherence bandwidth variation with distance has also been examined. Results corresponding to a correlation level of 0.9 are shown in Figure 6-8 with the values of the coherence bandwidth given in Table 6.4. It can be seen that the coherence bandwidth varies with distance in a similar fashion to that obtained at 11GHz with large values measured at small distances. Results obtained using this second method yield lower coherence bandwidth values than those given in Table 6.2 because, as explained in Chapter 5, the frequency correlation function at each position in the microcell is not necessarily a monotonously decreasing one.

	c	n
70%	0.33	0.36
80%	0.20	0.37
90%	0.11	0.39
95%	0.06	0.44
99%	0.04	0.42

Table 6.1: coefficients of the best fit function $\rho = 1/(1 + c\Delta f^n)$

Signal envelopes considering reflections up to the second and third order were separately predicted in order to examine the effect of the order of reflection on the results. Predicted frequency correlation functions are presented for 90 % of the time in Figure 6-9 with the coherence bandwidth values given in Table 6.5. It can be seen that the correlation coefficient between the simulated signal envelopes decreases significantly with increasing the order of reflection and is much higher than the measured value. Results given in Table 6.5 also show that the values of the coherence bandwidth computed by considering double and triple reflections differ significantly, and are larger than the measured ones.

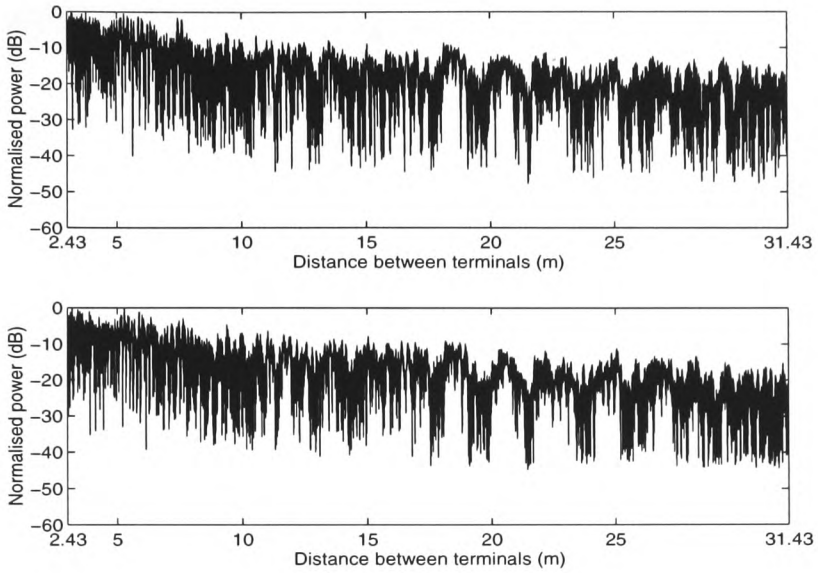

Figure 6-1: Received envelopes for a frequency spacing of 5 MHz in corridor J2 using a horn to omnidirectional antenna at 62.4 GHz

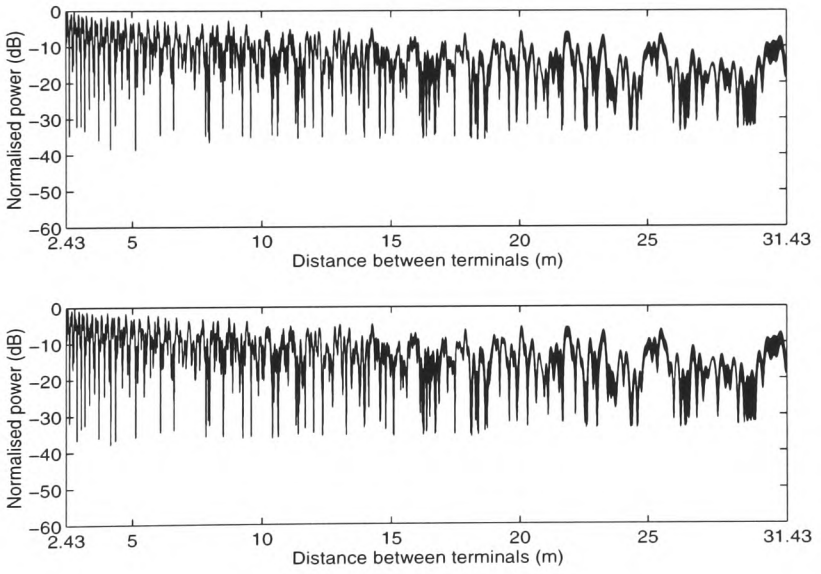

Figure 6-2: Predicted envelopes using third order ray-tracing with a frequency spacing of 5 MHz in corridor J2 using a horn to omnidirectional antenna at 62.4 GHz

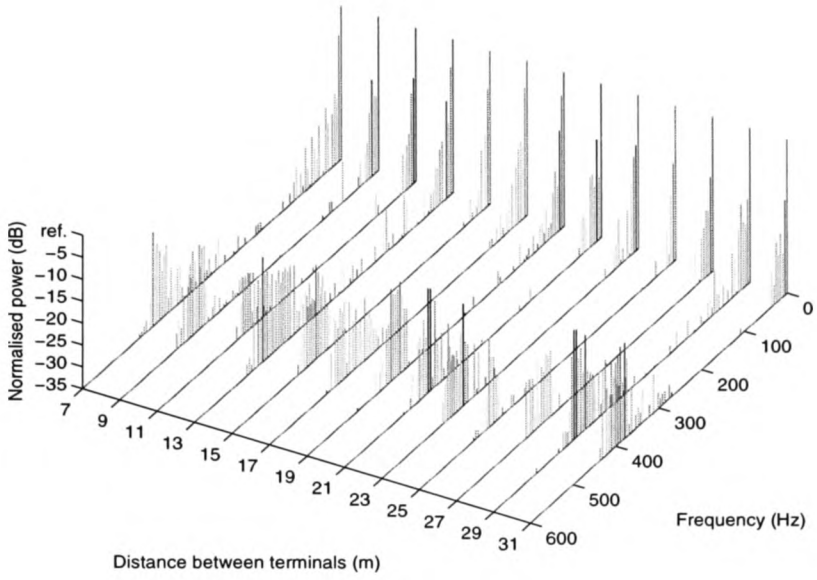

Figure 6-3: Power spectra of the signal envelope as function of distance between terminals in corridor J2 using a horn to omnidirectional antenna at 62.4 GHz

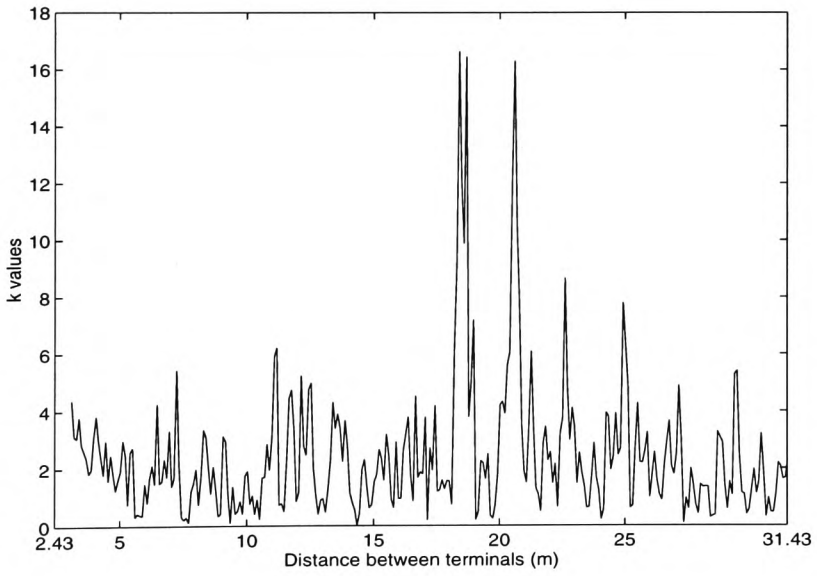

Figure 6-4: K factor in the Rice distribution with distance between terminals in corridor J2 using a horn to omnidirectional antenna at 62.4 GHz

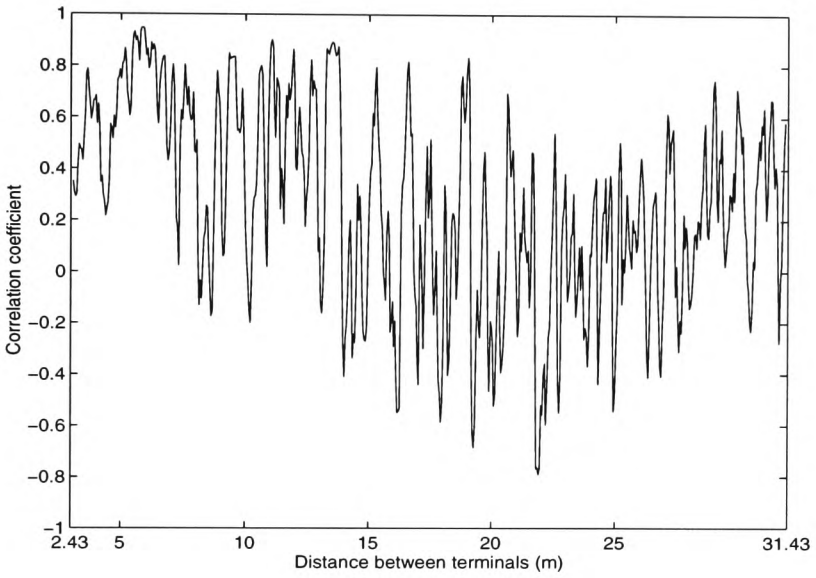

Figure 6-5: Correlation between the envelopes separated by 5 MHz versus distance between terminals

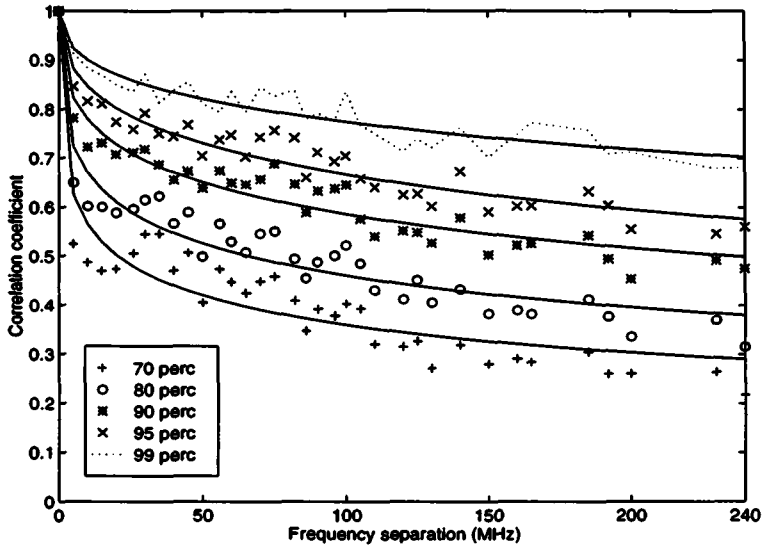

Figure 6-6: Frequency correlation functions mesured in corridor J2 using a horn to omni-directional antenna at 62.4 GHz

	Percentage of time				
Coherence bandwidth (MHz)	70%	80%	90%	95%	99%
$B_{0.9}$	1.1	1.4	2.3	3.2	7.2
$B_{0.7}$	3.1	4.3	32.8	84.0	210.9
$B_{0.5}$	8.3	49.9	191.2	-	-

Table 6.2: Coherence bandwidth for 0.5 ($B_{0.5}$), 0.7 ($B_{0.7}$) and 0.9 ($B_{0.9}$) correlation levels computed from the above frequency correlation function

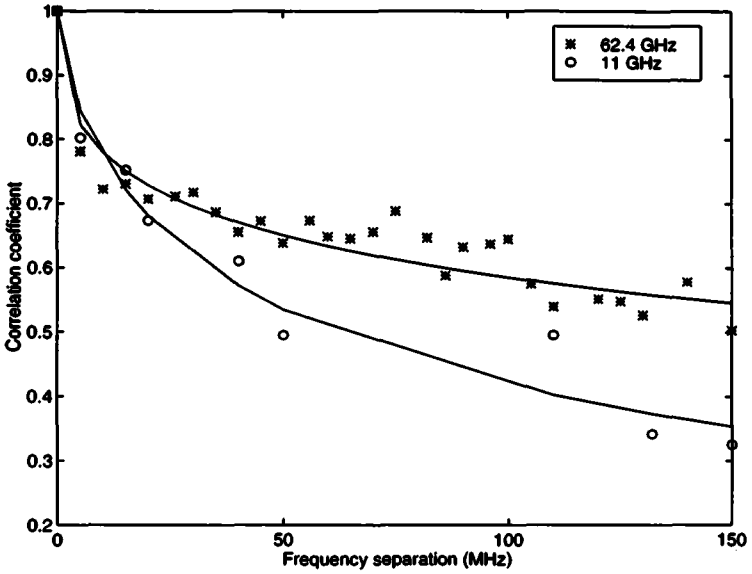

Figure 6-7: Frequency correlation function measured in corridor J2 for 90 % of the time using a horn to omnidirectional antenna at 11.0 GHz and 62.4 GHz

90% of time			
Coherence bandwidth (MHz)	$B_{0.5}$	$B_{0.7}$	$B_{0.9}$
62.4 GHz	191.2	32.8	2.32
11.0 GHz	49.5	18.3	2.5

Table 6.3: Coherence bandwidth for 0.5 ($B_{0.5}$), 0.7 ($B_{0.7}$) and 0.9 ($B_{0.9}$) correlation levels computed from the above frequency correlation functions

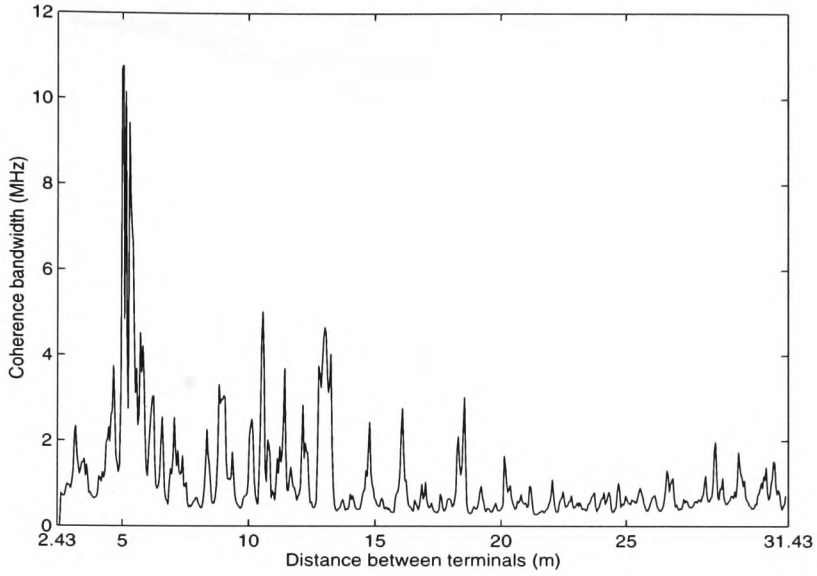

Figure 6-8: Coherence bandwidth for a correlation level of 0.9 as a function of distance between terminals in corridor J2 using a horn to omnidirectional antenna at 62.4 GHz

	Percentage of time				
Coherence bandwidth (MHz)	70%	80%	90%	95%	99%
$B_{0.9}$	1.0	1.4	2.3	3.2	6.6
$B_{0.7}$	3.1	4.2	6.3	11.9	32.6
$B_{0.5}$	5.5	7.5	13.4	34.9	122.9

Table 6.4: Coherence bandwidth for 0.5 ($B_{0.5}$), 0.7 ($B_{0.7}$) and 0.9 ($B_{0.9}$) correlation levels computed from the coherence bandwidth functions in corridor J2 using a horn to omnidirectional antenna configuration at 62.4 GHz

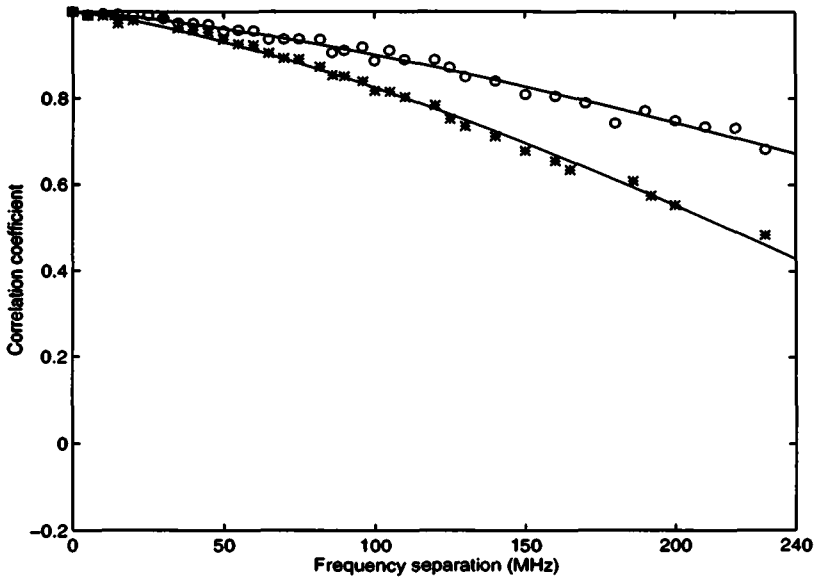

Figure 6-9: Frequency correlation functions predicted for 90 % of the time using double (o) and triple (*) order ray-tracing in corridor J2 at 62.4 GHz

Coherence bandwidth (MHz)	$B_{0.5}$	$B_{0.7}$	$B_{0.9}$
measurement	191.2	32.8	2.3
simulation (tripple)	222.9	143.4	66.6
simulation (double)	>240	226.3	98.2

Table 6.5: Predicted and measured Coherence bandwidth for 0.5 ($B_{0.5}$), 0.7 ($B_{0.7}$) and 0.9 ($B_{0.9}$) correlation levels computed from the frequency correlation function for 90 % of the time in corridor J2 using a horn to omnidirectional antenna configuration at 62.4 GHz

6.3 Room B68

Measurement in the room (12.8 m × 6.92 m × 2.6 m) was undertaken at 62.4 GHz using a frequency separation varying from 0 to 240 MHz. Furniture from the room was removed and the measurement set up was identical to that at 11 GHz as described in section 5.2.5. The receiver, with its antenna set at a height of 1.73 m, was located at 0.5 m from Wall A and 0.98 m from Wall D. The transmitter, with its antenna set at a height of 1.74 m, was moved on the same diagonal as for the 11 GHz measurement.

The received signal envelopes measured, with a frequency separation of 5 MHz, are shown in Figure 6-10 with the predicted envelopes given in Figure 6-11.

The frequency spectra of the measured signal envelopes are shown in Figure 6-12. These results, when compared with the frequency spectra given in Figure 6-12 at 11.0 GHz, are similar.

The statistical distribution of the signal envelope, modeled as Rician with the value of k expressed as a function of distance between terminals, behaves in a similar manner to that at 11 GHz as shown in Figure 6-13. However the values of k, measured at small distances at 62.4 GHz, are larger than those obtained at 11 GHz. This suggests that reflections at millimetre waves in such microcell are weaker.

The frequency correlation functions for different percentages of time are shown in Figure 6-14 with the coherence bandwidth values in the Table 6.6. It can be clearly seen that the value of the correlation drops rapidly at small frequency separations and then start fluctuating significantly when the frequency spacing is increased. These functions, therefore, may not be considered monotonous. These results exhibit similar behaviour to the ones obtained at 11 GHz for the same microcell as shown in Figure 6-15 for 90 % of the time. Table 6.7 indicates that the coherence bandwidth at 62.4 GHz is higher than the one at 11 GHz. For instance, 11.2 MHz is required to achieve a level of correlation below 0.7 for 95 % of the time at 62.4 GHz and only 7.0 MHz at 11.0 GHz. This is a very interesting result because by definition the coherence bandwidth is directly related to the RMS delay spread which is independent of the frequency. Therefore, such results

would indicate that there are additional factors that influence the value of the coherence bandwidth.

The coherence bandwidth at 62.4 GHz is also expressed as a function of distance between terminals and is shown in Figure 6-16 for a correlation level of 0.9 together with results at 11 GHz. Values of the coherence bandwidth at both frequencies are given in Table 6.8. This observations confirm that the coherence bandwidth at 62.4 GHz is larger than that at 11 GHz.

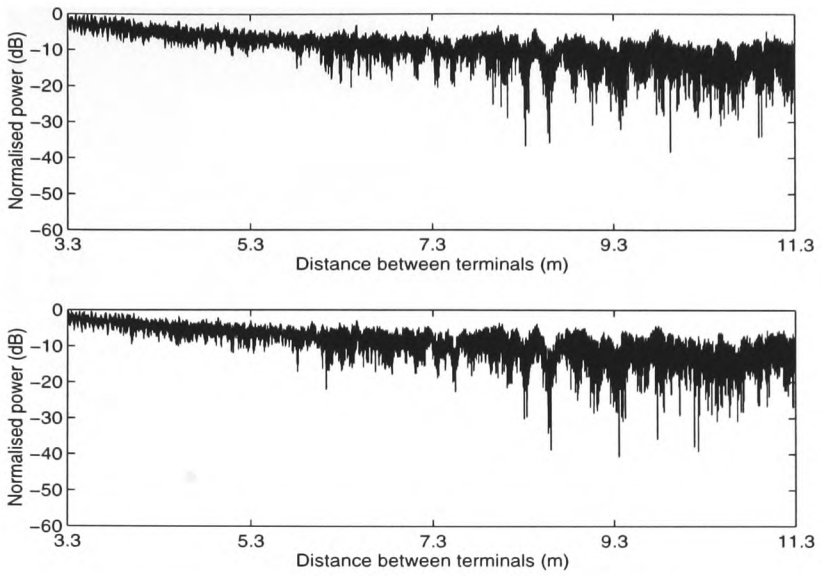

Figure 6-10: Received envelopes for a frequency separation of 5 MHz in room B68 empty using a horn to omnidirectional antenna at 62.4 GHz

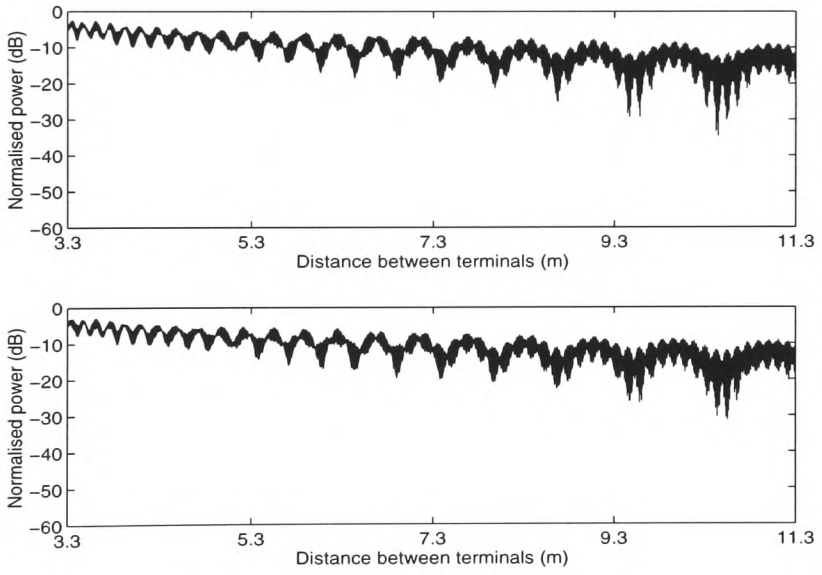

Figure 6-11: Predicted received envelopes using a third order ray-tracing model computed with a frequency spacing of 5 MHz in room B68 using a horn to omnidirectional antenna at 62.4 GHz

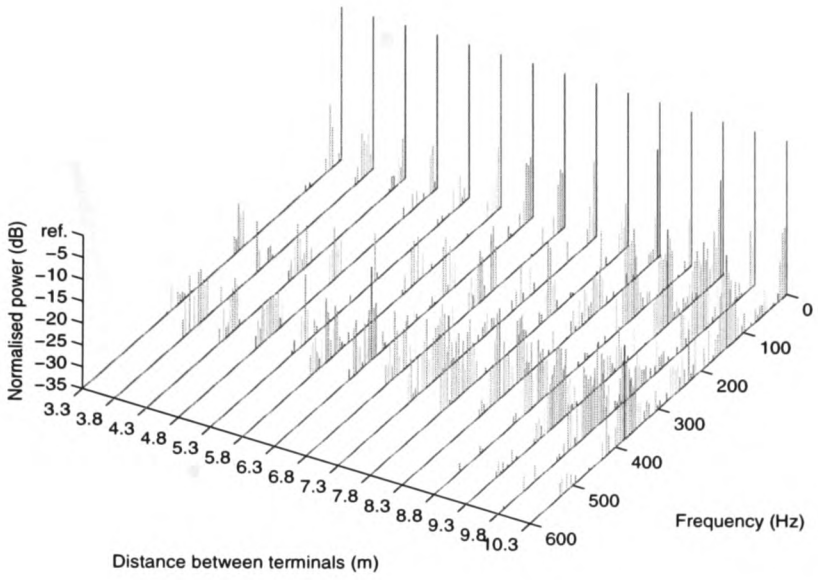

Figure 6-12: Power spectra of the signal envelope as a function of distance between terminals in room B68 empty using horn to omnidirectional antenna at 62.4 GHz

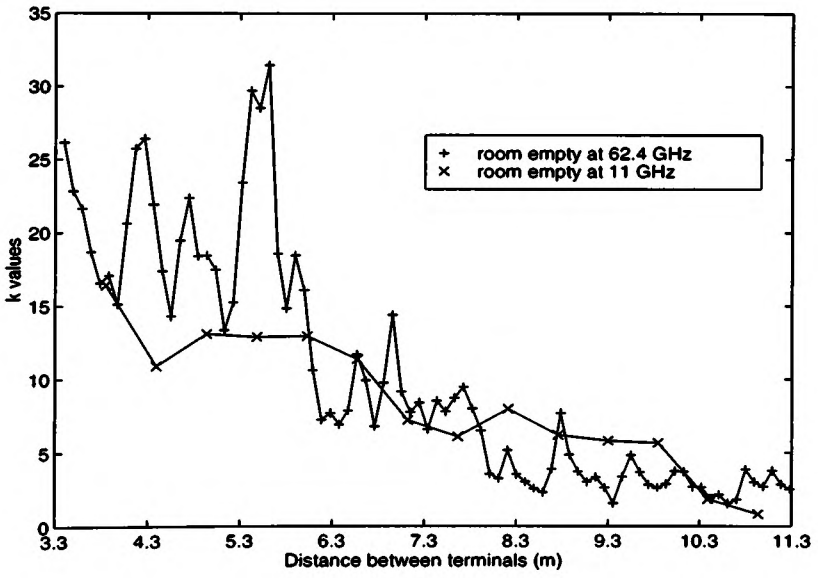

Figure 6-13: K factor in the Rice distribution with distance between terminals in room B68 empty using horn to omnidirectional antenna at 62.4 GHz and 11 GHz

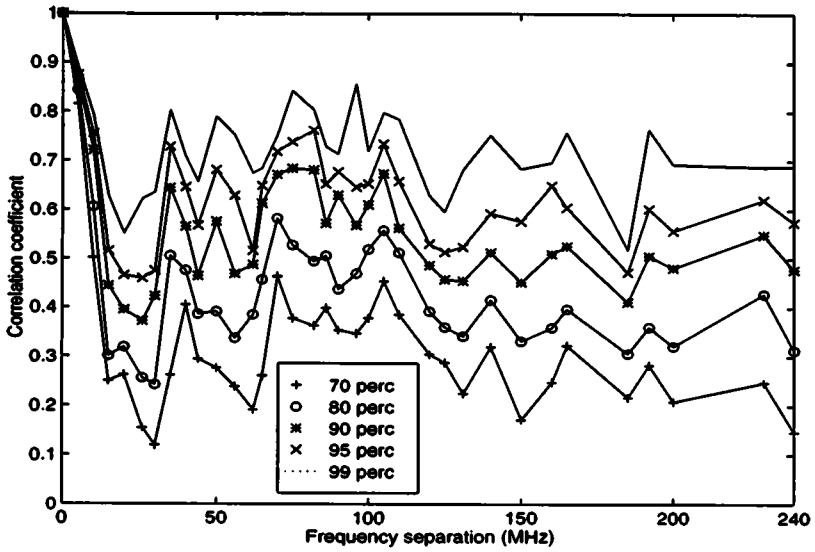

Figure 6-14: Frequency correlation function measured in room B68 empty using a horn to omnidirectional antenna at 62.4 GHz

	Percentage of time				
Coherence bandwidth (MHz)	70%	80%	90%	95%	99%
$B_{0.9}$	2.7	3.2	3.7	3.9	4.6
$B_{0.7}$	6.8	8.0	10.4	11.2	12.8
$B_{0.5}$	10.0	11.7	13.9	16.6	>190

Table 6.6: Coherence bandwidth for 0.5 ($B_{0.5}$), 0.7 ($B_{0.7}$) and 0.9 ($B_{0.9}$) correlation levels computed from the above frequency correlation functions

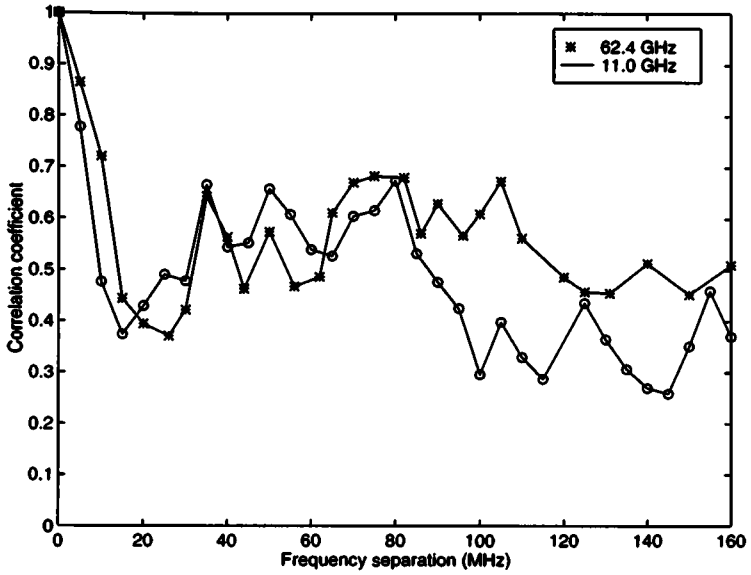

Figure 6-15: Frequency correlation function measured for 90 % of the time in room B68 empty at 62.4 GHz and 11.0 GHz

90% of time			
Coherence bandwidth (MHz)	$B_{0.5}$	$B_{0.7}$	$B_{0.9}$
62.4 GHz	13.9	10.4	3.7
11.0 GHz	9.6	6.3	2.2

Table 6.7: Coherence bandwidth for 0.5 ($B_{0.5}$), 0.7 ($B_{0.7}$) and 0.9 ($B_{0.9}$) correlation levels computed from the above frequency correlation functions

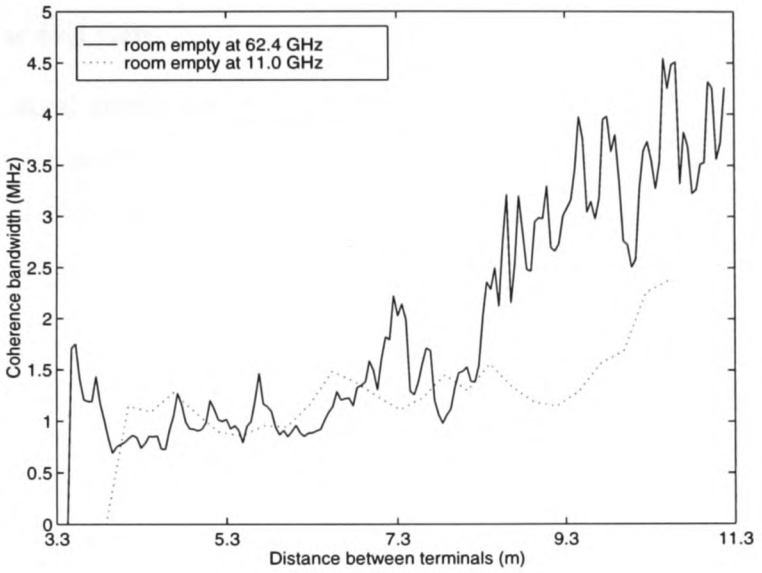

Figure 6-16: Coherence bandwidth for a correlation level of 0.9 as a function of distance between terminals using a horn to omnidirectional antenna at 11.0 GHz and 62.4 GHz

$B_{0.9}$	Percentage of time				
Coherence bandwidth (MHz)	70%	80%	90%	95%	99%
62.4 GHz	2.7	3.2	3.7	3.9	4.5
11.0 GHz	1.38	1.5	1.7	2.3	2.4

Table 6.8: Coherence bandwidth for different percentage of time computed from the above coherence bandwidth functions

6.4 Effects of furniture on the coherence bandwidth

Measurements, with the room furnished, were made under identical conditions to those conducted at 11 GHz. The locations of the terminals were identical to the one used for the empty room at 62.4 GHz.

The received signal envelopes, obtained with 5 MHz separation, are shown in Figure 6-17 with their power spectra given in Figure 6-18. The spectra, when compared to those given in Figure 6-12 between 5.3 m and 5.8 m, exhibit additional strong low frequency components.

The value of k, in the Rice distribution, versus distance for the room with and without furniture is shown in Figure 6-19. It can be seen that values of k, in both cases, decrease in a similar fashion except when the terminals are 5.3 to 5.8 m apart. Over these distances the values of k drop significantly when the room is furnished. This indicates that the presence of furniture at this frequency influences the statistical distribution of the envelopes.

The frequency correlation functions, obtained in the room for 70 % and 95 % of the time, with and without furniture are shown in Figure 6-20 with values of the coherence bandwidth given in Table 6.9. It can be seen that the coherence bandwidth values are comparable for low percentages of time. However at larger perecntages of time the coherence bandwidth in the presence of furniture becomes higher.

The coherence bandwidth, corresponding to a correlation level of 0.9, is expressed as a function of distance and is shown in Figure 6-21. It can be clearly seen that, when the terminals are 5.3 to 5.8 m apart, the coherence bandwidth is significantly different. It has already been shown, using the power spectra, that a strong middle frequency components appear at these distances. Such components cause a correlated amplitude variations resulting in higher correlation levels and therefore larger coherence bandwidth.

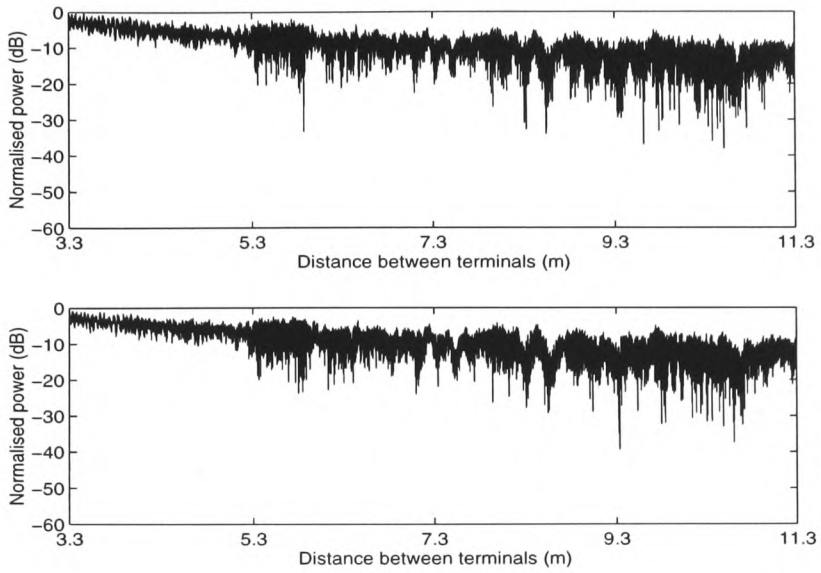

Figure 6-17: Received envelopes for a frequency spacing of 5 MHz in room B68 with furniture using a horn to omnidirectional antenna at 62.4 GHz

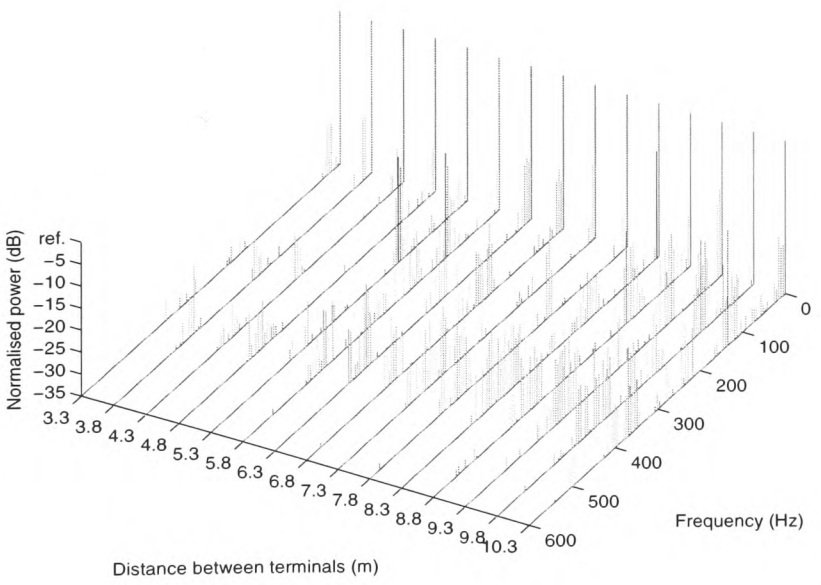

Figure 6-18: Power spectra of the signal envelope as function of distance between terminals in room B68 with furniture using a horn to omnidirectional antenna at 62.4 GHz

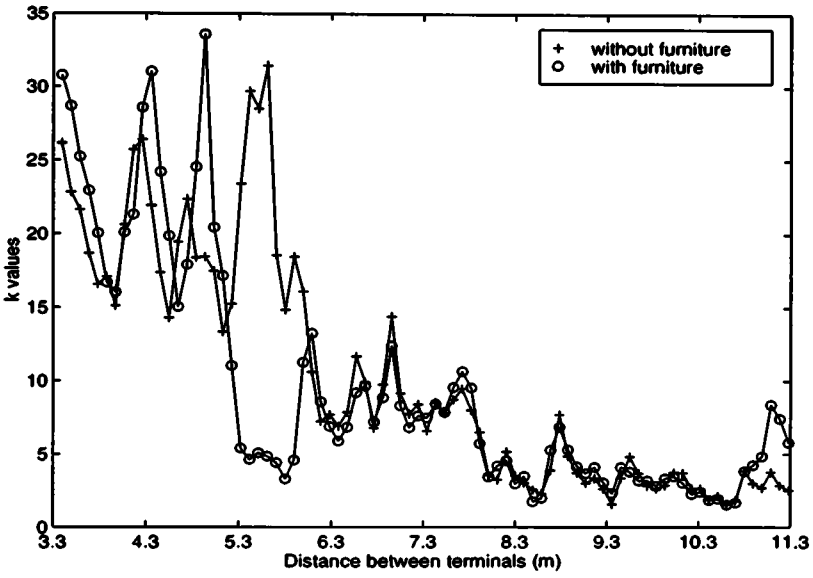

Figure 6-19: K factor in the Rice distribution with distance between terminals for B68 with and without furniture using a horn to omnidirectional antenna at 62.4 GHz

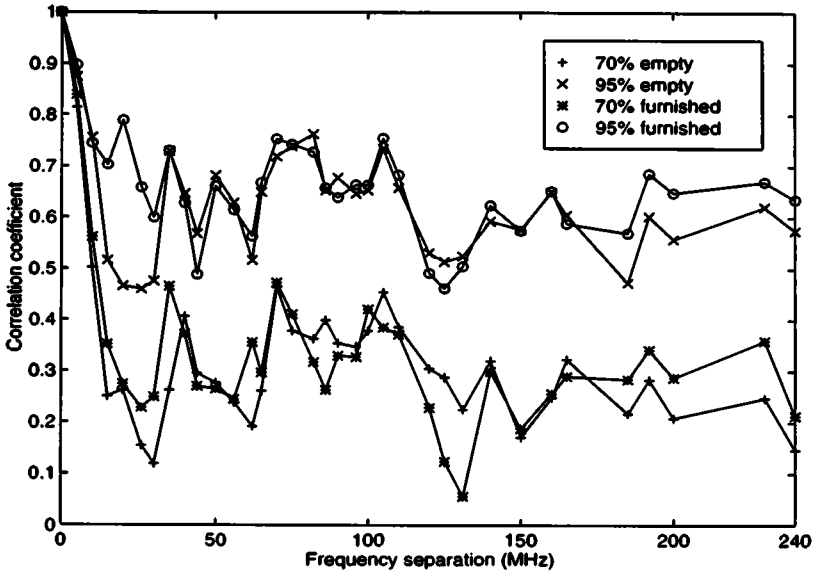

Figure 6-20: Frequency correlation functions measured for 70 % and 90 % of the time in room B68 with and without furniture using a horn to omnidirectional antenna at 62.4 GHz

	Percentage of time			
Coherence bandwidth (MHz)	70%		95%	
room	empty	furnished	empty	furnished
$B_{0.9}$	2.7	3.1	3.9	4.9
$B_{0.7}$	6.8	7.5	11.1	24.1
$B_{0.5}$	10.0	11.4	16.6	43.6

Table 6.9: Coherence bandwidth for 0.5 ($B_{0.5}$), 0.7 ($B_{0.7}$) and 0.9 ($B_{0.9}$) correlation levels computed from the above frequency correlation functions in room B68 with and without furniture using a horn to omnidirectional antenna at 62.4 GHz

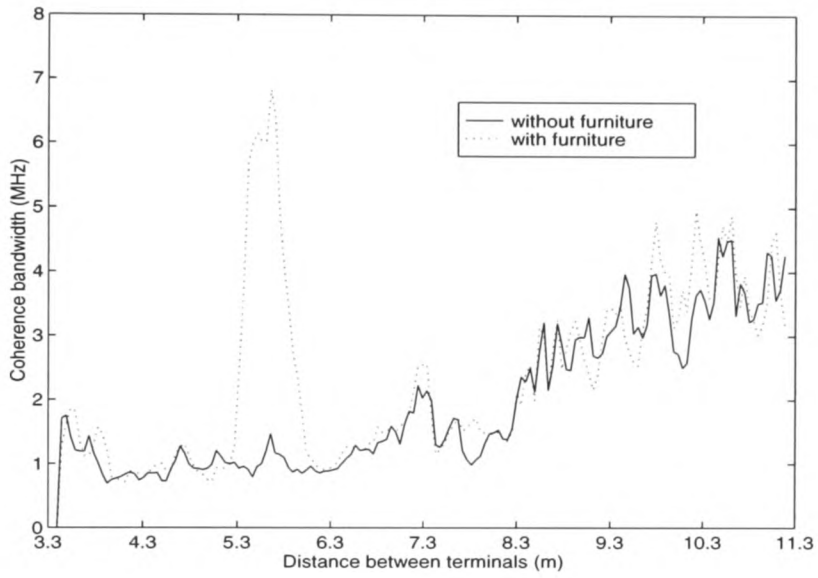

Figure 6-21: Coherence bandwidth for a correlation level of 0.9 as function of distance between terminals with and without furniture using a horn to omnidirectional antenna at 62.4 GHz

Chapter 7

Conclusion and further work

7.1 Conclusion

This thesis reports experimental and theoretical work undertaken at 11 GHz and 62.4 GHz to fully characterise the coherence bandwidth of an indoor mobile radio channel. Measurements, at both frequencies, have been made in a number of indoor environments. The influence of the antennas radiation patterns on the value of the coherence bandwidth has been investigated, by conducting experiments under identical conditions, but using a combination of different antennas. The effect of furniture on the coherence bandwidth value has also been examined. Comparison between results obtained at both frequencies is presented and differences explained.

Measurements have been made by simultaneously transmitting and receiving two side-band signals separated in frequency. A two branch frequency diversity system has been developed and used at both 11 GHz and 62.4 GHz. A controlled mechanical measurement set up has been developed utilizing a motor driven terminal along a specified route.

It has been illustrated that the amplitude variations of the signal envelopes are caused by reflections from all surfaces of the enclosed environment. Their distributions are found to be Rician, with the power ratio of the line-of-sight to that in the reflected rays varies significantly with distance between terminals.

Experimental and theoretical results have shown that the correlation coefficient be-

tween signal envelopes separated in frequency is highly variable with the position of terminals in the microcell. Due to this varying nature, the coherence bandwidth has been estimated by measuring the level below which the correlation stays for a given percentage of time. This has facilitated the construction of the frequency correlation function in the microcell. On the other hand, a second method based on measuring the coherence bandwidth at each terminal positions in the microcell has been used. Results obtained using both techniques are different. This is because, as explained in this thesis, the frequency correlation functions are not necessarily monotonously decreasing at each position in the microcell. However, it has been shown that the function behaviour changes with the geometry of the indoor environment. In a long narrow corridor, with one of the terminals located at one end, the frequency correlation function is found to exhibit a monotonous decreasing characteristic. Whereas in an almost square room, with or without furniture, this function exhibits a rapid reduction in the correlation value at small frequency spacings and becomes highly variable at larger frequency separations.

Measurements made at 11 GHz, under identical conditions in two corridors of similar dimensions but one with metal sidewalls and the other with metal and glass sidewalls, have shown that frequency spacings of 12.4 MHz and 59.6 MHz are needed to ensure a correlation level below 0.7 for 99 % of the time respectively. However, for a correlation level of 0.9, the frequency spacings become 2.5 MHz and 3.9 MHz. The difference between values obtained in both corridors is due to the fact that the corridor with metal sidewalls gives rise to additional multiple sidewall reflections and stronger reflections coming from the endwall opposite the receiver after being reflected from the sidewall.

Measurements made, under identical conditions in a shorter corridor with metal sidewalls, have shown larger coherence bandwidth values compared with those obtained in a longer corridor with metal sidewalls as well. This is believed to be due to the lower time delays associated with rays in the shorter corridor.

In an almost square empty room, with the receiver located at one corner and the transmitter moving along the diagonal away from the receiver, the behaviour of the frequency correlation function is somewhat different. To ensure levels of correlation below 0.7 and

0.9 for 99 % of the time, frequency separations of 7.7 MHz and 2.7 MHz are required respectively. These values are in general smaller than those obtained in the corridors.

Influence of the antennas radiation patterns on the coherence bandwidth has been investigated. It has been shown that, when the omnidirectional antenna at the transmitter was replaced by a 15 dBi horn antenna, larger values of the coherence bandwidth have been measured. This is explained by the fact that components, with a long time delays, coming from the endwall opposite the receiver are attenuated by the front-to-back ratio of the antenna radiation pattern. Measurements made in the corridor, with metal sidewalls using two horn antennas, have shown that the frequency spacing required to achieve a level of correlation of 0.7 for 95 % of the time is 106.6 MHz compared to only 11.7 MHz when an omnidirectional antenna is used.

Results of experiments conducted, under identical conditions in the same environments, have shown that the propagation mechanism at both 11 GHz and 62.4 GHz is similar. Higher values of the coherence bandwidth are measured at 62.4 GHz. The reason behind this is that the 62.4 GHz omnidirectional antenna has a narrower elevation beamwidth which precludes reflections from the ceiling, floor and those from the endwall of the corridor opposite the receiver after being reflected from these surfaces. It has also been shown that the effect of furniture in an almost square room is more noticeable at 62.4 GHz.

A three dimensional ray-tracing reflection model, based on the image method, has been developed and used to assist in explaining experimental results. The model considers 54 rays and reflections up to the third order and takes into account the antennas radiation patterns. The surfaces of the enclosed environment are assumed to be smooth all with the same dielectric parameters. Theoretical results obtained from the ray-tracing algorithm have shown similar trend at both 11 GHz and 62.4 GHz.

The most important of the work presented in this thesis is that the correlation coefficient must be measured at a significantly large number of points in the microcell in order to fully characterise the frequency correlation function. It has also been demonstrated that calculating the coherence bandwidth from the frequency correlation function at each position in the microcell may lead to inaccurate estimate.

7.2 Further work

- To improve the ray-tracing model allowing higher order of reflections and taking into account different sidewall materials.
- Measurements of power delay profile to examine the relationship between RMS delay spread and coherence bandwidth.
- Measurements of the correlation coefficients and power delay profiles in urban micro-cells to determine the coherence bandwidth and its dependence on the RMS delay spread

References

[1] J. E. Padgett, C. G. Günther, and T. Hattori, "Overview of wireless personal communications," *IEEE Communications Magazine*, vol. 33, pp. 28–41, January 1995.

[2] R. Steele, "An update on personal communications," *IEEE Communications Magazine*, vol. 30, pp. 30–31, December 1992.

[3] K. A. Wimmer and J. B. Jones, "Global development of PCS," *IEEE Communications Magazine*, pp. 22–27, June 1992.

[4] J. S. DaSilva, B. Arroyo-Fernádez, B. Barani, and D. Ikonomou, "European third-generation mobile systems," *IEEE Communications Magazine*, vol. 34, pp. 68–83, October 1996.

[5] J. G. Proakis, *Digital Communications.* Mc Graw-Hill International editions, third ed., 1995.

[6] M. Rahnema, "Overview of the GSM system and protocol architecture," *IEEE Communications Magazine*, vol. 31, pp. 92–100, April 1993.

[7] R. Pandya, "Emerging mobile and personal communication systems," *IEEE Communications Magazine*, vol. 33, pp. 44–52, June 1995.

[8] P. W. Baier, P. Jung, and A. Klein, "Taking the challenge of multiple access for third-generation cellular mobile radio systems - a european view," *IEEE Communications Magazine*, vol. 34, pp. 82–89, February 1996.

[9] R. S. Cole, H. J. Thomas, and G. L. Siqueira., "Two frequency coherence measurements on a 55 GHz mobile radio link," *Journal of the Institution of Electronic and radio Engineers*, vol. 58, pp. 140–144, September-December 1988.

[10] J. S. DaSilva, B. Barani, and B. Arroyo-Fernández, "European mobile communications on the move," *IEEE Communications Magazine*, vol. 34, pp. 60–69, February 1996.

[11] L. M. Correia and R. Prasad, "An overview of wireless broadband communications," *IEEE Communications Magazine*, vol. 35, pp. 28–33, January 1997.

[12] A. Hammoudeh and C. Haslett, "Characterisation and modelling of obstructed line-of-sight millimetre wave mobile radio signals," *ICAP'95, 9th International Conference on Antennas and Propagation*, vol. 2, pp. 283–287, April 1995. Eindhoven, The Netherlands.

[13] P. F. M. Smulders and A. G. Wagemans, "Wideband indoor radio propagation measurements at 58 GHz," *Electronics Letters*, vol. 28, pp. 1270–1272, June 1992.

[14] P. F. M. Smulders, *Broadband Wireless LANs : A Feasibility Study.* PhD thesis, Technische Universiteit Eindhoven, 1995.

[15] M. Bensebti, J. McGeehan, and M. A. Beach, "Indoor multipath radio propagation measurements and characterisation at 60 GHz," *21st European Microwave Conference*, pp. 1217–1222, September 1991. Stuttgart, Germany.

[16] R. Davies, M. Bensebti, M. A. Beach, and J. P. McGeehan, "Wireless propagation measurements in indoor multipath environments at 1.7 GHz and 60 GHz for small cell systems," *Proceeding of the 41st IEEE Vehic. Tech. Soc. Conf.*, pp. 589–593, 1991. St Louis, USA.

[17] S. E. Alexander and G. Pugliese, "Cordless communication within buildings : Results of measurements at 900 MHz and 60 GHz," *Br Telecom Technol J*, vol. 1, pp. 99–105, July 1983.

[18] P. W. Huish and G. Pugliese, "A 60 GHz radio system for propagation studies in buildings," *International Conference on Antennas and Propagation*, pp. 181–185, 1983.

[19] P. Nobles, D. Ashworth, and F. Halsall, "Propagation measurements in an indoor radio environment at 2, 5 and 17 GHz," *IEE colloquium on high bit rate UHF/SHF channel sounders-technology and measurement*, pp. 4/1–4/6, December 1993.

[20] R. O. LaMaire, A. Krishna, P. Bhagwat, and J. Panian, "Wireless LANs and mobile networking : Standards and future directions," *IEEE Communications Magazine*, vol. 34, pp. 86–94, August 1996.

[21] K. Pahlavan, T. H. Probert, and M. E. Chase, "Trends in local wireless networks," *IEEE Communications Magazine*, vol. 33, pp. 88–95, March 1995.

[22] P. Beckmann and A. Spizzichino, *The Scattering of Electromagnetic Waves from Rough Surfaces.* Artech House, Inc, 1987.

[23] M. P. M. Hall, L. W. Barclay, and M. T. Hewitt, *Propagation of Radiowaves.* The Institution of Electrical Engineers, 1996.

[24] A. J. Rustako, Jr., N. Amitay, G. J. Owens, and R. S. Roman, "Radio propagation at microwave frequencies for line-of-sight microcellular mobile and personal communications," *IEEE Transactions on Vehicular Technology*, vol. 40, pp. 203–210, February 1991.

[25] A. Hammoudeh and G. Allen, "Millimetric wavelengths radiowave propagation for line-of-sight indoor microcellular mobile communications," *IEEE Transactions on Vehicular Technology*, vol. 44, pp. 449–460, August 1995.

[26] A. Kajiwara, "Millimetre-wave indoor radio channel with artificial reflector," *IEEE Transactions on Vehicular Technology*, vol. 46, pp. 486–493, May 1997.

[27] R. A. Valenzuela, O. Landron, and D. L. Jacobs, "Estimating local mean signal strength of indoor multipath propagation," *IEEE Transactions on Vehicular Technology*, vol. 46, pp. 203–212, February 1997.

[28] T. Manabe, T. Ihara, A. Kato, K. Sato, and H. Saito, "Wideband millimeter wave channel sounder and indoor propagation experiment at 60 GHz," *Proceeding of the ISAP'96, International Symposium Antennas and Propagation*, pp. 201–204, September 1996. Chiba, Japan.

[29] G. Kalivas, M. El-Tanany, and S. Mahmoud, "The performance of a radio link for indoor communications at 29 GHz," *ANTEM'94, Proceeding of Symposium on Antenna Technology and Applied Electromagnetics*, pp. 24–29, August 1994.

[30] H. Hashemi and D. Tholl, "Statistical modeling and simulation of the RMS delay spread of indoor radio propagation channels," *IEEE Transactions on Vehicular Technology*, vol. 43, pp. 110–120, February 1994.

[31] D. Molkdar, "Review on radio propagation into and within buildings," *IEE Proceeding*, vol. 138, pp. 61–73, February 1991.

[32] J. B. Andersen, T. S. Rappaport, and S. Yoshida, "Propagation measurements and models for wireless communications channels," *IEEE Communications Magazine*, vol. 33, pp. 42–49, January 1995.

[33] W. K. Tam and V. N. Tran, "Propagation modelling for indoor wireless communication," *Electronics and Communication Engineering Journal*, vol. 7, pp. 221–228, October 1995.

[34] S. R. Todd, M. El-Tanany, G. Kalivas, and S. Mahmoud, "Indoor radio path loss comparison between the 1.7 GHz and 37 GHz bands," *Proceeding of the IEEE International Conference on Universal Personnal Communications*, pp. 621–625, October 1993.

[35] G. Kalivas, M. El-Tanany, and S. Mahmoud, "Channel charcterization for indoor wireless communications at 21.6 GHz and 37.2 GHz," *ICUPC'93 Proceeding of the IEEE International Conference on Universal Personnal Communications*, pp. 626–630, October 1993.

[36] G. Allen and A. Hammoudeh, "Frequency diversity propagation measurements for an indoor 60 GHz mobile radio link," *7th International Conference on Antennas and Propagation*, pp. 298–301, April 1991.

[37] P. F. M. Smulders and J. Lähteenmäki, "Measurements of indoor radio channels at 60 GHz," *Joint COST 231/235 Workshop on Mobile Communication*, April 1994. Prague.

[38] S. Y. Tan and H. S. Tan, "Modelling and measurements of channel impulse response for an indoor wireless communication system," *IEE Proceeding Microwave Antennas Propagation*, vol. 142, pp. 405–410, October 1995.

[39] J. D. Parsons, *The Mobile Radio Propagation Channel.* Pentech Press, 1992.

[40] R. C. V. Macario, *Personal and Mobile Radio Systems.* Peter Peregrinus Ltd, 1991.

[41] D. A. Hawbaker and T. S. Rappaport, "Indoor wideband radiowave propagation measurements at 1.3 GHz and 4.0 GHz," *Electronics Letters*, vol. 26, pp. 1800–1802, October 1990.

[42] H. Hashemi, "A study of temporal and spatial variations of the indoor radio propagation channel," *PIMRC'94, Proceeding of the 5th IEEE International Symposium on Personal Indoor and Mobile Radio Communication*, pp. 127–134, September 1994. The Hague, The Netherlands.

[43] R. Ganesh and K. Pahlavan, "Effects of traffic and local movements on multipath characteristics of an indoor radio channel," *Electronics Letters*, vol. 26, pp. 810–812, June 1990.

[44] G. J. M. Janssen, P. A. Stigter, and R. Prasad, "Wideband indoor channel measurements and BER analysis of frequency selective multipath channels at 2.4, 4.75, and 11.5 GHz," *IEEE Transactions on Communications*, vol. 44, pp. 1272–1288, October 1996.

[45] Y. Qi, B. Currie, W. Wang, P. Y. Chung, C. Wu, and J. Litva, "Measurement and simulation of radio wave propagation in two indoor environments," *PIMRC'95,*

Proceeding of the 6th IEEE International Symposium on Personal Indoor and Mobile Radio Communication, pp. 1171–1174, September 1995. Toronto, Canada.

[46] M. G. Sánchez, L. de Haro, A. G. Pino, and M. Calvo, "Human operator effect on wide-band radio channel characteristics," *IEEE Transactions on Antennas and Propagation*, vol. 45, pp. 1318–1320, August 1997.

[47] S. J. Howard and K. Pahlavan, "Doppler spread measurements of indoor radio channel," *Electronics Letters*, vol. 26, pp. 107–108, January 1990.

[48] P. Melançon and J. Lebel, "Effects of fluorescent lights on signal fading characteristics for indoor radio channels," *Electronics Letters*, vol. 28, pp. 1740–1741, August 1992.

[49] A. A. M. Saleh and R. A. Valenzuela, "A statistical model for indoor multipath propagation," *IEEE Journal on Selected areas in communications*, vol. 5, pp. 128–137, February 1987.

[50] J. H. Tarng, W. R. Chang, and B. J. Hsu, "Three-dimensional modelling of 900-MHz radio propagation in corridors," *IEEE Transactions on Vehicular Technology*, vol. 46, pp. 519–527, May 1997.

[51] J. P. Kermoal and A. Hammoudeh, "Measurements of correlation degree using frequency diversity at 62.4 GHz in indoor environment for mobile radio communication systems," *Propagation Électromagnétique du Décamétrique à l' Angström*, pp. 194 – 199, October 1997. Rennes, France.

[52] P. A. Bello, "Characterization of randomly time-variant linear channels," *IEEE Transactions on Communications Systems*, pp. 360–393, December 1963.

[53] A. Gersho, "Characterization of time-varying linear systems," *Proceedings of the IEEE*, vol. 51, pp. 238–239, January 1963.

[54] M. J. Gans, "A power-spectral theory of propagation in the mobile-radio environment," *IEEE Transactions on Vehicular Technology*, vol. 21, pp. 27–38, February 1972.

[55] J. W. C. Jakes, *Microwave Mobile Communications.* John Wiley and Sons, Inc, 1974.

[56] R. C. V. Macario, *Cellular Radio. Principles and Design.* The Macmillan Press Ltd, 1993.

[57] R. H. Clarke, "A statistical theory of mobile-radio reception," *The Bell System Technical Journal*, vol. 47, pp. 957–1000, July-August 1968.

[58] W. C. Jake and D. O. Reudink, "Comparison of mobile radio transmission at UHF and x band," *IEEE Transactions on Vehicular Technology*, vol. 16, pp. 10–14, October 1967.

[59] F. Hanssen and F. I. Meno, "Mobile fading - rayleigh and lognormal superimposed," *IEEE Transactions on Vehicular Technology*, vol. 26, pp. 332–335, November 1977.

[60] S. O. Rice, "Statistical properties of a sine wave plus random noise," *The Bell System Technical Journal*, vol. 27, pp. 109–157, January 1948.

[61] T. Aulin, "A modified model for the fading signal at a mobile radio channel," *IEEE Transactions on Vehicular Technology*, vol. 28, pp. 182–203, August 1979.

[62] W. C. Y. Lee, "Estimate of local average power of a mobile radio signal," *IEEE Transactions on Vehicular Technology*, vol. 34, pp. 22–27, February 1985.

[63] R. Prasad and L. M. Correia, "Wireless broadband multimedia communications," *International Workshop on Telecommunication Systems*, pp. 1–15, May 1997. Saha Alam, Malaysia. Invited paper.

[64] P. F. Driessen, "Gigabit/s indoor wireless systems with directional antennas," *IEEE Transactions on Communications*, vol. 44, pp. 1034–1043, August 1996.

[65] G. Kalivas, M. El-Tanany, and S. Mahmoud, "The design of a radio link for indoor wireless communications at 29 GHz," *ICUPC'94, Proceeding of the 3rd IEEE International Conference on Universal Personal Communications*, pp. 6–10, September 1994.

[66] T. Manabe, Y. Miura, and T. Ihara, "Effects of antenna directivity and polarization on indoor multipath propagation charcateristics at 60 GHz," *IEEE Journal on Selected Areas in Communications*, vol. 14, pp. 441–448, April 1996.

[67] T. Manabe, K. Sato, H. Masuzawa, K. Taira, T. Ihara, Y. Kasashima, and K. Yamaki, "Polarization dependence of multipath propagation and high-speed transmission characteristics of indoor millimeter-wave channel at 60 GHz," *IEEE Transactions on Vehicular Technology*, vol. 44, pp. 268–274, May 1995.

[68] A. Kajiwara, "Effects of polarization, antenna directivity, and room size on delay spread in LOS indoor radio channel," *IEEE Transactions on Vehicular Technology*, vol. 46, pp. 169–175, February 1997.

[69] A. R. Tharek and J. P. McGeehan, "Propagation and bit error rate measurements within buildings in the millimetre wave band about 60 GHz," *ICC'88, IEEE International Conference Communication*, pp. 318–321, 1988.

[70] J. P. Pugliese, A. Hammoudeh, and M. Al-Nuaimi, "Estimation of dielectric parameters from reflection and transmission coefficients of building materials at 62.4 GHz," *ICAP'97, 10th International Conference on Antennas and Propagation*, pp. 2.1–2.4, April 1997.

[71] K. Sato, T. Manabe, J. Polivka, T. Ihara, Y. Kasashima, and K. Yamaki, "Measurement of the complex refractive index of concrete at 57.5 GHz," *IEEE Transactions on Antennas and Propagation*, vol. 44, pp. 35–40, January 1996.

[72] K. Sato, T. Manabe, T.Ihara, H. Saito, S. Ito, T. Tanaka, K. Sugai, N. Ohmi, Y. Murakami, M. Shibayama, Y. Konishi, and T. Kimura, "Measurements of reflection and transmission characteristics of interior structures of office in building in the 60-GHz band," *IEEE Transactions on Antennas and Propagation*, vol. 45, pp. 1783–1792, December 1997.

[73] J. D. Gibson, *The Mobile Communications Handbook.* CRC Press, Inc, 1996.

[74] A. S. Bajwa, *Wideband Characterisatio of UHF Mobile Radio Propagation in Urban and Suburban Areas.* PhD thesis, University of Birmingham, 1979.

[75] R. Kattenbach and H. Früchting, "Calculation of system and correlation functions for WSSUS channels from wideband measurements," *Frequenz*, vol. 49, pp. 42–47, 1995.

[76] A. Papoulis, *Signal Analysis.* McGraw-Hill, 1984.

[77] I. Siaud, "A mobile radio propagation channel model with frequency hopping for the performance evaluation of the third generation radiocommunication systems in an urban area," *Propagation Électromagnétique du décamétrique á l'Angström*, pp. 277–282, October 1997. Rennes, France.

[78] S. Kim, H. L. Bertoni, and M. Stern, "Pulse propagation characteristics at 2.4 GHz inside buildings," *IEEE Transactions on Vehicular Technology*, vol. 45, pp. 579–592, August 1996.

[79] B. H. Fleury, "An uncertainty relation for WSS processes and its application to WSSUS systems," *IEEE Transactions on Communications*, vol. 44, pp. 1632–1634, December 1996.

[80] R. Kattenbach and H. Früchting, "Wideband measurements of channel characteristics in deterministic indoor environment at 1.8 GHz and 5.2 GHz," *PIMRC'95, Proceeding of the 6th IEEE International Symposium on Personal Indoor and Mobile Radio Communication*, pp. 1166–1170, September 1995. Toronto, Canada.

[81] I. Siaud and D. Gérome, "Radio propagation channel characterisation in hilly terrain at 850 MHz for the radio link extension of the wired communication networks," *Propagation Électromagnétique du décamétrique á l'Angström*, pp. 91–96, October 1997. Rennes, France.

[82] T. Felhauer, W. König, and W. Mohr, "Wideband propagation measurements for characterizing the mobile radio channel and its parameters," *AEÜ- Archiv für Elektronik und Übertragungstechnik*, vol. 48, no. 6, pp. 321–331, 1994.

[83] H. R. Anderson and J. P. McGeehan, "Direct calculation of coherence bandwidth in urban microcels using a ray-tracing propagation model," *PIMRC'94, Proceeding of the 5th IEEE International Symposium on Personal Indoor and Mobile Radio Communication*, pp. 20–24, September 1994.

[84] W. K. Tam and V. N. Tran, "Multi-ray propagation model for indoor wireless communications," *Electronics Letters*, vol. 32, pp. 135–137, January 1996.

[85] N. Amitay, "Modelling and computer simulation of wave propagation in lineal line-of-sight microcells," *IEEE Transactions on Vehicular Technology*, vol. 41, pp. 337–342, November 1992.

[86] P. Driessen, M. Gimersky, and T. Rhodes, "Ray model of indoor propagation," *Proceeding of the 2nd Virginia Technology Symposium*, pp. 225–249, June 1992.

[87] H. R. Anderson, "A ray-tracing propagation model for digital broadcast systems in urban areas," *IEEE Transactions on Broadcasting*, vol. 39, pp. 309–317, September 1993.

[88] P. F. M. Smulders, "Deterministic modelling of mm-wave indoor radio propagation," *Proceeding of IEEE first Symposium on Communication and Vehicular Technology in the Benelux*, pp. 3.1–1 – 3.1–7, October 1993. Delft, Netherlands.

[89] H. Yamamura and S. Sasaki, "Millimeter wave propagation model and delay spread along the maglev guideway," *IECE Transaction Communication*, vol. 78, p. 12041207, August 1995.

[90] M. C. Lawton and J. P. McGeehan, "The application of a deterministic ray launching algorithm for the prediction of radio channel characteristics in small-cell environments," *IEEE Transactions on Vehicular Technology*, vol. 43, pp. 955–969, November 1994.

[91] S. Y. Seidel and T. S. Rappaport, "Site-specific propagation prediction for wireless in-building personal communication system design," *IEEE Transactions on Vehicular Technology*, vol. 43, pp. 879–891, November 1994.

[92] D. I. Laurenson, A. Sheikh, and S. McLaughlin, "Characterisation of the indoor mobile radio channel using a ray tracing technique," *ICWC'92, Proceeding of the IEEE Internatioanl Conference on Selected Topics in Wireless Communications*, pp. 65–68, June 1992. Vancouver, Canada.

[93] J. W. McKown and J. R. L. Hamilton, "Ray tracing as a design tool for radio networks," *IEEE Network Magazine*, vol. 5, pp. 27–30, November 1991.

[94] S. Y. Tan and H. S. Tan, "Improved three-dimensional ray tracing technique for microcellular propagation models," *Electronics Letters*, vol. 31, pp. 1503–1505, August 1995.

[95] S. S. Y and T. S. Rappaport, "A ray tracing technique to predict path loss and delay spread inside buuildings," *Proceeding of the IEEE Globe Com' 92 Conference*, pp. 649–653, December 1992. Orlando, USA.

[96] K. R. Schaubach, N. J. D. IV, and T. S. Rappaport, "A ray tracing method for predicting path loss and delay spread in microcellular environments," *Proceedings of the 1992 Vehicular Technology Society Conference*, pp. 932–935, May 1992. Denver, USA.

[97] H. Suzuki and A. S. Mohan, "Ray tube tracing method for predicting indoor channel chracteristics map," *Electronics Letters*, vol. 33, pp. 1495–1496, August 1997.

[98] G. Durgin, N. Patwari, and T. S. Rappaport, "Improved 3d ray launching method for wireless propagation prediction," *Electronics Letters*, vol. 33, pp. 1412–1413, July 1997.

[99] T. Holt, K. Pahlavan, and J. F. Lee, "A graphical indoor radio channel simulator using 2d ray tracing," *PIMRC'92, Proceeding of the 3rd IEEE International Symposium on Personal Indoor and Mobile Radio Communication*, pp. 411–416, October 1992. Boston, USA.

[100] C. A. Balanis, *Advanced Engineering Electromagnetics*. Hamilton Printing Company, 1989.

[101] H. R. Reed and C. M. Russell, *Ultra High Frequency Propagation.* Chapman and Hall Ltd, second ed., 1965.

[102] J. D. Kraus, *Electromagnetics.* Mc Graw-Hill International Editions, 1984.

[103] U. Dersch, J. Troger, and E. Zollinger, "Multiple reflections of radio waves in a corridor," *IEEE Transactions on Antennas and Propagation*, vol. 42, pp. 1571–1574, September 1994.

[104] S. R. Todd, M. S. El-Tanany, and S. A. Mahmoud, "Space and frequency diversity measurements of the 1.7 GHz indoor radio channel using a four-branch receiver," *IEEE Transactions on Vehicular Technology*, vol. 41, pp. 312–320, August 1992.

[105] J. F. Lemieux, M. S. El-Tanany, and H. M. Hafez, "Experimental evaluation of space frequency polarization diversity in the indoor wireless channel," *IEEE Transactions on Vehicular Technology*, vol. 40, pp. 569–574, August 1991.

[106] H. B. Abdullah, *Microwave and Millimetre-Wave Omnidirectional Antennas in the Azimuth Plane for Mobile Communications.* PhD thesis, University of Bath, 1994.

[107] J. P. Kermoal, A. Hammoudeh, and C. J. Haslett, "An evaluation of frequency diversity performance in microwave frequency mobile radio communication systems," *ICAP'97, 10th International Conference on Antennas and Propagation*, pp. 2.123 – 2.127, April 1997. Edinburgh, UK.